CRANFIELD UNIVERSITY

Ömer Faruk Eker

A Hybrid Prognostic Methodology and its Application to Well-Controlled Engineering Systems

School of Aerospace, Transport and Manufacturing
IVHM Centre

PhD Thesis
Academic Year: 2014 - 2015

Supervisors: Assoc Prof Fatih Camci
Prof Ian K. Jennions

January 2015

CRANFIELD UNIVERSITY

School of Aerospace, Transport and Manufacturing
IVHM Centre

PhD Thesis

Academic Year 2014 - 2015

Ömer Faruk Eker

A Hybrid Prognostic Methodology and its Application to Well-Controlled Engineering Systems

Supervisors: Assoc Prof Fatih Camci
Prof Ian K. Jennions

January 2015

Abstract

This thesis presents a novel hybrid prognostic methodology, integrating physics-based and data-driven prognostic models, to enhance the prognostic accuracy, robustness, and applicability. The presented prognostic methodology integrates the short-term predictions of a physics-based model with the longer term projection of a similarity-based data-driven model, to obtain remaining useful life estimations. The hybrid prognostic methodology has been applied on specific components of two different engineering systems, one which represents accelerated, and the other a nominal degradation process.

Clogged filter and fatigue crack propagation failure cases are selected as case studies. An experimental rig has been developed to investigate the accelerated clogging phenomena whereas the publicly available Virkler fatigue crack propagation dataset is chosen after an extensive literature search and dataset analysis. The filter clogging experimental rig is designed to obtain reproducible filter clogging data under different operational profiles. This data is thought to be a good benchmark dataset for prognostic models.

The performance of the presented methodology has been evaluated by comparing remaining useful life estimations obtained from both hybrid and individual prognostic models. This comparison has been based on the most recent prognostic evaluation metrics. The results show that the presented methodology improves accuracy, robustness and applicability. The work contained herein is therefore expected to contribute to scientific knowledge as well as industrial technology development.

Keywords:

Integrated Vehicle Health Management, Prognostics and Health Management, Condition Based Maintenance, Hybrid Prognostics, Physics-based Prognostics, Data-driven Prognostics, Similarity-based Prognostics, Filter Clogging Modelling, Fatigue Crack Growth Modelling.

Acknowledgements

I would like to express sincere gratitude to my supervisor Professor Fatih Camci, for all his help and guidance carrying out the work presented in this thesis. I would also like to extend my gratitude to my co-supervisor Professor Ian K. Jennions, providing specialist knowledge in fluid dynamics as well as the IVHM field. I am also grateful to Professor Andrew Starr for his valuable feedback who was the subject advisor to this project. I would also thank Professor Philip Irving for his collaboration in fatigue crack modelling studies.

I would like to acknowledge the full sponsorship and feedbacks for this project provided by the Cranfield University IVHM Centre and its industrial partners: The Boeing, Rolls-Royce, Meggitt, BAE Systems, Thales, Alstom, and the UK Ministry of Defence.

I would also like to thank to my colleagues in IVHM centre for all kinds of support and assistance. In particular, I would like to thank to Faisal Khan for technical discussions on all sorts of interesting engineering topics which indirectly helped on this thesis completion.

Finally, I would like to thank my parents, my brothers and sisters who have supported me at every stage.

Table of Contents

List of Figures

List of Tables

List of Abbreviations

AI	Artificial Intelligence
ANFIS	Adaptive Neuro-Fuzzy Inference System
ANN	Artificial Neural Networks
ARIMA	Auto-Regressive Integrated Moving-Average
ARMA	Auto-Regressive Moving-Average
ASTM	American Society for Testing and Materials
BBN	Bayesian Belief Networks
BPNN	Back Propagation Neural Networks
CBM	Condition-Based Modelling
CDF	Cumulative Density Function
CM	Condition Monitoring
C-MAPSS	Commercial Modular Aero-Propulsion System Simulation
CPNN	Confidence Prediction Neural Networks
CRA	Cumulative Relative Accuracy
DBN	Dynamic Bayesian Networks
DDM	Data-Driven Modelling
DP	Damage Prognosis
DWNN	Dynamic Wavelet Neural Networks
EKF	Extended Kalman Filter
EoL	End-of-Life
eUAV	Electric Unmanned Aerial Vehicle
FFNN	Feed Forward Neural Networks
FMECA	Failure Mode, Effects, and Criticality Analysis
GM	Gray Model
GPR	Gaussian Process Regression
HHMM	Hierarchical Hidden Markov Models
HMM	Hidden Markov Models
HPC	High Pressure Compressor
HSMM	Hidden Semi Markov Models
HUMS	Health and Usage Monitoring Systems
IGBT	Insulated Gate Bipolar Transistor
ISHM	Integrated System Health Management
IVHM	Integrated Vehicle Health Management
KBM	Knowledge-Based Modelling
KF	Kalman Filters
kNN	k-Nearest Neighbour
LSSVR	Least Squares Support Vector Regression

MAD	Mean Absolute Deviation
MAPE	Mean Absolute Percentage Error
MLE	Maximum-Likelihood Estimation
MLP	Multi-Layer Perceptron
MQE	Minimum Quantisation Error
MSE	Mean Squared Error
MTBF	Mean Time Between Failures
MTTR	Mean Time To Restore
NASA	National Aeronautics and Space Administration
NDE	Non-Destructive Evaluation
NI	National Instruments
NN	Neural Networks
nRMSE	Normalized RMSE
OSA-CBM	Open Systems Architecture for CBM
PbM	Physics-Based Modelling
PCA	Principle Component Analysis
PDF	Probability Density Function
PEEK	Poly-ether-ether-ketone
PF	Particle Filters
PH	Prognostic Horizon
PHM	Prognostics and Health Management
PoF	Physics of Failure
RA	Relative Accuracy
RBF	Radial Basis Function
RCM	Reliability Centred Maintenance
RMSE	Root Mean Squared Error
RNN	Recurrent Neural Networks
RUL	Remaining Useful Life
RVM	Relevance Vector Machine
SBP	Similarity Based Prognostics
SHM	Structural Health Monitoring
SIR	Sequential Importance Resampling
SOM	Self-Organising Maps
SPC	Statistical Process Control
SVM	Support Vector Machines
SVR	Support Vector Regression
TDNN	Time Delay Neural Networks
TLFN	Time Lagged Feed forward Networks
WAEP	Weight Application to Exponential Parameters
WAFT	Weight Application to Failure Times

Chapter 1

Introduction

This chapter briefly describes the basics of Integrated Vehicle Health Management (IVHM), a capability that enables a number of maintenance philosophies emphasizing prognostics, one of the most attractive research topics in this area. Also, the research problem found in the literature of engineering applications is discussed. Finally, the aims and objectives of this study are outlined and the PhD contribution is presented.

IVHM is a relatively new comprehensive technology, enabling many disciplines with an integrated framework. Maintenance strategies such as Condition Based Maintenance (CBM) or Reliability Centred Maintenance (RCM) are enabled using IVHM. Prognostics and diagnostics are integrated into the framework involving the monitoring of sensory information and predicting the future health level of the system, based on the monitored data. IVHM technology has potential applications in many fields such as aerospace, military systems, electronics, machinery, energy, and manufacturing. In IVHM, real-time sensory data obtained from the equipment is analysed continuously to detect and forecast the health states and to plan maintenance based on the forecasted health.

Prognostics is challenging and the fundamental technology within IVHM, where it requires identification of the current health level and extrapolating

it to a predefined failure threshold, concluded with the estimation of remaining useful life (RUL). The output of prognostics (i.e. RUL) is the duration between the current time and the time at which the forecasted health level reaches to a predefined threshold. Benefits of the prognostics motivate researchers and the industry to achieve reduced costs, increased safety and availability via better maintenance planning. In contrast with traditional maintenance philosophies, the IVHM approach enables modelling and tracking of individual equipment deterioration leading to a maintenance action only when it is necessary rather than performing scheduled maintenance. Note that, Prognostics and Health Management (PHM) is a relevant technology to IVHM where slight differences may appear which are reported in the in the literature. IVHM endeavours bringing a business model within the integrated scheme which is missing in the PHM. However, this research coverage involves both PHM and IVHM.

1.1 Research Problem Definition

Prognostics applications are relatively immature compared to diagnostics applications in the literature. Prognostic models can be categorised into two major categories. These are: 1) Physics-based models 2) Data-driven models.

Physics-based models, also called model-based prognostics, consist of mathematical abstractions of a degradation path derived from first principles. They can be incorporated with Bayesian tracking methods (e.g. Particle Filters, Kalman Filters) in order to learn state of health parameters in the model and to cope with the sources of uncertainty (e.g. measurement noise) in measurement processes.

Alternatively, data-driven approaches employ historical run-to-failure data to construct a statistical or artificial intelligence based model aiming to accommodate the degradation process and predict the remaining useful life of the system. Extracted patterns from the signals, or raw data reflecting

the degradation pattern is used for predicting the time-to-failure with confidence bounds.

Approaches in both categories have their own advantages and disadvantages in real life applications. Data-driven models suffer from the inability to learn in portions of the operations where no such data exists. On the other side, physics-based models require high expertise in application field and tend to be computationally prohibitive to apply at system level. Approaches under both data-driven and physics-based categories require many conditions to be met. Besides, there is no universally accepted best model to perform prognostics due to variations on limitations of data availability, application constraints, and system complexity (Liao and Kottig, 2014). Furthermore, in real life applications, unmet requirements make the model imperfect, resulting in ineffective RUL predictions. Hence, a hybrid prognostic approach is aimed at leveraging the advantages of both approaches and to compensate for their limitations. In this research, these limitations and their effects are analysed in five different categories. The fifth scenario imitates the real world prognostic application limitations and presents an integration solution to enhance the prognostic applicability.

1.2 Research Aims & Objectives

The PhD aim is to develop a hybrid prognostic approach that integrates physics-based and data-driven prognostics in order to enhance the prognostic results and to increase the applicability of prognostics in real applications.

The core objectives of this research are:

- To build an experimental rig with a high degree of accuracy, capable of taking data to validate prognostic algorithms.
- To develop physics-based models (PbM) for the degrading components of two engineering systems.

- To develop a data-driven model (DDM) for the degrading components of two engineering systems.
- To develop an integration scheme for combining physics based and data driven prognostic approaches.
- To investigate the applicability & performance of the hybrid model for the application scenarios mentioned.

The developed prognostic models (PbM, DDM, and Hybrid) have been implemented on two datasets: 1. Fatigue crack propagation dataset, 2. Filter clogging dataset. The former is a publicly available dataset, where a new experimental test rig has been designed and developed for the latter one. The experimental prognostic rig has been setup to produce a benchmark degradation dataset under different operational profiles. Variation under the same operation profile group is very low, whereas the spread in the complete dataset, consisting of all profiles, is significantly higher. On the other hand, the fatigue crack propagation dataset is a well-controlled set of crack growth experiments where the test specimens are exposed to a constant amplitude cyclic fatigue load. The dataset is publicly available and is known as the 'Virkler Dataset'.

For the filter clogging experiment, a physics-based prognostic model is derived from the porous flow pressure drop equations to model the differential pressure in the system and predict future pressure levels. For the Virkler fatigue crack growth dataset, a physics-based model employing the Paris and Erdogan crack propagation formulation is used. The hybrid integration scheme is applied on both case studies. Performance and applicability analysis is conducted by investigating the prognostic outputs obtained from the two application scenarios. The outcome of the analysis helps in decision making on the level of integration in hybrid model. In addition, the development of a continuous learning environment that enhances the level of integration within product life cycle is studied.

1.3 Contributions

The intellectual contributions of this research are outlined below:

1. The development of a novel prognostic integration scheme enabling hybrid prognostic modelling to enhance prediction accuracy and robustness.
2. The collection of a prognostic benchmark dataset consisting of fifty six run-to-failure samples for filter clogging failure, obtained under sixteen different operational profiles.
3. A physics-based prognostic model of the clogging filter phenomena.
4. Introducing a new parameter to improve a data-driven prognostic approach.
5. A literature survey and prognostic eligibility study on benchmark prognostic datasets available on the Internet.

1.4 List of Publications

A list of publications that contributes to the literature regarding this research is listed below:

Journal papers:

1. Eker, O.F., Camci, F., Jennions, I.K., "*An Integration Scheme for Hybrid Prognostics*", IEEE Transactions on Reliability, to be submitted, Mar. 2015.
2. Eker, O.F., Camci, F., Jennions, I.K., "*Physics-based Prognostic Modelling of Filter Clogging Phenomena*", Reliability Engineering and System Safety, submitted, Feb. 2015.

Conference Proceedings:

1. Eker, O.F., Skaf, Z., Camci, F., Jennions, I.K., "*State-based Prognostics with State Duration information of Cracks in Structures*",

Proceedings of the 3rd International Conference in Through-life Engineering Systems, Volume 22, pp. 122-126, Nov. 2014.

2. Eker, O.F., Camci, F., Jennions, I.K., "*A Similarity-Based Prognostics Approach for Remaining Useful Life Prediction*", Second European Conference of the Prognostics and Health Management Society, Nantes, France, 8-10 Jul. 2014.
3. Eker, O.F., Camci, F., Jennions, I.K., "*Physics-based Degradation Modelling for Filter Clogging*", 2nd European Conference of the Prognostics and Health Management Society, Nantes, France, 8-10 Jul. 2014.
4. Eker O. F., Camci F., Jennions I.K., "*Filter Clogging Data Collection for Prognostics*", Proceedings of the Annual Conference of the PHM Society 2013, New Orleans LA, USA, 14-17 Oct 2013.
5. Eker O. F., Camci F., Jennions I. K., "*Major Challenges in Prognostics: Study on Benchmarking Prognostics Datasets*", 1st European Conference of the Prognostics and Health Management Society, Dresden, Germany, 3-6 July 2012.

1.5 Thesis Layout

Organisation of the thesis is as follows:

Chapter 2 introduces the maintenance technologies enabled by IVHM. A detailed prognostic literature survey consisting of the prognostic categorizations and comparisons of each category is presented.

Chapter 3 discusses publicly available prognostic datasets and the properties of each set with a comparison of prognostic eligibility analysis. Also, the details of filter clogging prognostic rig test design, setup, and data collection is presented.

Chapter 4 describes in detail the integration scheme for hybrid prognostic modelling. Data-driven and physics-based modelling methodologies are also discussed in this section.

Chapter 5 brings forward the prognostic results obtained from each methodology for different application scenarios. Prognostic performance analysis and results are given and a discussion section added in order to refer to the capabilities and imperfections of the proposed model.

Chapter 6 summarises the research presented in this thesis and the future work on this research is laid out.

Chapter 2

Literature Review

The primary aim of this chapter is to provide a detailed literature review regarding IVHM and Prognostics along with a review of maintenance strategies. The prognostics approaches are categorised and discussed in detail. Furthermore, an analysis on strengths and weaknesses of the approaches has been conducted for each class. This chapter is concluded with the prognostic modelling challenge analysis conducted by the researcher.

2.1 Integrated Vehicle Health Management

The Integrated Vehicle Health Management (IVHM) concept as introduced by NASA is defined as:

"… the capability to efficiently perform checkout, testing, and monitoring of space transportation vehicles, subsystems, and components before, during, and after operation(s)…must support fault-tolerant response including system/subsystem reconfiguration to prevent catastrophic failure; and IVHM must support the planning and scheduling of post-operational maintenance." (NASA, Oct. 1992)

As mentioned in the above definition, IVHM acts an imperative role in aircraft operation management, and continues to offer the potential for a

paradigm shift in the way that aircraft organisations conduct business operations. Benedettini et al. (2009) postulate that IVHM is also potentially applicable to non-vehicle systems such as industrial process plants and power generation plants.

However, IVHM is not suitable for all manufactured assets due to the IVHM solution may be more expensive than the asset or service itself (Jennions, 2011). Therefore the technology is recommended to be applied for high-value complex products such as aircrafts, power generating equipment (e.g. wind turbines), or medical scanners.

Jennions (2011) documents the generic IVHM taxonomy consisting of following sub-categories:

- Maintenance service offerings (e.g. CBM, Total Care, RCM)
- Business (e.g. Business models, IVHM mapping)
- System design
- Architecture
- Analytics (e.g. Diagnostics, Prognostics)
- Technologies (e.g. Structural Health Management (SHM))

IVHM enables many disciplines with an integrated framework. CBM, Health and Usage Monitoring Systems (HUMS), and RCM are some of the maintenance strategies offered under IVHM where diagnostics and prognostics considered under the analytics category. IVHM builds the background of this thesis along with the relevant technology, PHM.

Following sections present the maintenance strategies including CBM and its sub-disciplines which provide a basis for this research.

2.2 Maintenance Strategies Overview

Maintenance philosophies are classified into two categories, these are:

1. Reactive Maintenance (unplanned)

- ❖ Corrective Maintenance

2. Proactive Maintenance (pre-planned)
    - ❖ Preventative Maintenance
    - ❖ Predictive Maintenance

From the historical perspective of maintenance, it can be stated that the most spectacular changes have occurred in the last sixty years following World War II (Brown and Sondalini, 2014). Until then, corrective maintenance was the only option for a maintainer where equipment used to be fixed or replaced on a breakdown basis. Nevertheless, corrective maintenance is still in use for simple components such as light bulbs or a basic pipeline which are less risky and where the failure consequences are not fatal.

From the 1950's, mechanisation and automation steps have risen due to the increasing intolerance of downtime and the significantly increasing cost of labour. Improved machinery was of lighter construction and ran at higher speeds provoking wear out more quickly which lead to the development of proactive maintenance.

Preventative maintenance is a sub-discipline of proactive maintenance in which the maintenance tasks are performed periodically. Periods are fixed intervals determined by using historical data (e.g. MTBF: Mean-Time-Between-Failures) and without any input from the individual equipment itself. Equipment is serviced on a routine schedule whether the service is actually needed or not. However, both reactive and blindly proactive (preventative maintenance) maintenance approaches have financial and safety implications associated with them. Routine inspection rounds and lubrication, bi-monthly bearing replacements, or maintenance inspections and overhauls on aircraft systems are some of the examples of preventative maintenance activities.

In the late 1970s, the effectiveness of conducting preventative maintenance started to be questioned. A common concern about 'over-maintaining' arose which led to the development of predictive maintenance. Adaptively determined scheduling of maintenance actions are the main features of predictive maintenance that distinguishes it from preventative maintenance. On the contrary, predictive maintenance is limited to those applications where the cost and consequences are critical and technically feasible (Pintelon and Parodi-Herz, 2008). Predictive maintenance is classified as two: Condition-based Maintenance (CBM) and Reliability-Centred Maintenance (RCM). RCM performs two tasks: first, analyse and categorise failure modes (e.g. FMEA) and second, assess the impact of maintenance schedules on system reliability (Kothamasu et al., 2006). RCM is based on manual inspections and basic data trending. CBM is discussed in further detail later in this chapter.

From the 1980's systems became progressively more complex in nature, bringing a more competitive marketplace and intolerance of increased downtimes. As an example from the 21st century, Murthy et al. (2002) reports that the daily loss of revenue due to downtime is £320,000 for Boeing 747 aircraft. Increasingly, risk analysis and environmental safety issues have become paramount. New concepts such as condition monitoring and expert systems have emerged. The Institute of Asset Management has been established in the UK in mid-90's which has been received significant attention from most organisations. In 2000's, terms such as prognostics, IVHM, and integrated system health monitoring (ISHM) have emerged and taken place in literature gradually thus far.

To conclude, in engineering practices today, maintenance activities are predominantly intuitive and based on the expert's or personnel's experience that are familiar with the equipment. However, experience is becoming difficult to accumulate due to an ageing engineering workforce and improved asset reliability. In addition, when dealing with complex

equipment, human decision making is not always sufficiently reliable due to the multitude of interrelating failure modes (Sikorska et al., 2011). Industrial and military areas have become increasingly concerned about system availability and reliability, due to the fact that current systems became more complex and expensive which lead to an increase in competition drive more than ever. Maximised system availability and reliability, minimised failure and downtime cost are of great importance for many industries. Today's sophisticated sensor technology enables engineers to track degradation processes and empowers for prognostic reasoning of equipment being monitored (Lee et al., 2006).

2.2.1 Condition-Based Maintenance

Condition-Based Maintenance (CBM) is a predictive maintenance strategy, whereby the maintenance tasks are performed when the need arises. The necessity concept is determined by assessing the health condition of the equipment continuously and extrapolating it to a predefined failure threshold (Camci and Chinnam, 2010; Eker et al., 2011).

The hierarchical steps of standardised Open Systems Architecture for Condition-Based Maintenance (OSA-CBM) are depicted in Figure 2.1. OSA-CBM is a layered approach, describing a standardised information delivery system in between its functional blocks. The process starts with acquisition of data and transmitting it to the higher level where the signal is processed (e.g. feature extraction). Third layer stands for diagnostics in which the comparisons are performed in order to detect and isolate different fault types (e.g. FMECA failure mode analysis). In the next level, the degradation level is identified to provide an input to prognostic block in order to be able to predict the remaining useful life of the asset. The top two layers are responsible for the intelligent decisions for a maintenance activity by means of the prognostic results and instrumentation, respectively.

An example of degradation in health level of an asset is shown in Figure 2.2. The P-F interval is the time interval between potential failure which is identified by health indicators, and an eventual functional failure. With CBM, it's necessary that the P-F interval is long enough to enable corrective maintenance action to be taken (Jennions, 2011).

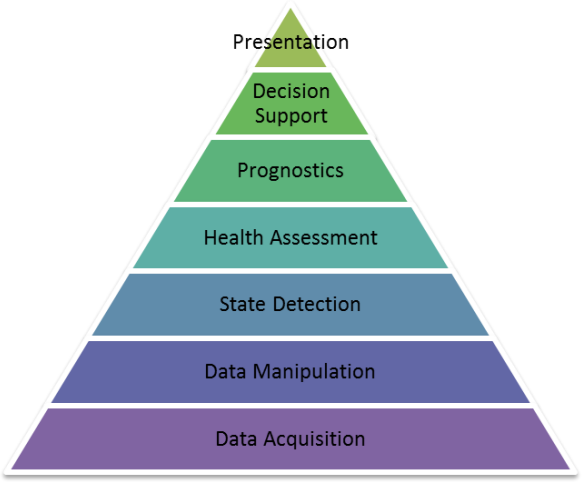

Figure 2.1 The OSA-CBM architecture

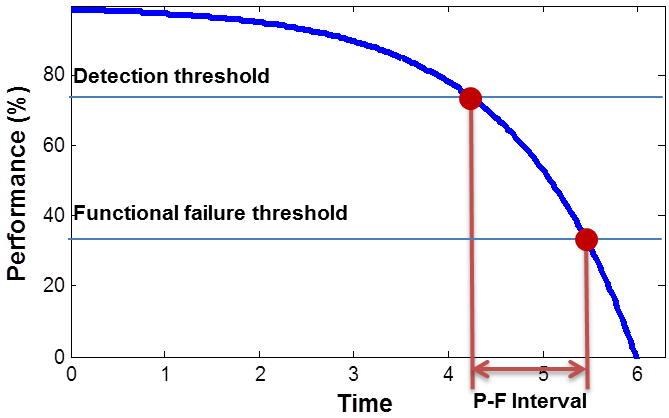

Figure 2.2. P-F curve of an equipment

Performing maintenance preparation when the system is up and running has a great effect on reducing the operation and support costs. In addition to the reduced down time, the inventory cost will be reduced as more time will be available for obtaining required parts. Moreover, the efficiency in logistics & supply chain will be increased by means of better preparation for

maintenance. Eventually, the life cycle cost of the equipment will be reduced, as they are used until the end of their lives.

2.2.1.1 Diagnostics and Prognostics in CBM

Diagnostics and prognostics are two of the major disciplines of CBM. In the literature, there is a minor disagreement that prognostics is related to and highly dependent upon diagnostics (Sikorska et al., 2011). Diagnostics involves detecting and reporting abnormalities in signal as well as identifying the fault type, and quantification of current health status of an asset, being the relatively mature area compared to prognostics. CBM with diagnostics outputs aims to stop and schedule a maintenance task for the system once an abnormality has been detected otherwise the system continues to operate. Once degradation is detected, unscheduled maintenance should be performed to prevent the failure consequences. It is not uncommon to spend more time in maintenance preparation than in performing the actual maintenance due to the lack of resources.

Ideally, in prognostics, maintenance preparation could be performed when the system is up and running, since the time-to-failure is known early enough. Thus, only the actual maintenance duration becomes the major contributor of the downtime which is way less than the fault diagnostic approach in CBM. As an example if prognostics can present a warning of a failure of an asset before 10 flight hours, re-test and installation steps can be pre-planned, yielding in saving of maintainer time and significant reduction in its variability (Hecht, 2006). Figure 2.3 illustrates the comparison of diagnostics and prognostics in CBM.

In general, incipient failures follow a progressive degradation path (Kwan et al., 2003). Detection of failure progression is more valuable compared to the detection of failure once it has reached to a severe point. Furthermore, it is a prerequisite for prognostics (Xiong et al., 2008). In other words, prognostic utilise the health severity or health status information transmitted from the

diagnostics base. Hecht (2006) states that prognostics for avionics is essential as the increasing of the number of complex systems comprising of electro-mechanical components in current and future aircrafts and a possible shortage of technicians capable of servicing them.

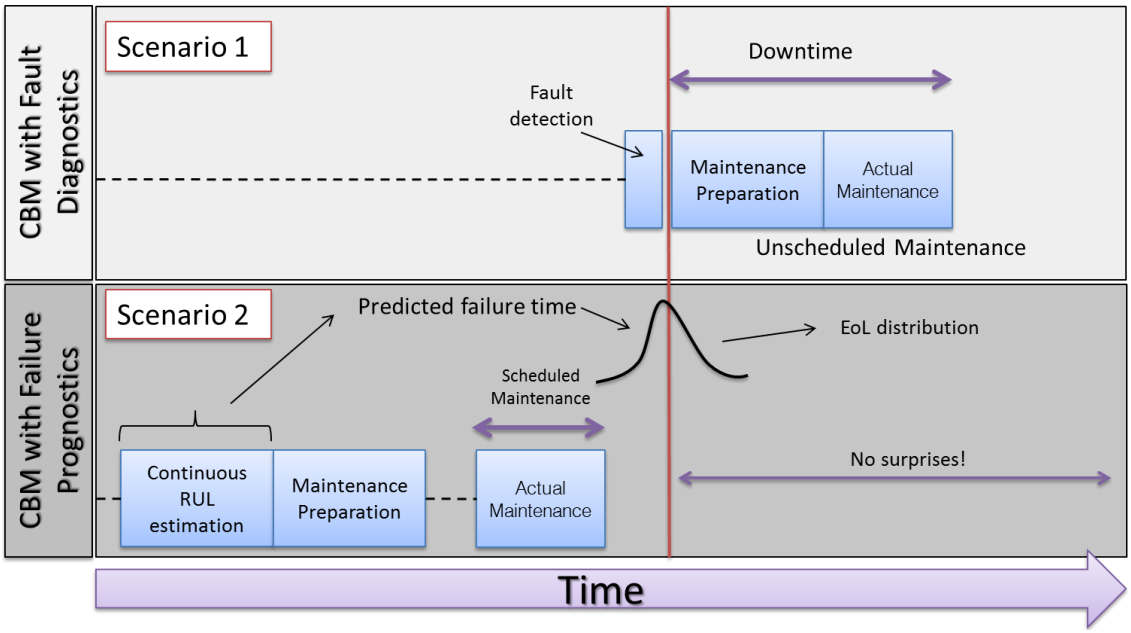

Figure 2.3. Fault Diagnostics vs. Failure Prognostics in CBM

Prognostics involve two phases as shown in Figure 2.4. The goal of the first phase of prognostics is to assess the current health status. Severity detection, health assessment, and degradation identification are the terms used for describing this phase in the literature. This phase could also be considered under diagnostics as mentioned before. Usually, Bayesian filtering and/or pattern recognition techniques such as classification or clustering are employed in the health assessment part. The second phase, which is so-called the true prognostics, aims to predict the failure time by forecasting the degradation trend leading to the estimation of remaining useful life (RUL). Time series analysis, extrapolation, propagation, trending, projection and tracking are the terms used for describing this phase.

Prognostics imply forecasting of the system's/component's future health level by propagating the current health level until a failure threshold.

Consequently, it enables an ability to provide an estimate of the remaining useful life (RUL). Prognostics is considered to be one of the most challenging and key enabling technologies among the CBM steps (Zhang et al., 2006b; Peng et al., 2010; Daigle and Goebel, 2010).

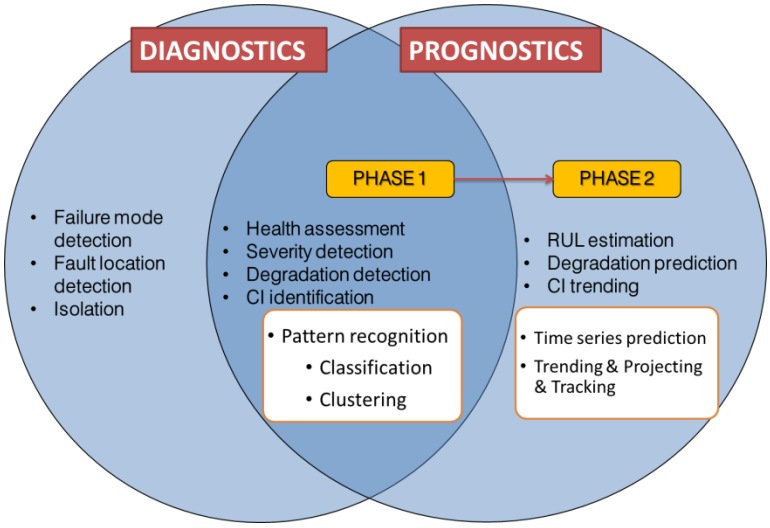

Figure 2.4. Prognostic and diagnostic phases

2.2.1.2 Benefits of Prognostics with CBM

CBM approach has significant advantages on reducing the support and operating costs and leading to a more effective planning and operational decision making. An unexpected one-day stoppage in machinery industry may cost up to £160,000 (Peng et al., 2010). Another example from the return on investment for companies is the investment of £9,500 on monitoring the condition of systems prevents £315,000 of maintenance costs per year (Kothamasu et al., 2006).

In another example, FAA's BRITE radar was maintained either with pre-arranged (proactive) or unscheduled (reactive) maintenance. Pre-arranged maintenance decisions were taken reasonably before the potential failure utilising prognostics by monitoring of degradation in the radar. Unscheduled maintenance took seventeen hours higher than pre-arranged maintenance in mean time to restore (MTTR) which was fifteen times

higher than that of the pre-arranged maintenance in comparison (Hecht, 2006). A detailed review of prognostic approaches is presented in the following section.

2.3 Review of Prognostics Approaches

Amongst those papers reviewed, there is little consensus of prognostic field as to what categorisation is the most appropriate for prognostic models. In general, prognostic models can be categorised into four classes, these are:

1. Data-driven models
2. Physics-based models
3. Knowledge-based models
4. Hybrid models

First three categories are illustrated in Figure 2.5, whereas a hybrid model implies fusion or combination of other methods is not shown in (Vachtsevanos et al., 2006) categorisation chart. This chart depicts the hierarchy of prognostic models based on the range of applicability, cost, and accuracy where knowledge-based models, being the most cost effective, find themselves a maximum applicability range in systems/components, albeit the accuracy of these models is less than the high accurate and costly physics-based models. Data-driven models fit in the middle of these models mentioned. Detailed discussion on comparison of the prognostic models will be presented in section 2.3.4.

Several literature surveys covering the prognostic models have been presented by (Liao and Kottig, 2014; Kothamasu et al., 2006; Lee et al., 2006; Zhang et al., 2006b; Peng et al., 2010; Vachtsevanos et al., 2006; Heng et al., 2009; Si et al., 2011; Luo et al., 2003b; Jardine et al., 2006). This literature review builds on the surveys referred in this section. In addition, current prognostic applications have emerged in the literature are further

discussed. In the following sections, a literature review of prognostic approaches within these categories is presented.

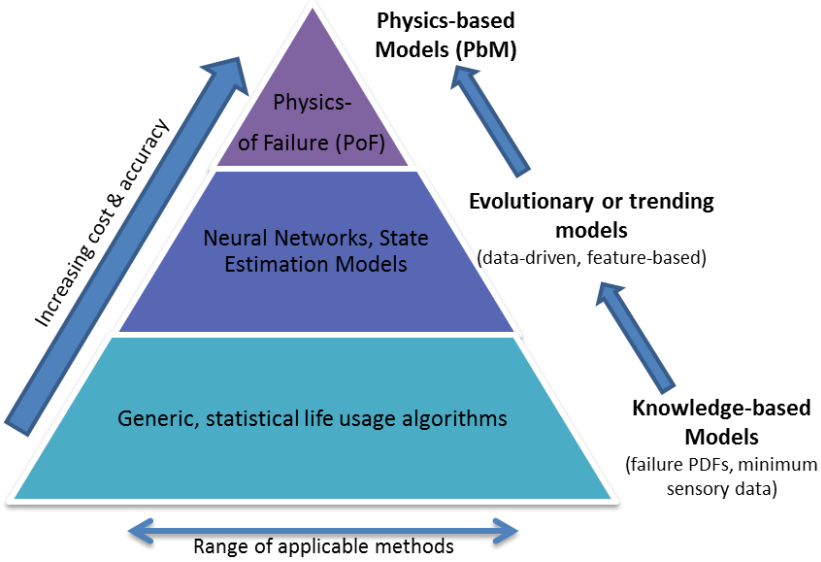

Figure 2.5. Prognostic models hierarchy (Vachtsevanos et al., 2006)

2.3.1 Data-Driven Models

Data-driven models (DDM) employ routinely collected condition monitoring data and/or historical event data instead of building a model based on system physics or human expertise. DDMs attempt to track the degradation of an asset using extrapolation or projection techniques (e.g. regression, exponential smoothing, and neural networks) or match similar patterns in the history of relevant samples to infer RUL (Liao and Kottig, 2014). They also rely on the past patterns of deterioration to forecast future degradation. Usually system or loading inputs are not involved in data driven prognostic modelling. Assumption for models in this category is that the future system inputs or operational profile remains constant or consistent with the past data. Since data-driven prognostics have no elaborate information (e.g. physical information) related to the asset or system, it is considered to be a black-box operation (Zhang et al., 2009). Data-driven models are divided into two categories: Statistical models and Artificial Intelligence-Based (i.e. machine learning) models.

2.3.1.1 Statistical Models

Statistical approaches construct models by fitting a probabilistic model to the data without depending on any engineering or physical principle. These approaches rely on statistical models and observed data to support the forecasting of the RUL of equipment. A comprehensive study on statistical data-driven models for remaining useful life estimation was conducted by Si et al. (2011). They divided statistical models into two categories based on the nature of condition monitoring (CM) data type used.

Typically, CM data can be divided into two categories: direct CM data, and indirect CM data. Direct CM data indicates the health level of system directly (e.g. crack size, wear level) whereas indirect CM reflects the underlying system health partially or indirectly (e.g. sensor information, vibration, oil based monitoring). Wiener and Gamma processes, regression-based models, and Markovian-based models find place under the models based on direct CM data; whereas, Stochastic Filtering-Based Models, Covariate-Based Hazard Models, Hidden Markov Models (HMMs) and, Hidden Semi Markov Models (HSMMs) are under the indirect CM category.

Brownian Motion (or Wiener Processes) are a continuous state prognostics data driven models and their probability density function (PDF) is considered to be inverse Gaussian distribution. Wiener Processes use only the current health status instead of using past event data. Wang and Carr (2010) proposed an improved version of Brownian motion-based stochastic degradation model for remaining useful life prediction of monitored plants. They contributed to the literature in two ways: Firstly, drifting the parameters of Brownian motion model by using Kalman Filters. Secondly, they used failure distribution threshold instead of using a constant threshold.

Gamma process is known for its simplicity. It's a special version of Markovian-Based processes with continuous state representation (Si et al.,

2011). A Gamma process-based deterioration model on (Hudak et al., 1978) crack growth data was implemented by Lawless and Crowder (2004). They incorporated covariates and a random effect to characterise the different rates among the different individuals.

Bunks et al. (2000), Camci (2005), Baruah and Chinnam (2005) referred that the HMM based models could be applied in the field of prognostics in machining processes. Zhang et al. (2005) have investigated the use of Hidden Markov Models (HMMs) in bearing fault prognosis. They applied a combination of Principle Component Analysis (PCA) and HMM in order to obtain the degradation index of bearings, and they implemented Li et al.'s (2000) stochastic defect propagation model for predicting the RUL's of components.

Marjanovic et al. (2011) presented a combination of Auto-Regressive Moving-Average (ARMA) & hypothesis testing and HMMs on a steam separator subsystem of thermal plants. However, both techniques provide inaccurate RUL results. They accounted for the problem as the methods were not taking into consideration of system's current state. They supplied prognostics results with a literature review. Auto-Regressive Integrated Moving-Average (ARIMA) models are an extended version classic ARMA models, enabling to model non-stationary time series signals. Typical ARMA models found to be less reliable for long-term predictions (Liao and Kottig, 2014). Examples of ARIMA model in prognostic application is found in (Wei Wu et al., 2007; Saha et al., 2009)

Camci (2005) developed an integrated diagnostics and prognostics methodology that employ support vector machines (SVM) and HMMs. Camci and Chinnam (2010) compared the results of HMMs and Hierarchical Hidden Markov Models (HHMMs) on a CNC drilling machine degradation dataset, reporting that the proposed model, HHMM, outperform regular HMMs in the literature. Another application of HMMs

in prognostics can be found in (Medjaher et al., 2012) in which they present a Gaussian Hidden Markov Models represented by Dynamic Bayesian Networks (DBN) for bearings.

As an extension to SVMs, the Support Vector Regression (SVR) models are highly capable of addressing regression problems especially in cases where data is sparse (Khawaja, 2011). Applications of SVR on pattern recognition and prediction problems can be found in (Zhang et al., 2006a; Thissen et al., 2003; Mattera and Haykin, 1999).

Dong et al. (2006), Dong and He (2007b) Dong and He (2007a) proposed several Hidden Semi-Markov Model (HSMM) fault classification and prognostics applications on UH-60A Blackhawk main transmission planetary carriers in which HSMMs generate a segment of observations and estimate the durations from training data unlike HMMs which generate single observation for each state. Examples of discrete state-based approach for prognostic approaches can be found in (Eker et al., 2011; Eker and Camci, 2012; Guclu et al., 2010a).

Proportional Hazard Model and Proportional Intensity Model (PIM) are also useful approaches for RUL estimation in combination with a trending model for the fault propagation process. Cox (1972) introduced the proportional hazard model to estimate the influences of diverse covariates affecting the RUL of a system. RUL prediction for a Markov failure time process which involves a joint model of hazard model and Markov property for covariate evolution as a special case has been discussed by (Banjevic and Jardine, 2006). Another hazard rate algorithm was developed by (Li et al., 2007) to extract the repeated failure indications. A proportional hazard model for catastrophic failures and multiple degradation features of single equipment was introduced by (Liao et al., 2005).

The Statistical Process Control (SPC) has been applied by (Goode et al., 2000) where they employed SPC to separate the whole machine life into two

intervals: First, the installation–potential failure (I-P); second, potential failure-functional failure (P-F).

Sheppard and Kaufman (2005) proposed a prognostics approach using Dynamic Bayesian Network (DBN) to model the changes over time. Bayesian Belief Networks (BBN) is recommended by (Przytula and Choi, 2007) for prognostic purposes, since the estimation of RUL can be done within the framework of BBNs.

Lastly, similarity-based prognostic approaches are usually effective when large amounts of historical data are available where a similarity matrix in between the current and historical data contributes to the estimation of RUL. Examples of Similarity-based Models for prognostics can be found in (Wegerich, 2004; Zio and Di Maio, 2010; Wang et al., 2008; Cheng and Pecht, 2007; Cheng and Pecht, 2007; Liu et al., 2007). Note that, some of the similarity-based approaches are categorised under the knowledge-based prognostic approaches (Wang, 2010). Details of the similarity based modelling approach are discussed in Chapter 0.

2.3.1.2 Artificial Intelligence-Based Models

Artificial Intelligence (AI) based or machine learning models attempt to recognise complex patterns and make intelligent decisions based on the empirical data. Machine learning approaches are adaptable to the situations where problem solutions require knowledge that is difficult to specify however enough data or observations are available. Artificial Neural Networks (ANN), Self-Organising Maps (SOM), and decision trees are common examples of machine learning approaches to be used for supporting the detection and diagnostics as well as prediction processes.

ANNs are perhaps the most commonly used machine learning techniques for prognostics; consisting of input, hidden, and output layers that interact with each other with numerically weighted connections inspired by the

neural structure of the human brain. ANNs are as multi-input-multi-output nonlinear blackbox function approximators, categorised into two classes; these are, supervised and unsupervised learning. The supervised learning models employ input data (i.e. sensor information, condition monitoring data) and target data (i.e. direct health indicators, health state) in order to train the weights and learn the complex patterns. The unsupervised learning models adapt to find hidden structure in the unlabelled data. Clustering algorithms (e.g. k-means clustering, SOM) are examples of unsupervised learning algorithms. Eker et al. (2011) used k-means clustering algorithm along with Calinski-Harabasz clustering evaluation index for the health state identification of railway turnout mechanisms, whereas the RUL prediction part is carried out by means of a state-based prognostic algorithm they developed.

Back propagation (BP) neural networks is a type of ANN, was utilised with a grey model in (Dong et al., 2004) for predicting the machine health condition. Gebraeel and Lawley (2008) proposed a degradation model based on dynamic wavelet neural networks (DWNN) in which the condition monitoring data was employed to estimate the RUL of partially degraded assets. Another example of DWNN in prognostics can be found in (Vachtsevanos and Wang, 2001). Huang et al. (2007) applied quantisation error indicator method (i.e. a derivation of SOM network) to assess the ball bearing degradation process and predict the remaining life. Time Delay Neural Networks (TDNN) is used for forecasting of a railway turnout systems in (Yilboga et al., 2010). A multi-layer perceptron NN along with regression NN is employed in (Herzog et al., 2009) for estimation through two application scenario. Ak et al. (2013) integrated a genetic algorithm to train ANN for predicting wind power under high uncertainty conditions. Mahamad et al. (2010) used Feed-Forward Neural Networks (FFNN) to predict RUL for a bearing failure case study.

Recurrent Neural Networks (RNN) with feedback connections can be considered as a non-linear extended version of classical ARMA models (Wang et al., 2004). RNNs have an advantage over generalised FFNNs where the uncertainty presentation of predictions is more robust. Zemouri et al. (2003) used recurrent radial basis neural networks to dynamically detect breakdowns and predict time series of nonlinear system states of gas ovens. Other examples for Recurrent Neural Networks for predicting machine condition trend can be found in (Yam et al., 2001; Heimes, 2008; Zhigang Tian, 2009). In the next section, literature review of physics-based models is provided.

2.3.2 Physics-Based Models

Physics-based models (PbM), also called 'Model-based Prognostics or Model-based Approaches', typically involve describing the physics of the equipment and the failure mechanism. The author prefers to use the term 'physics-based models' rather than 'model-based prognostics' since the most data-driven approaches use models as well. This way of categorization gives a better ability to distinguish physics-based and data-driven models (Daigle, 2014).

In PbMs, mathematical models of failure are usually employed which is directly tied to health degradation. In order to provide knowledge rich prognostics output; PbMs are attempted to combine defect growth formulas, system specific mechanistic knowledge and condition monitoring data. These models assume that an accurate mathematical model for component degradation can be constructed from first principles. Residuals, the outcomes of consistency checks between sensor measurements and mathematical model outputs, are utilised as features of health condition in PbM approaches. Thresholds to detect the presence of faults are determined by using statistical techniques. In addition, model parameters are identified using empirical data obtained from specifically designed experiments (Liao

and Kottig, 2014). Physics-Based Models are implemented in three different ways (Sikorska et al., 2011); firstly, dynamic ordinary or partial differential equations that can be solved with approximation approaches (e.g. Lagrangian or Hamiltonian dynamics), secondly, state-space methods (i.e. no differential equations), thirdly, simulation methods.

Kacprzynski et al. (2002) employed a physical stochastic model on gears. They calibrated the parameters for physical stochastic prognostics & diagnostics using system level features extracted from test specimens. Byington et al. (2004b) developed a fault detection and prediction algorithm for flight actuators which applies parametric identification and physical modelling techniques. Cempel et al. (1997) and Qiu et al. (2002) applied physics-based approaches to prognostics which have involved deriving the explicit relationship between condition variables and the current lifetime and failure lifetime via mechanistic modelling. Both of them applied their model for energy processors and bearings by employing vibration sensor measurements respectively. A general method for tracking the progress of a hidden damage process was proposed by (Chelidze and Cusumano, 2004). The proposed model is applicable for a given situation where a slowly evolving damage process is connected to a fast, directly observable dynamic system. Kacprzynski et al. (2004) fused diagnostic information and physics of failure modelling and applied for helicopter gear prognostics. A hierarchical modelling approach proposed by (Lesieutre et al., 1997) for system simulation to determine remaining useful life.

A physics-of-failure approach reinforced with Kalman filters were used to track the dynamics of the frequency of accelerometer sensor signals in tensioned steel band by (Swanson, 2001). Phelps et al. (2001) used a Kalman Filter with an associated interacting multiple model to perform tracking of sensor-level test-failure probability vectors for prognostics. Assumptions for Kalman Filters are that the system exhibits a linear process and the noise in the system follows Gaussian distribution. Extended Kalman Filters and

Unscented Kalman Filters are some of the extensions to the traditional Kalman Filters in which the system is not bounded by the linear process. Hu et al. (2012) presented an Extended Kalman Filter approach for estimation of Lithium-ion battery life. Particle filters are a generic type of Bayesian tracking methods used with physics laws (i.e. in the form of differential equations) in which the model is not bounded by the assumption of linearity in the system and Gaussian noise. Instead of using deterministic probability distributions, significant numbers of particles are employed representing the health state of the system distribution. A number of examples are available in prognostic modelling literature for particle filters (Daigle and Goebel, 2010; Zio and Peloni, 2011; An et al., 2013). Detailed discussion of particle filters is given in section 4.2.1.

Crack growth modelling is a widely used physics-based approach. Paris & Erdogan Law (Paris and Erdogan, 1963) is being used in several physics-based prognostics applications. Li et al. (2000) and Li et al. (1999) correlated defect growth rate of rolling element bearings to the material constants (i.e. C and m) and to defect area size based on Paris & Erdogan's law. They tuned both their defect diagnostic and defect propagation model parameters by monitoring of the system signals. Luo et al. (2003b) described an integrated prognostic process based on model-based simulation data under nominal and degraded conditions. Forman law of linear elastic fracture mechanics was used by (Oppenheimer and Loparo, 2002) in order to model rotor shaft crack propagation. Orsagh et al. (2003) and Orsagh et al. (2004) employed a version of the Yu-Harris life equation for estimating the spall initiation. They used Kotzalas-Harris spall progression model to forecast the time to failure. Paris & Erdogan Law is also used in (Li and Choi, 2002; Li and Lee, 2005) to model gear crack growth. Most of the crack growth prediction models mentioned here are assumed that defect area size can be estimated using vibration data as the defect area size measurements are usually not available without interrupting the machine condition. A

comprehensive case study on modelling of fatigue crack propagation is provided in section 4.2.2.

Physics-based models are considered to be more accurate if an accurate mathematical model representing the degradation process is fitted in the model thoroughly (Liao and Kottig, 2014). And the requirement concept on the data is significantly less, compared to the data-driven models. However, PbMs are usually component or system specific models which mean usually they cannot be applied to other type of components or systems in which the physics of failure mechanism is different. Another disadvantage is that the PbMs are costly compared to other approaches whereas they are the most suitable approach for cost-justified applications where accuracy weighs most other factors (Heng et al., 2009).

2.3.3 Knowledge-Based Models

It is usually difficult to obtain an accurate mathematical model in real-world applications which limits the use of physics-based prognostic models. Due to the absence of a complex model, systems tend to be maintained with simpler models such as knowledge-based models (KbM). Knowledge or experience-based prognostic approaches are the simplest way of performing prognostics where the statistical historical failure information of systems is utilised for predicting the RUL (Vachtsevanos et al., 2006). The use of knowledge-based models is automated representation of how a human domain expert solves a problem (Liao and Kottig, 2014). Expert systems and fuzzy logic are two generic examples of these models.

Disadvantages of knowledge based systems can be listed as:

- Hard to obtain domain knowledge and extract rules
- Handling of new situations which are not stored in knowledge base is limited

- ❖ Computational difficulty increases dramatically as the number of rules increases (i.e. combinational explosion problem)
- ❖ No confidence limits are supplied

2.3.3.1 Expert Systems

Expert systems have been used since 1960s, and are considered as an artificial intelligence (AI) program that represent domain expert knowledge in solving a problem related to a particular domain. In expert systems, knowledge of domain experts is stored in the knowledge base where the extracted rules are applied into the failure situations by the maintainer. Knowledge-based rules are generated from collections of real experiments. Basic IF-THEN statement rules are often based on heuristic facts acquired by experts over a number of years (Sikorska et al., 2011). Outputs of expert systems are singular rather than a distribution of RUL.

Expert systems have traditionally been used in failure diagnostics cases and it has started to be implemented in prognostics applications as well. Lembessis et al. (1989) developed an online expert system called CASSANDRA, which was built to monitor the condition of industrial equipment with the intent of fault prognostics.

Biagetti and Sciubba (2004) developed an expert system called PROMISE (Prognostics and Intelligent Monitoring Expert System) which carries out both diagnostic and prognostic duties and provides solutions to system maintenance in plants. However no RUL information was provided with their proposed method.

Butler (1996) developed an expert system based framework called FDPM (Failure Detection and Predictive Maintenance) which consists of several expert-system-related databases and components. It was applied on a power distribution system component for predicting maintenance demands.

2.3.3.2 Fuzzy Logic

Similar to expert systems, fuzzy logic is a problem solving mechanism providing a robust mathematical framework to deal with non-statistical uncertainty and real world imprecision. A fuzzy system consists of a knowledge base; fuzzy rule, and the implementation algorithms for applying the logic. Fuzzy logic has a wide application area from simple small components to large workstations. Unlike expert systems, the fuzzy logic system has the ability to model system behaviours in continuum mathematics of fuzzy sets rather than with traditional discrete values. Fuzzy logic systems are usually incorporated with other methodologies such as neural networks (NN) or expert systems.

Choi et al. (1995) proposed a fuzzy expert system called 'Alarm Filtering' and Diagnostic System (AFDS) which provide clean alarm pictures and system wide failure information during abnormal states. And also providing alarm prognosis to notify the operator of process abnormalities.

Dmitry and Dmitry (2004) presented a fuzzy logic process in which the input data is mapped into fuzzy variables (i.e. fuzzification) using membership functions and de-mapping the fuzzy variables processed into numerically precise outputs (i.e. defuzzification). This methodology has been used widely in control applications such as in (Lee, 1990).

Feng et al. (1998) proposed a dynamic fuzzy system for real-time condition monitoring and incident prevention. However, the RUL was not calculated whereas the applicability of fuzzy logic into prognostics was demonstrated.

A comparison of a fuzzy logic model and neural networks is conducted by (Majidian and Saidi, 2007) for predicting the life of boiler tubes. Results show that neural network performed better where the applicability of NNs was favourable compared to the fuzzy logic model.

Unlike Majidian and Saidi's (2007) work, fuzzy logic is usually integrated in RUL calculation as an auxiliary method for the primary method to enhance prediction results. Fuzzy logic has an ability of dealing with incomplete or imprecise input information with the use of linguistic variables such as 'low', 'very low', which provides an intuitive way of reasoning and representing of failure health level. On the other hand; having no memory, limited capability of learning, and difficulties of determining good fuzzy rules and membership functions are some of the disadvantages of fuzzy logic.

2.3.4 Hybrid Models

It has been found to be difficult to predict the trends of all characteristic parameters by using an individual prognostic approach since the parameters are diversified in real world cases (Peng et al., 2010). The prognostic models under hybrid category combine multiple prognostic approaches in order to leverage the strengths of prognostic methods leading to enhanced prognostic results. Combination, fusion, integration, and hybrid terms are used for prognostic approaches in the literature for hybrid prognostic approaches. It is relatively a new area in prognostics and offers a promising concept for prognostics.

Hybrid prognostic approaches consist of several advantages, some of these are:

- Imperfections of individual approaches will be compensated; furthermore, merits of them could be utilised;
- Prediction accuracy; hence prognostics performance can be enhanced;
- Computation complexity may be reduced.

Summarisation of advantages and disadvantages of prognostic approaches are shown in Table 2-1. A highly detailed comparison of prognostic models from an industrial point of view can be found in (Sikorska et al., 2011).

Table 2-1. Comparison of the benefits of prognostic approaches

	Advantages	Disadvantages
Physics-Based Models	Accurate compared to other approaches (if a good representative of mathematical model is available) Higher precision Requires less data compared to other approaches Suitable for creation in design phase	Difficult to create a model especially for complex systems Sensitive to the design and material properties Sufficient component information and a good insight of the failure mechanism is required High cost of implementation Component or system specific
Data-Driven Models	Easy to conduct & simplicity in implementation Flexible and adaptable Suitable to all levels (component, system) More robust to changes in material or design compared to physics based Low cost	Need data representing the failure progression, which is often not possible to obtain Computational complexity may be high Difficulty in determining of the failure thresholds
Knowledge-Based Models	Simple and easy to understand No model is required Wide application area and lower cost Ability of dealing with incomplete, noisy or imprecise input information	Not always easy to obtain domain knowledge and extract rules Handling of new situations which are not stored in knowledge base is limited Computational difficulty increases dramatically as the number of rules increases Limited capability of learning No confidence limits are provided

Liao and Kottig (2014) have conducted an extensive research on hybrid prognostic model categorisation. According to their study, hybrid models are classified into five different categories as shown in Figure 2.6 where:

- ❖ Knowledge-Based Model + Data-Driven Model (H1)
- ❖ Knowledge-Based Model + Physics-Based Model (H2)
- ❖ Data-Driven Model + Data-Driven Model (H3)
- ❖ Data-Driven Model + Physics-Based Model (H4)
- ❖ Knowledge-Based Model + Data-Driven Model + Physics-Based Model (H5)

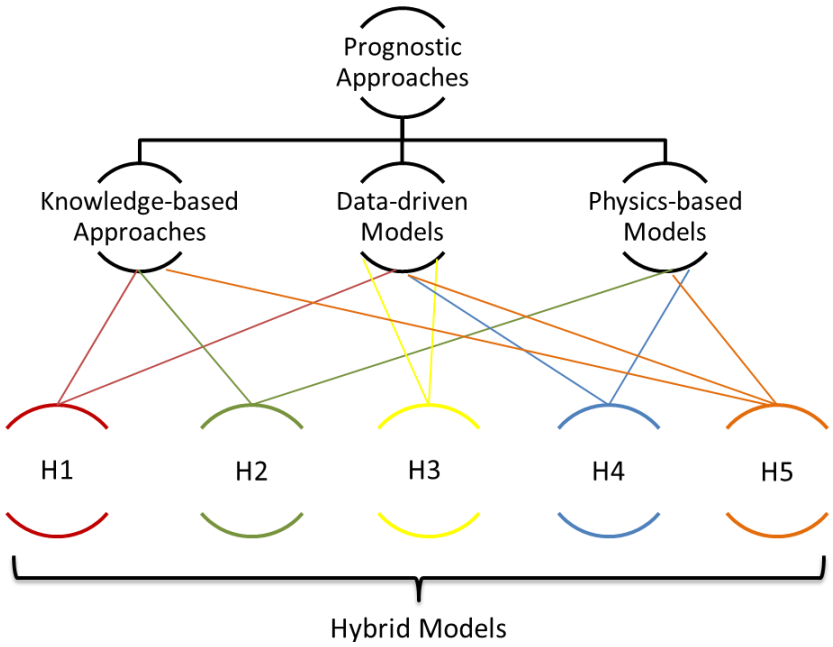

Figure 2.6. Hybrid prognostic model types (Liao and Kottig, 2014)

2.3.4.1 Knowledge-Based Model & Data-Driven Model

Hybrid prognostic models under this category represent incorporation of expert systems or fuzzy logic systems along with data-driven approaches. These approaches can add the flexibility of integrating domain knowledge into data-driven models for health state estimation where the RUL calculation is performed by a data-driven model.

Artificial Neural Networks (ANN) is usually incorporated with expert systems or fuzzy logic systems. Brotherton et al. (2000) applied a neurofuzzy (NN & FL) combination method on gas turbine engines. NN learning procedures are combined with fuzzy interference system linguistic

description in the proposed model yielding an adaptive, robust, and flexible algorithm. Dong et al. (2004) proposed a multi-parameter condition prediction model by combining back propagation NN and gray model (GM (1, 1)) .The proposed combination model outperformed single characteristic parameter prediction results. Garga et al. (2001) presented a hybrid reasoning methodology for an industrial gearbox, integrating domain knowledge along with a feed forward neural network. However, in their study, the exact method for RUL prediction was not defined nor the results quantified.

Neurofuzzy combination models have also been studied in (Zhang et al., 2009; Wang et al., 2004; Chinnam and Baruah, 2004; Satish and Sarma, 2005; Xue et al., 2005; Kothamasu and Huang, 2007).

2.3.4.2 Knowledge-Based Model & Physics-Based Model

In this category, knowledge-based approach output is often used as an auxiliary source to enhance physics-based model prognostic model outputs.

Byington et al. (2004b) and Byington et al. (2004a) documented a methodology comprising of a fuzzy logic process and a physical model. The physical model incorporates actuator failure progression physics-of failure model with Kalman filters. Swanson (2001) combined a fuzzy logic system with a physics-based model where a crack propagation analytic model was combined with Kalman filters. In their study, fuzzy logic is also used for adapting failure thresholds to the operational profiles.

2.3.4.3 Data-Driven Model & Data-Driven Model

Hybrid models under this category consist of multiple data-driven approaches where one of the models is used for health state identification and the other model utilised for degradation state extrapolation and RUL estimation.

The author is involved in implementing a number of hybrid prognostic models incorporating different data-driven models in a research group before PhD studies. A clustering algorithm (e.g. k-means clustering) was trained to map the sensory data into discrete health index values. Then the health state of a turnout system was estimated using a classification algorithm (e.g. k-Nearest Neighbours) which maps the sensory data into health indexes by taking inputs from the trained clustering method. Finally, the future health state predictions leading to RUL estimations were performed with many different data-driven algorithms including Time Delay Neural Networks (TDNN), and Auto Regressive Moving Average. The articles describing these prognostic models can be found in (Eker et al., 2011; Eker and Camci, 2012; Yilboga et al., 2010; Guclu et al., 2010b).

Huang et al. (2007) presented a hybrid methodology in which the health state of the system is estimated by Self-Organising Maps baseline supported with the Minimum Quantisation Error (MQE), and RUL prediction is performed by a trained Back Propagation Neural Network (BPNN). Liu et al. (2012) proposed a model which integrates Least Squares Support Vector Regression (LSSVR) with HMMs where prognostic results are obtained for bearing degradation scenario.

For further reading, other articles fall into this category can be found in (Heimes, 2008; Yan and Lee, 2007; Gebraeel et al., 2004; Peel, 2008; Du et al., 2012).

2.3.4.4 Data-Driven Model & Physics-Based Model

Hybrid prognostic algorithms under this category have been extensively studied in the literature.

Hansen et al. (1995) fused data-driven and physics-based information in order to enhance the capabilities of failure diagnostics and prognostics. Hazard rate comparison is provided in the paper. Hazard rate (ß) is

considered to be 1 for electronic equipment which means that the degradation of the component exhibit a constant increase whereas ß>1 for mechanical equipment that is degradation of the component increases exponentially by time. Authors of the paper developed a methodology for combination of diagnostics and prognostics which involves the fusion of model-based and sensor-based approaches. However, only concept of the methodology is given. Results or model implementation details are not provided in the publication.

A hybrid prognostics model which combines the information from off-line data-driven and physics-based, and on-line system identification-based predictive models was proposed by (Mohanty et al., 2008). The model was built for real-time remaining useful life estimation of metallic aircraft structural components.

Many researchers have used a data-driven model to infer the measurement model, and used a physical model to predict RUL. The measurement model stands for mapping the sensory data to underlying system state, which is not measured. These studies can be found in (Zhang et al., 2009; Orchard and Vachtsevanos, 2007; Kumar et al., 2008; Patil et al., 2009; Cheng and Pecht, 2009; Pecht and Jaai, 2010; Xing et al., 2011; Mohanty et al., 2007; Rosunally et al., 2009; Peng et al., 2012; Irving et al., 2012; Saha et al., 2007; Baraldi et al., 2012).

Pecht is involved in implementing their hybrid approach on several electronic equipment (Zhang et al., 2009; Cheng and Pecht, 2009; Pecht and Jaai, 2010; Mathew et al., 2008; Vichare and Pecht, 2006). In (Cheng and Pecht, 2009), a fusion prognostics model is implemented for electronic products. Both physics-based model and data-driven models are utilised in order to advance the RUL estimation. PbM was employed for identification and prioritising the failure model parameters, failure mechanisms and determining failure threshold. DDM was used for feature extraction, failure

anomaly detection, and trending the isolated parameters. Mathew et al. (2008) used canaries (canary devices) with their hybrid prognostics model. Canary devices are designed to fail faster than normal product so that they are used as indicator of failures. Zhang et al. (2009) presented a novel hybrid prognostics approach combining physics-based and data-driven models. In their model, DDM calibrates PbM in return PbM assists DDM by defining the failure criteria threshold.

Another way of combining physics-based and data-driven models is to use a data-driven model to replace a system model in a physics-based model. System model is a degradation process model often involves physics-of-failure models. This concept is suitable when an analytical degradation model is not available (Chen et al., 2011; Chen et al., 2012; Shetty et al., 2008).

Liu et al. (2012) and Orchard (2007) used data-driven models to predict future measurements while a physics-based model was used for predicting the RUL of the equipment. Hybrid approaches of this type aim to address the issue of data availability when updating a physical model in extrapolation phase where no measurements are available.

Goebel and Eklund (2007) and Goebel et al. (2006) run data-driven and physics-based models simultaneously for prediction and fused their results to improve prediction efficiency. Liao and Kottig (2014) proposed a hybrid prognostic methodology and stated that the framework can be used in any application where knowledge about the degradation process and historical data or training data are available.

2.3.4.5 Knowledge-Based Model & Data-Driven Model & Physics-Based Model

Hybrid models under this section are designed as combination of data-driven, physics-based, and data-driven models.

Examples of this combinations can be found in (Orsagh et al., 2003; Xu and Xu, 2011; Bartram and Mahadevan, 2012; Gola and Nystad, 2011).

Table 2-2 is a chronologically ordered list of all hybrid models discussed in this chapter. Hybrid models belong to each category is listed as well as the individual prognostic models forming the hybrid architecture. Next section presents an analysis on prognostic applicability and challenges in the modelling of prognostics.

Table 2-2. Hybrid prognostic model reference table

	Hybrid Model Architecture	Reference
KbM + DDM	Fuzzy Logic + NN	(Brotherton et al., 2000)
	Expert System + FFNN	(Garga et al., 2001)
	Fuzzy Logic + (DWNN & CPNN)	(Zhang et al., 2002)
	Fuzzy Logic + TLFN	(Chinnam and Baruah, 2004)
	Fuzzy Logic + NN	(Wang et al., 2004)
	Gray Model + NN	(Dong et al., 2004)
	Fuzzy Logic + NN	(Xue et al., 2005)
	Fuzzy Logic + ANN	(Satish and Sarma, 2005)
	Fuzzy Logic + NN	(Kothamasu and Huang, 2007)
KbM + PbM	Fuzzy Logic + (Crack Growth Model & KF)	(Swanson, 2001)
	Fuzzy Logic + (Actuator Failure Progression & KF)	(Byington et al., 2004a)
DDM + DDM	FFNN + (WAFT & WAEP)	(Gebraeel et al., 2004)
	(MQE & SOM) + BPNN	(Huang et al., 2007)
	ARMA + (Logistic Regression & MLE)	(Yan and Lee, 2007)
	MLP + RBF + KF	(Peel, 2008)
	RNN + EKF	(Heimes, 2008)
	LSSVR + HMM	(Liu et al., 2012)
	NN ensemble (NN + NN)	(Du et al., 2012)
	(k-means clustering & kNN) + (different discrete future health	(Eker et al., 2011; Eker and Camci, 2012; Yilboga et al.,

	state prediction models)	2010; Guclu et al., 2010b)
	Hybrid concept only	(Hansen et al., 1995)
	Empirical Spall Length Model + Spall propagation model	(Goebel and Eklund, 2007; Goebel et al., 2006)
	Non-linear state-space model + (Paris Law + PF)	(Orchard and Vachtsevanos, 2007)
	Non-linear state-space model + PF	(Orchard, 2007)
	GPR + FASTRAN-II	(Mohanty et al., 2008; Mohanty et al., 2007)
	Multivariate state-space model + MLE	(Shetty et al., 2008)
	Mixture of different data driven and physics-based models for electronic equipment prognostics	CALCE Group Works (Zhang et al., 2009; Kumar et al., 2008; Patil et al., 2009; Cheng and Pecht, 2009; Pecht and Jaai, 2010; Xing et al., 2011; Rosunally et al., 2009; Mathew et al., 2008; Vichare and Pecht, 2006)
DDM + PbM	RVM + (Battery Health Model & PF)	(Saha et al., 2007; Saha et al., 2009)
	GPR + (Die-attach degradation model & EKF)	(Celaya et al., 2011)
	ANFIS + PF	(Chen et al., 2011; Chen et al., 2012)
	Bayesian updating: Max. relative entropy + Small time scale model for crack growth	(Peng et al., 2012)
	Dataset statistical validation + Paris Law	(Irving et al., 2012)
	Bagged ensemble NNs + PF	(Baraldi et al., 2012)
	ANN + (Battery Model &PF)	(Liu et al., 2012)
	(SVR & SBP) + (Battery Health Model & PF)	(Liao and Kottig, 2014)
KbM + DDM + PbM	Expert Systems + Feature Based RUL + Bearing spall propagation model	(Orsagh et al., 2003)
	(Fuzzy Logic & NN) + ARMA + SVM	(Xu and Xu, 2011)
	Expert Systems + FFNN + Choke valve fluid dynamic model	(Gola and Nystad, 2011)

	Expert Systems + DBN + (Crack Growth Model & PF)	(Bartram and Mahadevan, 2012)

2.3.5 Challenges in Prognostic Modelling

Wang (2010) reports that the examples of successful prognostic applications in complex engineering systems are still scarce, even though several improvements have been made in prognostic modelling. Such complex systems exhibit immensely stochastic and non-linear degradation profiles which make it difficult to model accurately. Therefore, the prognostics is considered as the 'Achilles' heel' in CBM (Vachtsevanos and Valavanis, 2009).

Both, data-driven and physics-based models have different requirements to capture the degradation process and predict the RUL of a system. Challenges and requirements of these approaches are given in distinct sub-sections below.

2.3.5.1 Data-Driven Models

In summary, data-driven models aim to model the system behaviour employing regularly collected condition monitoring data instead of using comprehensive system physics or human expertise. Generally, data-driven approaches are separated into two categories. These are statistical and machine learning (i.e. AI-based) prognostics approaches. In statistical approaches, models are constructed by fitting a probabilistic model to the available data; whereas, AI-based approaches attempt to recognise complex patterns and make intelligent decisions based on empirical data (Heng et al., 2009).

Both statistical and machine learning methods employ the degradation patterns of sufficient samples representing equipment failure progression. This requirement is the major challenge in data-driven prognostics since it is often not possible to obtain samples of failure progressions.

Predominantly, industrial systems are not allowed to run until failure, is due to its consequences especially for critical systems. However, quality and quantity (sample size) of system monitoring data has a high influence on data-driven methods. Virkler et al. (1979) reports that sample size of a dataset should be at least 50 in order to conduct a meaningful analysis. Sample sizes of prognostic datasets found in the literature are ranging from 10 to 100 (Camci and Chinnam, 2010; Eker et al., 2011; Baruah and Chinnam, 2005; Huang et al., 2007; NASA Ames, 2012; Gebraeel et al., 2005). Another challenge for data-driven models is that the higher computational complexity of modelling due to the high number of statistical calculations. In the absence of prior knowledge about the failure mechanism, determining the failure threshold is considered to be another challenge.

Majority of the electro-mechanical failures occur slowly, exhibiting a non-linear degradation path (Gebraeel et al., 2009). Failure degradation of such systems may take months or even years. This challenge has been addressed in the literature in the following ways:

1. Accelerated aging: Equipment is run in a lab environment with extreme loads and/or increased speed to allow faster failure. Structural health monitoring (SHM) applications are a good example of this type of failure progression. Test specimens are subjected to fatigue cyclic loading experiments so that cracks are propagated faster than normal degradation process (Camci et al., 2012; Diamanti and Soutis, 2010; Papazian et al., 2009). Camci and Chinnam (2010) used imitations of real components which are made of lighter materials so that failure progresses faster than normal.

2. Unnatural failure progression: A predefined degradation formula is used to define the discrete failure states and duration to be spent in each state. Failure progression in a railway turnout has been modelled using exponential degradation (Eker et al., 2011).

Each solution has its own strengths and weaknesses with some level of failure degradation representation capability.

2.3.5.2 Physics-Based Models

Physics-based models employ a physical understanding underlying the system degradation mechanism for estimating the remaining useful life of equipment. Unlike data-driven models, the samples of failure degradation usually do not play a significant role in physics-based prognostics; however, interrelated physical rules within the system should be known in detail which is often found to be significantly difficult, if not almost impossible. The first part of the physics-based modelling is to obtain the residuals that represent the dispersion of sensed measurements from their expected values of healthy systems (Luo et al., 2003a). The second phase in physics-based prognostics requires mathematical modelling of failure degradation.

There exist two major challenges in physics based prognostics: 1) the lack of sufficient knowledge on physics of failure degradation; and 2) the inability to obtain the values of the parameters in the model formulations. Thus, sufficient component/system information and good understanding of failure mechanisms are essential and skilled personnel is also required in physics based models (Zhang et al., 2009). Environmental and operating conditions may be used as inputs and constitute added dimensions to be considered.

2.3.5.3 Knowledge-Based Models

Usually, systems are maintained with simpler models such as knowledge-based approaches, due to the absence of a complex model. Knowledge or experience-based prognostic approaches are the simplest way of performing prognostics where the statistical historical failure information of systems is utilised for predicting the RUL. The use of knowledge-based models is an automated representation of how a human domain expert solves a problem. Expert systems and fuzzy logic are two generic examples of these models.

Similar to the physics-based models, it is often difficult to obtain domain knowledge and extract rules based on degradation phenomena. Handling of new situations which are not stored in knowledge base limits the ability of RUL predictions with knowledge-based models.

Equivalently as data-driven models, knowledge-based models suffer from the increase in computational difficulty as the number of rules increases (i.e. combinatorial explosion problem).

2.3.5.4 Research Gap

As discussed in the previous sections, prognostics approaches have their own advantages and disadvantages. Hybrid approaches aim to integrate their individual advantages as well as avoiding their characteristic disadvantages.

Engineering prognostic datasets that can be efficiently employed in a data-driven modelling as well as in a physics-based modelling approach are remarkably sparse in the literature. Either lacking of sufficient data samples or missing of an efficient physical modelling is the case for most of the examples. Thus, development of a data driven and physics based model for the same system and their integration is a great challenge. The prognostic data gap is discussed thoroughly in the next chapter.

In addition, hybrid prognostic models found in the literature are application specific and combination of models is achieved by using one method for health state estimation and the other for the RUL prediction. However, a generic prognostic integration scheme where multiple models are integrated in the RUL prediction phase (i.e. so called 'true prognostics phase') is found to be missing in the literature. This research aims to contribute in filling this gap.

This PhD research contributes to the literature by serving an experimental benchmark dataset consisting of degradation signals, whose sample size is

sufficient enough for a data-driven prognostics method. Additionally, the degradation mechanism is not too complex, enabling to model the failure progression using a physics-based model thoroughly. In this research, data driven and physics based prognostics models have been developed for the experimental dataset and a publicly available dataset. In addition, a hybrid prognostic integration scheme to overcome the weaknesses of performing prognostics with a respective modelling technique (i.e. a data-driven model or a physics-based model) has been developed. This research proposes a generic prognostic integration scheme where multiple models are integrated in RUL prediction phase.

Chapter 3

Data Selection & Data Collection

This chapter introduces the case studies for prognostic implementation and the determination processes are also described in detail. Throughout this chapter, several publicly available datasets are analysed for their suitability in testing prognostic approaches. Their applicability of physics based and data-driven approach are discussed in detail. The applicability is analysed based on the available degradation data sample size for a data-driven approach. For the physics-based model eligibility analysis, availability of a mathematical degradation model and the knowledge of its parameters served the basis. The applicability of data-driven and physics-based prognostics methods have been presented in following subsections.

3.1 Case Study 1: Available Prognostic Datasets

NASA Ames prognostics data repository (NASA Ames, 2012) is a growing source covering several sets of prognostic data contributed by universities, companies, and agencies. Datasets in the repository consist of run-to-failure time series data, representing the case study under examination. There are seven sets of prognostics dataset available. In this section, analysis of five datasets from NASA data repository and a fatigue crack growth dataset for data-driven or physics-based modelling are presented.

3.1.1 Milling Dataset & Tool Wear Modelling

The dataset was collected by (Agogino and Goebel, 2007). Sixteen milling inserts were aged by running them at different operating profiles. Once the flank wear on the milling insert exceeded a standard threshold level, the tool was considered to have failed. Flank wear was observed by a microscope on the flank face of the cutting tool caused by the abrasion of hard constituents of work piece material which is commonly observed during the machining of steels or cast irons. The acoustic emission, vibration and current readings, which are considered as the indirect health indicators, are collected from the tools. There are eight different operating conditions leading to only two samples for each operating condition. Effective data-driven modelling is very difficult, if not impossible, using only two samples of failure degradation.

Several tool life or tool-wear rate models, mostly based on Taylor's formula (Yen et al., 2004), are available for physics based prognostics, displayed in Table 3-1.

Tool life is described as the duration in which a tool can be operated properly before it starts to fail. In physics-based prognostics, Taylor tool life (Eq. 1) and its extended versions in Equations. 2-4, are well known life models employed in machining applications. Each of which can be applied into tool degradation scenarios separately.

In machining applications, a predetermined flank wear upper level is used as a failure criterion. Tool life and rate of wear are sensitive to changes in cutting conditions. The relationship between tool life and machining parameters (e.g. cutting speed, feed, and depth of cut) are described by the Equations (1-5). Cutting speed is considered as the difference in speed between the cutting tool and the work piece. Feed rate is the velocity of a tool moving laterally across the work piece which is perpendicular to the cutting speed. The depth of cut is how deep a work piece is penetrated.

Takeyama and Murata's tool wear rate model, shown in Eq. (5), describes the relationship between rate of volume loss on the tool insert, cutting distance and diffusive wear per cycle. Even though the parameters specific to the tool material or work piece (e.g. cutting tool hardness) can be found in machinery's handbooks, operating or environmental condition parameters such as cutting temperature and sliding speed are not provided with the dataset.

Table 3-1. Tool life and wear models

Tool Life Models		Tool Wear Rate Models	
$VL^n = C$	(1)	$\frac{dW}{dt} = \frac{C}{H}\frac{F_f}{Vf}V_s + Bexp^{\frac{-E}{RT_f}}$	(5)
$V^x f^y d^z L = C$	(2)		
$V = \frac{C}{L^p f^q d^r (BHN/200)^t}$	(3)		
$TL^n = C$	(4)		

C, x, y, z, n, p, q, r, t = Constants
V = Cutting speed
L = Tool life
f = Feed rate
d = Depth of cut
BHN (Brinell Hardness Number) = Workpiece hardness
H = Cutting tool hardness
T = Cutting temperature
T_f = Cutting temperature in tool flank
E = Process activation energy
R = Universal gas constant
F_f = Normal cutting force
V_s = Sliding speed

For these reasons, the dataset is found to be inadequate for data-driven and physics-based prognostic models.

3.1.2 Bearing Dataset & Spall Progression Modelling

Three sets of tapered rolling element bearings, each of which consist of four bearings, have been run to failure under the same operating conditions (Lee

et al., 2007). Accumulated mass of debris was collected for each experiment. The amount of debris is linked to bearing health status (Dempsey et al., 2006). In contrast to the milling dataset, the direct health indicator (i.e. the amount of debris collected) was not supplied with the dataset. Vibration data was collected regularly as an indirect health indicator. After approximately a hundred million revolutions, the bearings were failed due to a crack or outer race failure (Qiu et al., 2006).

Yu-Harris (Y-H) and Kotzalas-Harris (K-H) models can be selected to be used in a physics-based prognostic approach for bearing failure scenarios. Both bearing spall initiation and spall progression models found in (Orsagh et al., 2003; Yu and Harris, 2001) are shown in

Table 3-2. Y-H bearing stress-based spall initiation formula is a function of dynamic capacity (Q_c) and the applied load (Q) as shown in Eq. 6. The dynamic capacity is also a function of bearing geometry and stress. Once initiated, a spall grows rapidly and a bearing has only 3% to 20% of its remaining useful life left (Kotzalas and Harris, 2000).

The K-H spall progression rate model is a function of spall progression region width (W_{sp}), and is described with regards to maximum stress(σ_{max}), average shearing stress(τ_{avg}), and spall length(S_p). Similarly, some parameters used in physics based modelling are not provided within the dataset (e.g.$\sigma_{max}, \tau_{avg}, \tau_{avg}$).

The emerging challenges from this dataset are as follows:

- Three run-to-failure sets of samples are considered insufficient for data-driven modelling when compared to dataset sample sizes found in literature.
- Lack of parameters to be used in physics-based modelling.

Table 3-2. Bearing fatigue life models

Spall initiation model

$$L_{10} = \left(\frac{Q_c}{Q}\right)^{\frac{x+y+z}{3}} \quad (6)$$

where:

$$Q_c = A_1 \Phi D^{\frac{2z-x-y-3}{z+x+y}} \quad (7)$$

$$\Phi = \left[\left(\frac{T}{T_1}\right)^z \frac{u(D\Sigma\rho)^{\frac{2z-x-y}{3}}}{(a^*)^{z-x}(b^*)^{z-y}} \frac{d}{D}\right]^{\frac{-3}{z+x+y}} \quad (8)$$

Spall progression model

$$\frac{dS_p}{dN} = C(W_{sp})^m \quad (9)$$

where:

$$W_{sp} = (\sigma_{max} + \tau_{avg})\sqrt{\pi S_p} \quad (10)$$

x, y, z = constants

A_1 = material property

T = a function of the contact surface dimensions

T_1 = value of T (when a/b = 1)

u = number of stress cycles per revolution

D = ball diameter

ρ = curvature

d = component diameter

a^* , b^* = function of contact ellipse dimensions

S_p = spall length

W_{sp} = spall progression region width

C and m = constants

σ_{max} = maximum stress

τ_{avg} = average shearing stress

3.1.3 Li-Ion Battery Dataset & Capacity Modelling

Data collections from electric unmanned aerial vehicle (eUAV) Li-ion batteries were conducted by (Saha and Goebel, 2007).The batteries were

charged and discharged at different ambient temperatures and different load currents. There are four samples under the same operating conditions and 36 samples are provided in total. Battery capacity fade is chosen as a failure indicator for these experiments. It was assumed that 30% of a battery capacity fade (e.g. a reduction from 2000 to 1400 mAh) was determined as the failure threshold. Voltage, current, and battery temperature measurements are provided with the dataset as indirect health indicators. Impedance and capacity measurements were supplied within the dataset as damage criteria which are direct health indicators.

Only four sets of batteries, under the same operating and environmental conditions, are not enough to apply data-driven prognostics in an effective way. Typically, battery capacity and end of life (EOL) modelling have been conducted for physics-based prognostics purposes. A remaining battery capacity model can be found in the literature (Rong and Pedram, 2006). All parameters, other than the constant coefficients which are determined from experimental testing by curve fitting, are available to be serviced within their model. Therefore, this dataset is thought to be appropriate for physics-based modelling.

3.1.4 Turbofan Engine Degradation Simulation Dataset

This dataset contains four sets of data each of which is a combination of two failure modes and two operating conditions. Each set has at least 200 engine degradation simulations carried out using C-MAPSS, which are divided into training and test subsets (Saxena and Goebel, 2008). Twenty one different sensor measurements as well as RUL values for test subsets are given. However, health indicators are not provided with the dataset.

Degradation in the HPC and Fan of the turbofan engine is simulated, whilst the dataset consists of multiple multivariate time series data. The simulations employ several operating conditions. The model that the dataset suppliers applied is exponential degradation shown in Eq. 11 where (d) is

initial degradation, (A) is a scaling factor, (B(t)) time varying exponent, and (th_w) is upper wear threshold. The model is a generalised equation of common damage propagation models (e.g. Arrhenius, Coffin-Manson, and Eyring models).

$$h(t) = 1 - d - Ae^{B(t)}/th_w \quad (11)$$

The dataset is eligible for data-driven approach, as sufficient data and RUL values are available within dataset. Either statistical or machine learning data-driven models can be applied to predict the RUL of turbofan engines. However, it is found to be not appropriate for physics-based modelling as the physics-based degradation model for this complex system would be daunting and significantly complex. In addition, since it was used in a data challenge competition, the actual health index values are not provided within the dataset.

3.1.5 IGBT Aging Dataset & Package Failure Modelling

The dataset consist of thermal overstress aging experiments of Insulated Gate Bipolar Transistors (IGBTs) (Celaya et al., 2009). IGBTs are power semiconductor devices used in switching applications such as traction motor control, and switched-mode power supplies (SMPS). Five IGBTs were aged with a squared signal at the gate and one was aged with DC waveforms. The experiments were terminated after a thermal runaway and/or latch-up failure was detected. Collector current, gate voltage, collector-emitter voltage, and package temperature measurements are given as indirect health indicators.

There are five run-to-failure samples under the same operational profiles. The dataset providers have also declared that they experienced several problems with aging systems (Sonnenfeld et al., 2008). Thus, it is difficult to claim that the dataset could be employed for data-driven prognostics effectively.

The Coffin-Manson model (Eq. 12) can be utilised within a physics-based model for thermal cycling applications (Cui, 2005). It is a function of temperature parameters and Arrhenius term ($G(T_{max})$). Arrhenius term is evaluated when the temperature level gets to the maximum temperature (T_{max}) in each cycle. The temperature parameters to be used in the model are given with the dataset. The dataset is therefore found to be eligible for employing a physics-based approach.

Table 3-3. Physics-based models for temperature cycling

Coffin-Manson Model	
$N = Af^{-a}\Delta T^{-b}G(T_{max})$	(12)
$G(T_{max}) = e^{(E_A/K)(1/T_{max})}$	(13)
N = number of cycles to fail	
f = cycling frequency	
A = scaling factor	
ΔT = temperature range during a cycle	
a = cycling frequency exponent	
b = temperature range exponent	
T_{max} = maximum temperature reached in cycle	
$G(T_{max})$ = Arrhenius term	
E_A = activation energy	
K = Boltzman's constant	

3.1.6 Virkler Dataset & Fatigue Crack Growth Modelling

In structural health monitoring discipline, the fatigue cracks are defined as one of the primary structural damage mechanisms caused by cyclic loadings. Cracks at the structure surface grow gradually. Once a fatigue crack on a structure has reached to a critical length determined by standards, the structure will suddenly fracture and it may cause the system to fail catastrophically. Therefore, prediction of fatigue life or fatigue crack growth in structures is necessary.

The Virkler fatigue crack growth dataset (Virkler et al., 1979) contains 68 run-to-failure specimens. Specimens used for experiments are centre

cracked sheets of 2024-T3 aluminium. Each specimen was initiated with a notch of nine millimetre crack length. Data comprising of crack length and corresponding cycle information was recorded at consistently increasing discrete crack levels (e.g. 9.1mm, 9.2mm). The loading cycles were terminated once the crack length reached at 49.8mm for each experiment. Each specimen signal has 164 crack length observation points. Figure 3.1 depicts the sample trajectories within the dataset. The crack length information is provided as a direct health indicator of the specimens. However, indirect sensory measurements such as vibration and acoustic emission are not provided.

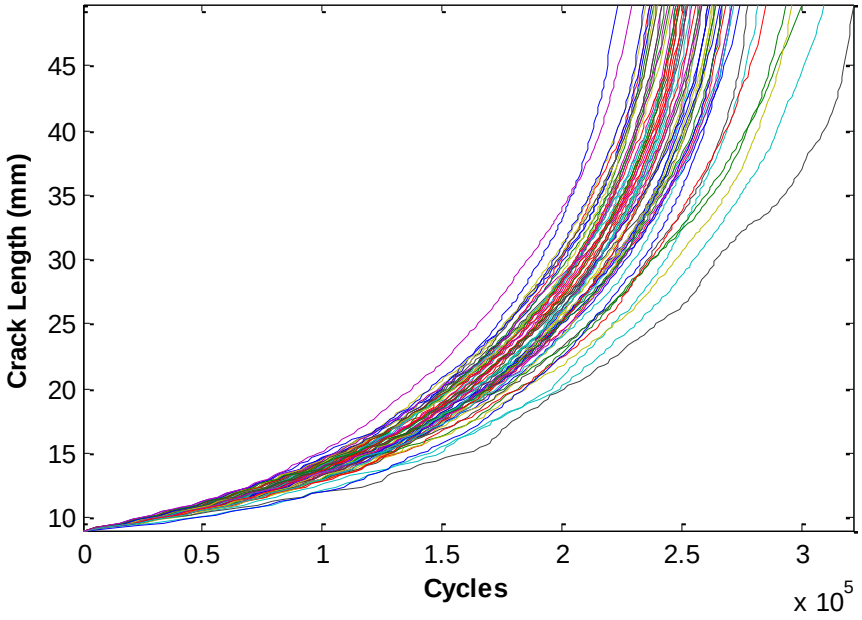

Figure 3.1. Virkler dataset visualisation

The Virkler dataset is found to be eligible for a data-driven prognostic application, as there are sufficient run-to-failure samples within the dataset. Sixty eight samples are sufficient for developing data-driven method for RUL estimation of specimens.

Physics-based modelling of fatigue crack propagation is a widely studied research area. Paris & Erdogan crack growth formulation as shown in Equations 14 and 15 describes the relationship in between crack growth

rate (da/dN); and previous crack length (a), loading specifications (Paris and Erdogan, 1963; Cross et al., 2006). The Paris & Erdogan crack growth rate (da/dN) equation consists of two material specific constants (i.e. 'C' and 'm') and the range of intensity factor (ΔK), where (Δσ) is the range of cyclic stress amplitude, (Y) is the geometric constant, and (a) is the crack length.

$$\frac{da}{dN} = C(\Delta K)^m \qquad (14)$$

Where:

$$\Delta K = \Delta\sigma Y\sqrt{\pi a} \qquad (15)$$

The equation can be employed in a physics-based prognostic implementation. Physics-based modelling of crack propagation is discussed in detail in section 4.2.2.

3.1.7 Dataset Comparison & Selection

The challenge and requirement analysis of six different dataset have been performed both considering data-driven and physics-based modelling demands. As a result, noticeably four out of six datasets can be modelled within a physics-based approach smoothly; whereas, only two of them are applicable for a data-driven prognostics modelling.

Table 3-4.Prognostic approach applicability table

Dataset	Data-Driven Modelling	Physics-Based Modelling
Milling Dataset	☒	☑
Bearing Dataset	☒	☒
Battery Dataset	☒	☑
Engine Dataset	☑	☒
IGBT Dataset	☒	☑
Virkler Dataset	☑	☑

A summary table of all datasets is shown in Table 3-4. In comparison to other datasets, the Virkler dataset was found to be the most applicable, considering the requirements of both data-driven and physics-based approaches. The fatigue crack growth scenario, specifically the Virkler Dataset is selected as the first case study for this research.

3.2 Case Study 2: Filter Clogging Data Collection

This section discusses thoroughly the filter clogging experimental scenario and the data collection for a hybrid prognostic task under the accelerated aging conditions.

Filtration phenomenon is interest of several engineering processes including automotive, chemical, reactor, and process engineering applications. Besides, several industrial applications such as food, petroleum, pharmaceuticals, metal production, and minerals embrace filtration process (Sparks, 2011).

The aim of the filtration systems is to keep the rest of the system running smoothly; moreover, they play a vital role in maintaining the process operating. Filtration and separation equipment plays a substantial portion (15%) in production of transport equipment manufacturing. Modern commercial vehicles and automobiles have numerous types of filters including fuel, lubricant, and intake air (Sutherland, 2010).

Sharing an important role with pumps, fuel filters filtrate dirt and other contaminants in the fuel system such as sulphates, polymers, paint chips, dust, and rust particulate which are released from a fuel tank due to moisture or other numerous types of dirt have been uplifted via supply tanker (Wilfong et al., 2010; Jones, 2008). Consequences like engine and pump performance degradation due to increased abrasion and inefficient burning in the engine are the main motivators for fuel filtration leading to a purified fuel. However, filtering the fuel associates with some complications

(e.g. clogging of filter) as well. System flow rate and engine performance declines once a fuel filter is clogged where it does not function well in its desired operation ranges. Jones (2008) reports that filter clogging indication due to fuel contamination may result in an aircraft having to return to the ground or divert for further fuel filter inspection or replacement. A fuel filter bypass indicator alarms the pilot and the crew to take an action when the pressure drop level reaches a predefined threshold (e.g. 11.5±1 PSI for GE CFM53-3 engine). A potential catastrophic failure such as engine shutdown may occur when both engines are exposed to unfiltered fuel due to the bypass operation.

In today's maintenance planning, fuel filters are replaced or cleansed on a regular basis. Jones (2008) reports that Boeing 777 fuel filter inspections are performed at every 2000 flight hours. Monitoring and implementation of prognostics on filtration system have the potential to avoid costs and increase safety.

3.2.1 Test Rig Design & Setup

An experimental rig to demonstrate filter clogging failure should consist of the following major components: Pump, liquid tanks, tank stirrer, pulsation dampener, filter, pressure and flow rate sensors, data acquisition system connected to a computer. Figure 3.2 illustrates the design of such experimental rig. Each component is discussed below.

Pump: There are different types of pumps enabling a liquid to flow through a complex system. Since the system will involve contaminants in the fluid, a peristaltic pump has been used as its mechanism is more tolerant to particles in the liquid. A Masterflex® SN-77921-70 (Drive: 07523-80, Two Heads: 77200-62, Tubing: L/S© 24) model peristaltic pump was installed in the system to maintain the flow of the prepared suspension. The pump is a positive displacement source, providing a flow rate ranging from 0.28 to 1700 ml/min (i.e. from 0.1 to 600 RPM). The practical part of peristaltic

pumps is that they confine the fluid to the tubing. In this way, the pump cannot contaminate the fluid and vice versa. Detailed design of the prognostic rig is illustrated in Figure 3.2. A photograph of the test system including all components is displayed in Figure 3.4.

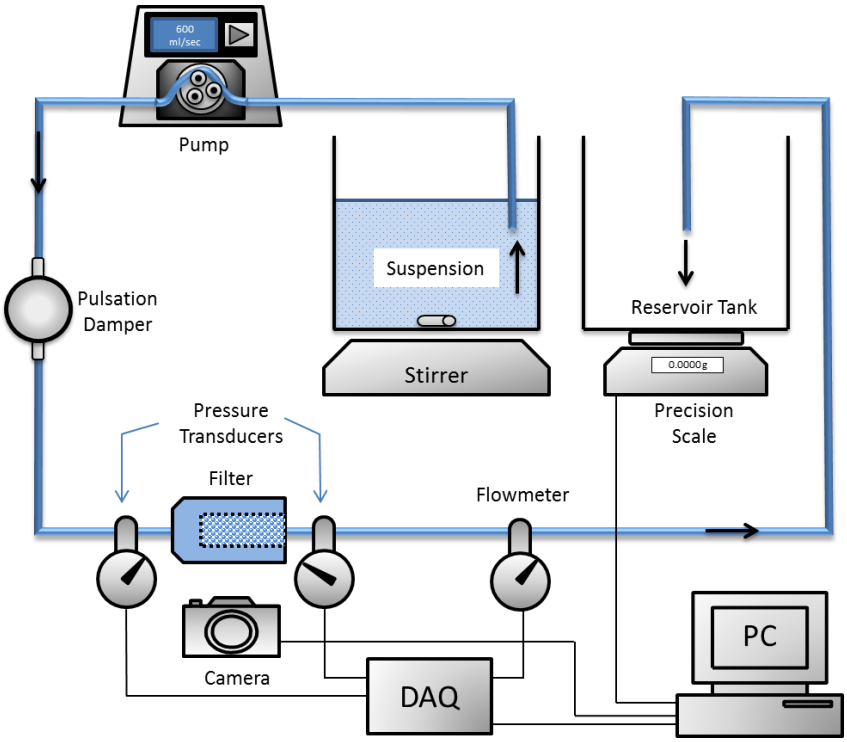

Figure 3.2. Filter clogging prognostic rig system design

Dampener: The aim of using rigid tubing is to prevent the system from the unwanted tubing expansion due to pressure build up which interrupts the actual pressure build up generated from filter clogging. A Masterflex® pulse dampener is installed on the downstream side of pump to eliminate the pulsation in flow, hence pressure drop across the filter. Majority of the system is furnished with a rigid polypropylene tubing whereas the pump side is covered with a flexible Tygon® LFL pump tubing.

Tank: One half-sphere-shaped main tank and two subsidiary tanks (i.e. reservoir tank and clean water tank) are installed in the system. The sphere shape tank bowl enables the stirrer work efficiently leading to homogeneously distributed slurry in the tank. The prepared suspension is

kept in the main tank and pumped through the filter and poured into the reservoir tank. The clean water tank is used to fill-up the system components (e.g. tubing and the filter chamber) with clean water prior to each test. A Kern® 10000-1N type high precision weighing scale (weighing range: 0.1 – 10,000 g.) is placed under the reservoir tank and connected to the PC with a serial cable to keep track of the amount of filtrated liquid continuously.

Particles: The suspension is composed of Polyetheretherketone (PEEK) particles and water. PEEK particles have a density (1.3g/cm^3) close to that of room temperature water and have significantly low water absorption level (0.1% / 24 hours, ASTM D570). Having a low water absorption level will prevent particles to expand their volume when they mix with water. Subsequently, closer density with water allows particles to suspend longer in water. Therefore, PEEK particles are selected to be used in the accelerated clogging of filter experiments. The particles have a large size distribution as seen in Figure 3.3. For this reason, narrowing the distribution by sieving is found to be necessary before conducting experiments.

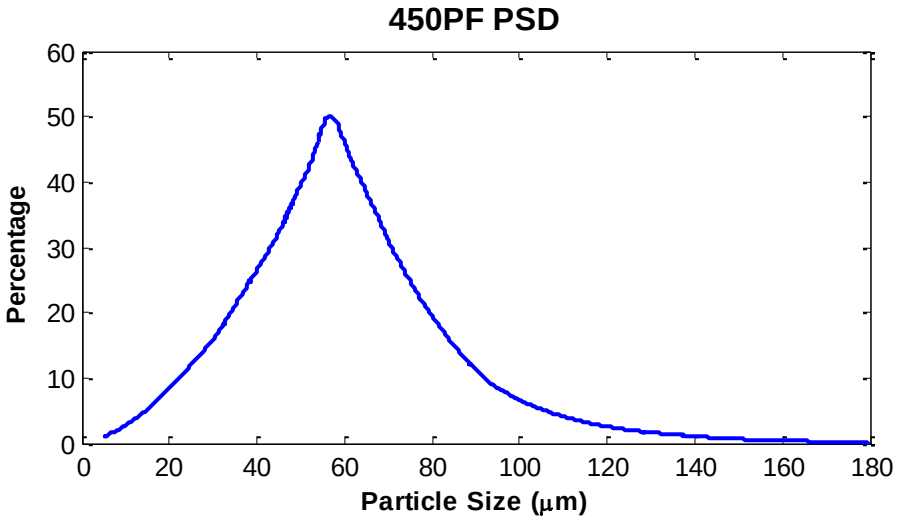

Figure 3.3. PEEK particle size distribution

Stirrer: An adjustable speed ceramic SC-1 type magnetic stirrer was installed in the system to ensure that the particles are distributed uniformly in the tank during the experiments. This is necessary as the particles, even though they are meant to be naturally buoyant, sink after a while leaving the water clean.

Pressure Sensors: Upstream and downstream Ashcroft® G2 pressure transducers (measurement range: 0 - 100 PSI) are installed in the system to capture the pressure drop (i.e. 'ΔP') across the filter, which is considered as the main indicator of clogging.

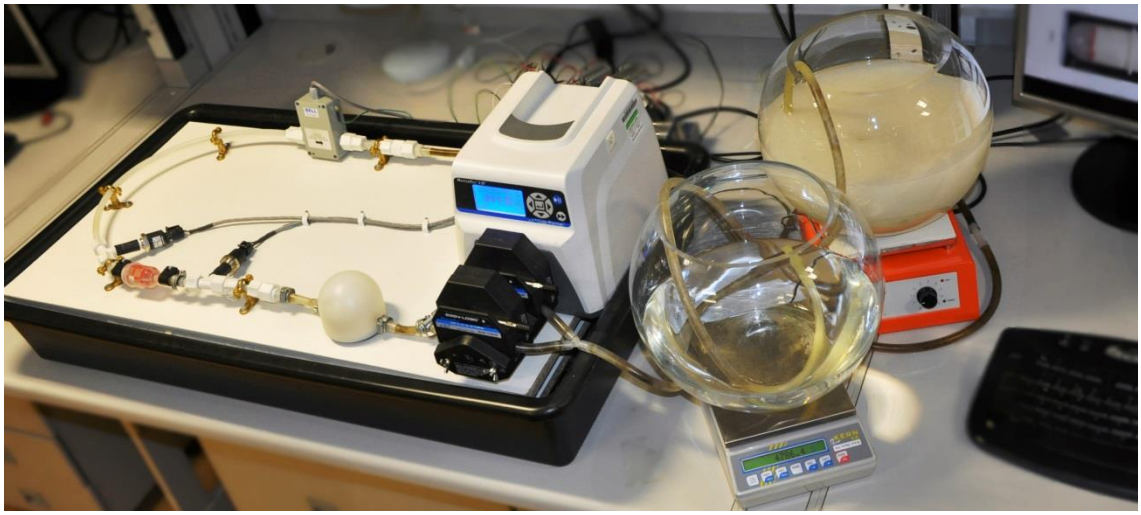

Figure 3.4. Filter clogging prognostic rig

Flow Rate Sensor: A GMAG100 series electromagnetic flow meter (measurement range: 3 – 25,000 millilitres per minute) is installed in the system to keep track of the flow rate in the system. The flow meter is also suitable for high pulsation flows. Magnetic flowmeters have no moving parts, which allow measuring the flow rate of slurry by means of the magneto-inductive principle. This type of flow meters has been selected for two reasons: 1) To enable measuring flow rate of water & PEEK suspension with no accuracy degradation; 2) They are reliable and very low unnecessary pressure loss across the flow meter. In addition, a pulse rate to current

converter is interfaced with the flow meter for converting frequency to proportional analogue 4-20mA current outputs.

Camera: A high quality macro lens camera is positioned on top the filter chamber, enabling to take macro pictures every two seconds. The mesh inside the filter; hence, the retained particles can clearly be captured and used in an image processing application for determining the ground truth clogging rate or an auxiliary source for modelling of the filter clogging phenomena. To be more precise, pressure and flow rate data can be compared or utilised with the features extracted from the macro picture data.

A box was designed to cover the filter container. The interior side of the box was masked with a white coloured material where a light source was projected inside the box to provide a constant uniform light so that the filter is isolated from varying environmental light. All components are placed on a grid style dripping tray in order to prevent potential problems due to a potential leakage.

The prognostic rig is designed so that no other component will deteriorate other than the filter. This means that, filter clogging is the only failure type to be targeted in the degradation modelling. This study is resulted in the publication of two conference proceedings (Eker et al., 2013; Eker et al., 2014).

3.2.2 Data Collection

This section provides the data collection details of the accelerated clogging experiments. Also, the 'finale prognostic data' is discussed thoroughly.

The PEEK particles are ordered in the powder form. As mentioned in the previous section, particle size distribution of the powder was in range between approximately 5 to 180 microns. In order to see the particle size effect on data collection, the particle size distribution is narrowed into

smaller distributions. Sieving of the particles is necessary to serve for this purpose. Wet sieve analysis is found to be helpful when working with fine polymer powders where particles exhibiting severe static charges (Advantech Mfg., 2013). Static electricity causes the particles to cling and agglomerate which makes the sieving process difficult, if not impossible. Therefore, particles are wet sieved, hence separated into different size ranges using American Society for Testing and Materials (ASTM) standard 45, 53, 63, and 75 micron pore sized sieves. For instance, the particles retained on top of the 45 micron sieve (i.e. 45-53 micron distribution) are used to obtain samples from the first four operational profiles shown in Table 3-5. On the other hand, the original sized (i.e. non-sieved) particles are used for the subsets under the last four operational profiles.

Table 3-5. Operational profiles

Profile No.	Particle Size (μm)	Solid Ratio (%)	Sample Size
1	45-53	0.4	4
2		0.425	4
3		0.45	4
4		0.475	4
5	53-63	0.4	4
6		0.425	4
7		0.45	4
8		0.475	4
9	63-75	0.4	4
10		0.425	4
11		0.45	4
12		0.475	4
13	Non-sieved	0.4	2
14		0.425	2
15		0.45	2
16		0.475	2

It is crucial to maintain the operational and environmental conditions consistent for the subset of data under the same operational profile. Hence, predefined operating conditions is kept as much as the same for sixteen different operational profiles each of which have four samples. Each operational profile is an outcome of a predefined combination of particle size distribution and solid ratio of the suspension. The entire dataset is

comprised of fifty six run-to-failure accelerated aging experiments. Operational profile details are shown in Table 3-5. Table 3-6 presents the amount of water and particles mixed for the first four operational profiles.

For instance, roughly 8kg of water is mixed with 32 grams of PEEK particles in order to obtain a suspension with 0.4% solid ratio. Jones (2008) states that airlines must ensure that the fuel supply hold less than 0.5 milligrams or contaminant particles per litre which corresponds to a maximum 0.00006% solid ratio is allowed in aviation fuel. This means that, in terms of the solid ratio values, the accelerated clogging experiments are approximately 6500 times faster compared to real life. However, there are many other parameters (e.g. flow rate, filtration rate, particle size, filter mesh size) to be considered in the mapping equation from accelerated times to real life scenarios.

Table 3-6. Profile details of 45-53 µm particle size distribution

	Profile No.			
	1	**2**	**3**	**4**
Water (g)	7968	7497	7079	6704
Particle (g)	32	32	32	32
Solid ratio	0.004 (0.40%)	0.00425 (0.43%)	0.0045 (0.45%)	0.00475 (0.48%)

125 micron pore sized Baldwin® BF7725 type of fuel filters is used for clogging experiments in the laboratory environment, shown in Figure 3.5. For this particular filter, both filter container and the mesh structure are cylindrical shape. The flow direction is from left to the right where suspension enters the filter chamber and passes through the mesh cylinder following the path out to right, leaving the particles on the surface of the filtration mesh. Captured particles form a cake on the mesh surface where the cake becomes the actual filtering element leading to a more effective

filtration. However, the flow becomes more restricted as more particles are captured by time hence the pressure builds up in the upstream side.

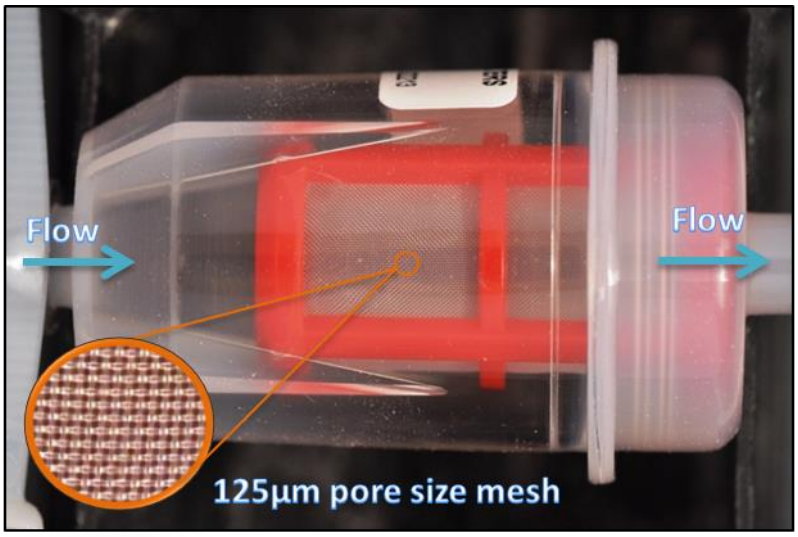

Figure 3.5. Baldwin fuel filter

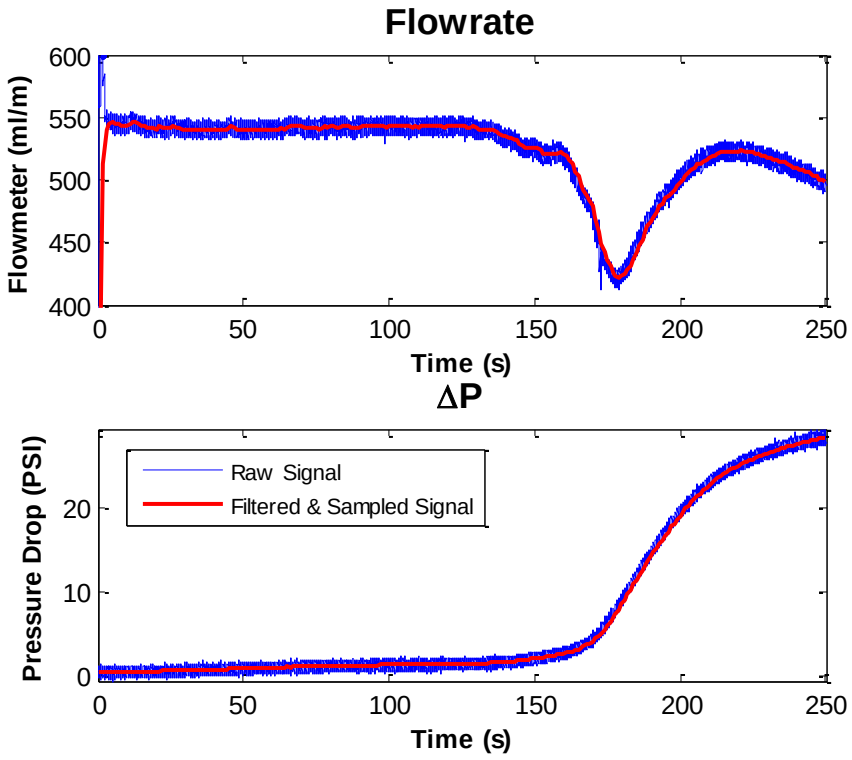

Figure 3.6. Pressure drop and flow rate measurements

Pressure and flow rate readings have been collected continuously which are the main indicators of clogging. Each clogging experiment has been run and

monitored until the filter has clogged where the pressure drop (i.e. differential pressure, $\Delta P = upstream\ pressure\ -downstream\ pressure$) has reached its peak and entered into a stable pressure region as shown Figure 3.6. In the figure, raw and low pass filtered signals are visualised against time. Fluctuations in the pressure measurements are generated due to the nature of peristaltic pump mechanism. Reflections of the pump RPM with regards to pressure pulsations are displayed in Figure 3.7. It has been found that the number of pulses in a second is proportional to the number of rollers in the pump mechanism. However this proportion rate changes when a pulsation damper and extra pump head added in the system.

Also in Figure 3.6, flow rate measurements remain relatively constant for considerable amount of the entire experiment times. This means that the pump provides a constant RPM; however, the flow becomes restricted gradually due to the clogging of filter. Moreover, the sudden drop curve regime reflects the pulse dampener effect where the dampener is being filled-up with the suspension due to the back pressure.

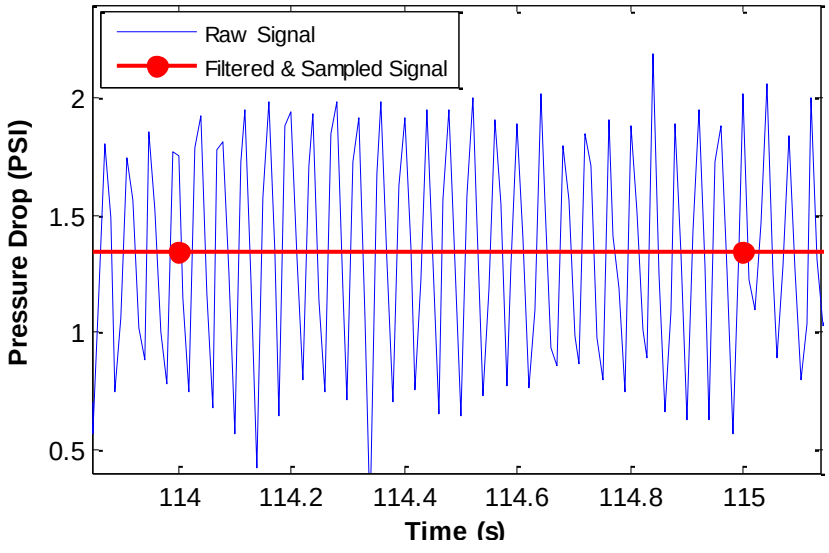

Figure 3.7. Magnified pressure plot of a sample

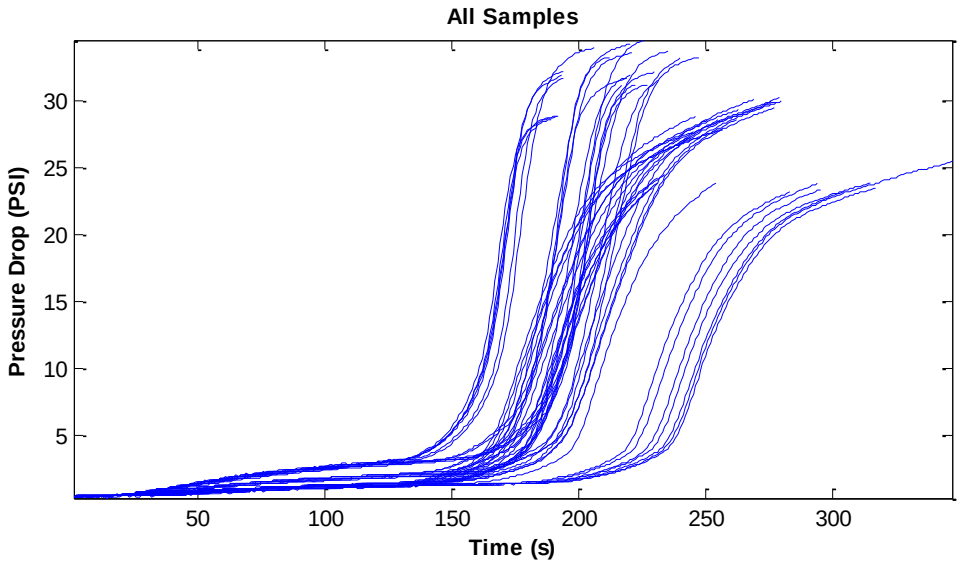

Figure 3.8. Filtered and sampled complete dataset

The data collection is conducted with an NI DAQ-9203 16 bit analogue current output module, which is connected to an NI cDAQ-9174 4-slot USB chassis. Sampling rate is adjusted as 100Hz within the LabVIEW environment which is eligible for capturing the pulses generated by the pump. For visualisation purposes, data is low pass filtered and down-sampled to 1Hz as displayed in Figure 3.8. Each trajectory in the figure represents differential pressure values for each distinct run-to-failure experiment. As seen from the figure, variation in the beginning is significantly lower than the critical clogging regime. However, the spread in the dataset increases as the experiment nears to the end of life. Variation in the experiments reflects the variation in sixteen different operational profiles.

Figure 3.9 associates the entire dataset and to different particle size distributions. Lightened colour scales represent different distribution of particles used in experiments, where the lighter colours correspond to lower solid ratios. As seen in the figure, the experiments conducted with lower solid ratios takes longer to time reach higher pressure drop levels comparatively to the higher solid ratio experiments. In the figure, red scale

trajectories represent the experiments under the first four operational profiles where particle size varies from 45 to 53 microns. This distribution is marked with a red band on top left hand side of the figure. Similarly, green and cyan coloured curves pertain to the 53-63 and 63-75 micron band of the distribution. Finally, the blue line trajectories obtained with non-sieved (i.e. original) particles whose distribution is shown with skewed normal distribution with a blue line.

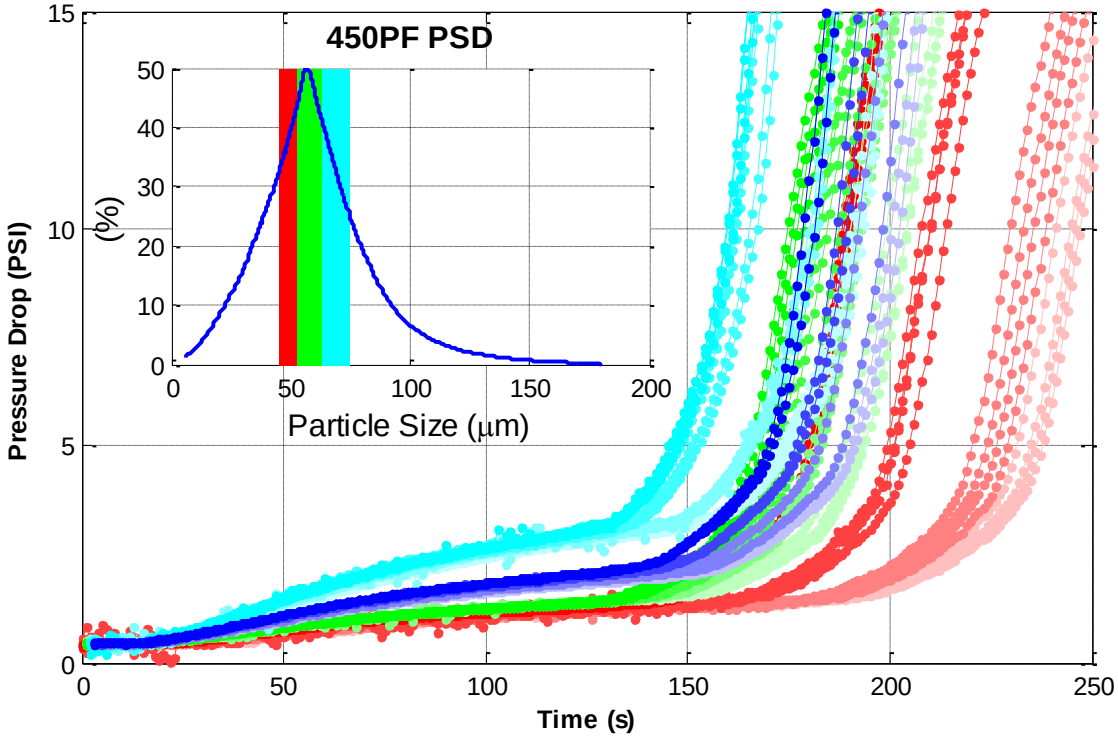

Figure 3.9. The dataset and sieved particle relation

Next section describes the challenges in the data collection process and presents the improvements that have been made for generating a reproducible prognostic benchmark dataset.

3.2.2.1 Challenges & Improvements

This section presents the challenges in data collection process and discusses the improvements that have been made on the system design, and the actual data collection process.

It is important to note that, all the improvements have been made in order to increase the controllability, repeatability, and to aid the modelling of the system. Initial design of the system was a circular continuous flow mechanism, where filtered liquid was poured into the same tank after passing through all components, which raises a significant change in the solid ratio in the tank. During the experiments, solid ratio was changing (i.e. ~30% decrease) due to the retainment of considerable amount of particles on the filter mesh. To capture this change in physics-based modelling, it was necessary to model the change in the solid ratio. However, modelling the solid ratio was not serving main purpose of the clogging modelling. Therefore, to cope with this problem, system design is changed by adding a reservoir tank. The initial pressure drop and flow rate data is visualised in Figure 3.10. This dataset comprises of thirteen run-to-failure filter specimens plugged under the same operational condition represented with different colours in the figure. However, the external and system parameters affecting clogging during the test were not controlled sufficiently. Therefore, end-of-life variation under the same conditions was unacceptably high (e.g. 25%). Besides, the chaos in the flow rate measurements is another indicator of non-controlled experiments.

After adding the reservoir tank in the system, a more controlled scheme was applied on the second attempt to data collection. Similar to the first attempt, the samples was obtained under a unique operational profile where solid ratio was fixed to 0.14%. Pressure drop and flow rate measurements are recorded for the six accelerated filter clogging experiments, displayed with different colours in Figure 3.11. In this figure, it can be observed that the lifetime variance in between the filters is reduced to 12%, which means that these experiments are relatively more repeatable compared to the first attempted set.

However, a higher variation in the flow rates was observed. This was due to poor handling of the pump and the flexible tubing passing through its head.

It was understood that several parameters can affect the lifetime of a clogging process and repeatability of the experiments. Henceforward, these parameters will be discussed in detail.

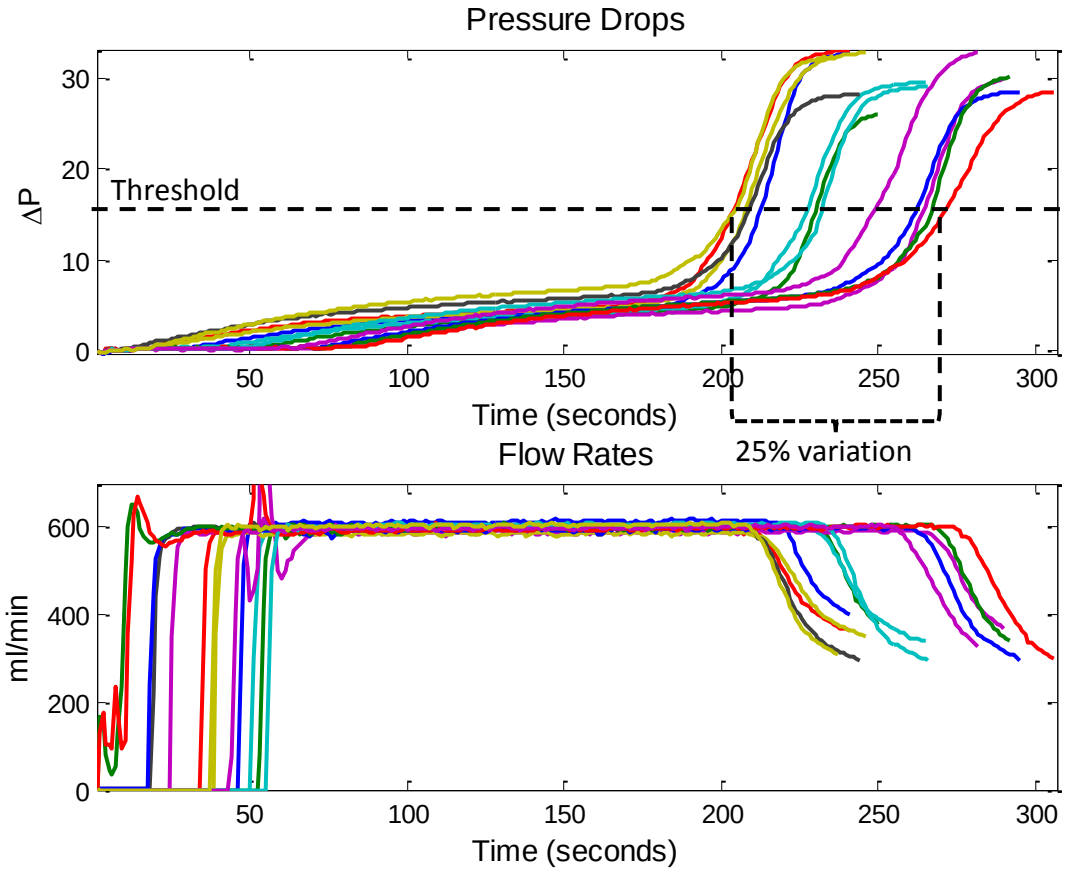

Figure 3.10. Initial data collection

Firstly, the solid ratio is the main factor which affects the duration of clogging process. Suspensions with high solid ratio values will plug the filter quicker assuming the flow rate is same. Flow rate is another parameter which is indirectly proportional to the clogging duration as well.

The shape and condition of the flexible tubing affects the flow rate, hence the duration of the clogging time. Therefore, before the start of each experiment, one needs to be sure that the tubing inside the pump heads are in the same condition in consideration of its geometry and heat. In this context, to cope with the uncertainty, pump RPM was adjusted precisely to provide the same initial flow rate before starting each experiment.

Another indicator, affecting the clogging process is the high pulses in the pressure measurements. Thus, we installed a pulsation dampener and stacked another pump head in the system to restrain the pulsations in the liquid flow. Essentially, stacking another head in the pump produces out-phase pulsations; hence, cancels the oscillations and doubles the flow rate. Note that, in this case, pump needs to be re-adjusted to half flow rate values than the desired flow rate. The dampening effects are visualised in Figure 3.12. This figure depicts the comparison of pressure pulsations scenarios with or without dampener and a stacked head.

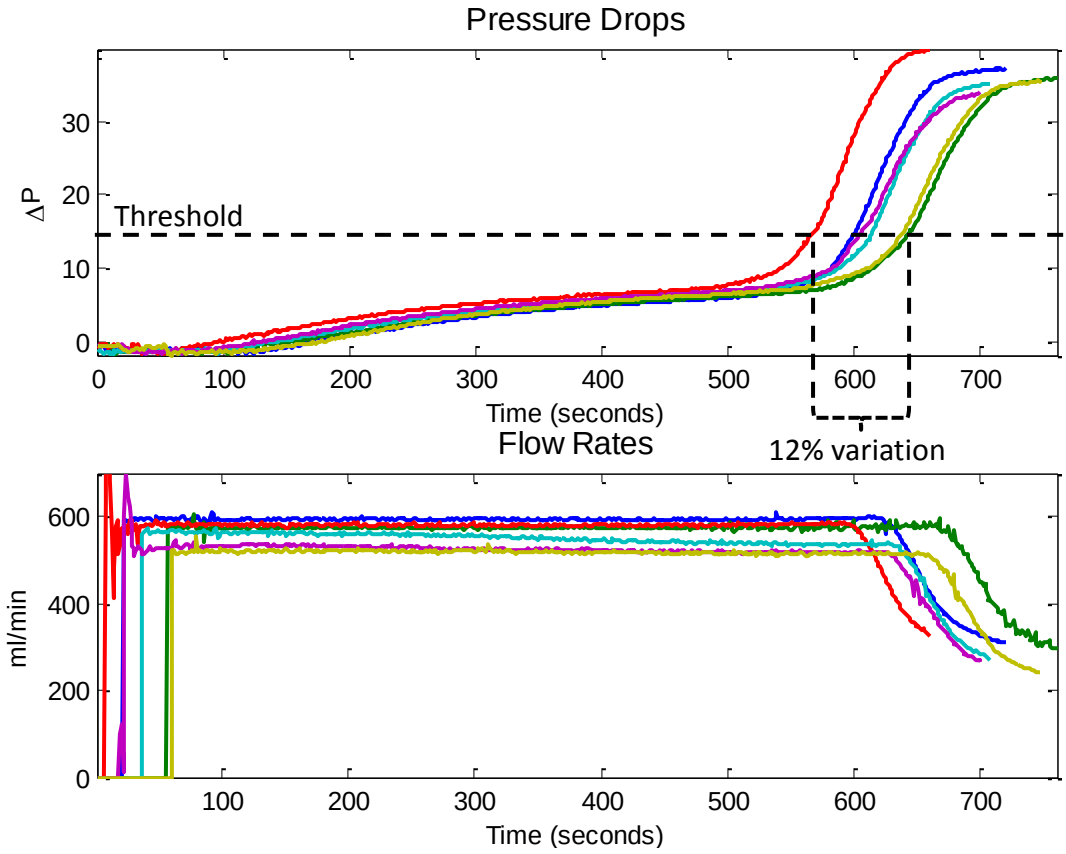

Figure 3.11. Second attempt for data collection

The top-left plot in the figure represents the pressure drop measurements where neither pulse dampener nor another pump head stacked in the system. Once we stacked another head in the pump or installed a pulsation dampener in the downstream side of the pump, a significant cancellation in the ΔP is distinguishable in the bottom-left and top right plots of the figure

respectively. The final experiments were conducted with two stacked heads and a pulsation dampener, shown in the bottom-right, where a compelling pulse cancellation is achievable.

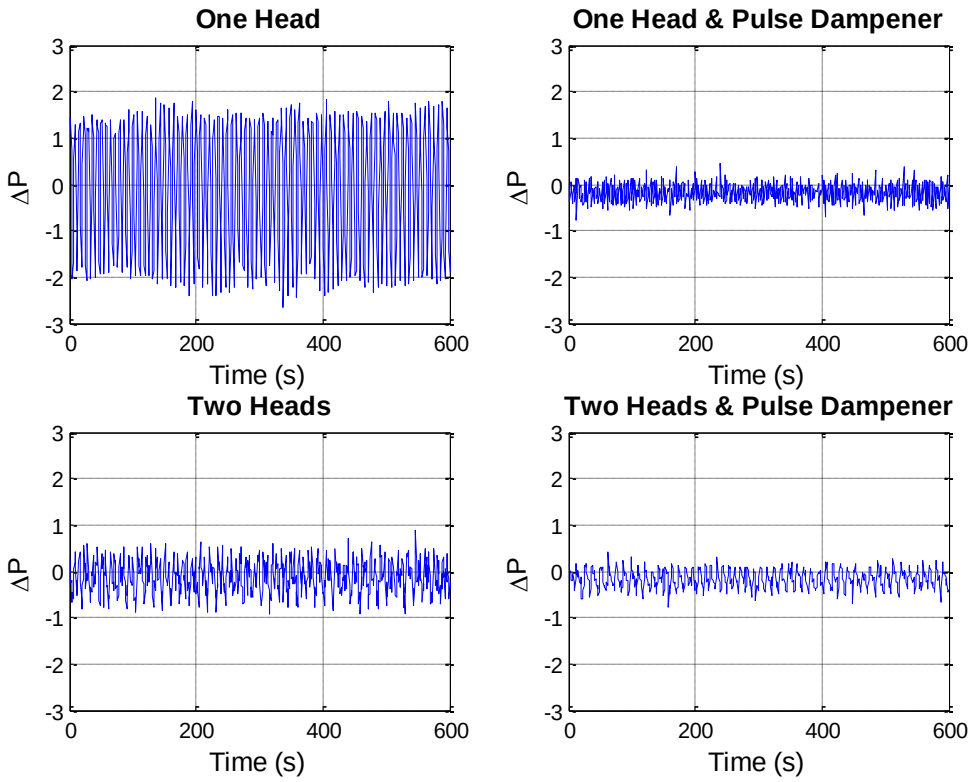

Figure 3.12. Pulsation dampening comparison

Head loss, which is the pressure drop in the tubing due to the friction in between tubing interior surface and the liquid, is another aspect influencing the system. In addition, sharp bends and fittings which reduce the tubing inside diameter will also contribute in the pressure loss. The clogging rig is designed to minimise this influence. It has also been experienced that head loss negligible compared to the pressure drop due to clogging, when working with lower flow rates and shorter tubing lengths. According to our pre-experiments, head loss increases exponentially when the flow rate is increased linearly. Therefore, we omit this phenomenon for filter clogging modelling.

Bubbles in the system, shown in Figure 3.13, are another factor which affects the repeatability of clogging experiments. Residual accumulation of bubbles in the filter container contributes to the stochasticity, which challenges the reproducibility of the data and also makes it difficult to model the clogging process. In addition, bubbles in the tubing have a potential effect in flow rate measurements as well. In order to eliminate these bubbles, the pump ran back and forth with clean water in opposite directions prior to each test until the entire system filled up with clean water.

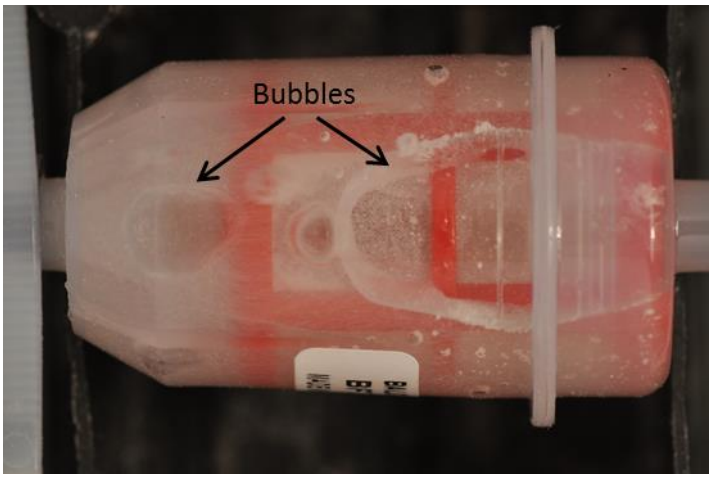

Figure 3.13. Accumulated bubbles inside the filter container

Another point to be taken into consideration is the steadiness of the test rig components which are needed to be properly fixed on to a bed to prevent from vibration effects. Besides, flexible tubing length is required to be fixed for reproducible experiment durations, pressure levels, and flow rate measurements. Therefore, tube brackets and holders are placed to tighten the components onto a fixed bed.

A final point to mention is that the PEEK particles naturally exhibit a hydrophobic character, or more evidently, mixing the particles in the water is burdensome. However; eventually, the particles were mixed sufficiently before starting the experiments by adding water on the particles slowly and constantly mixing them together.

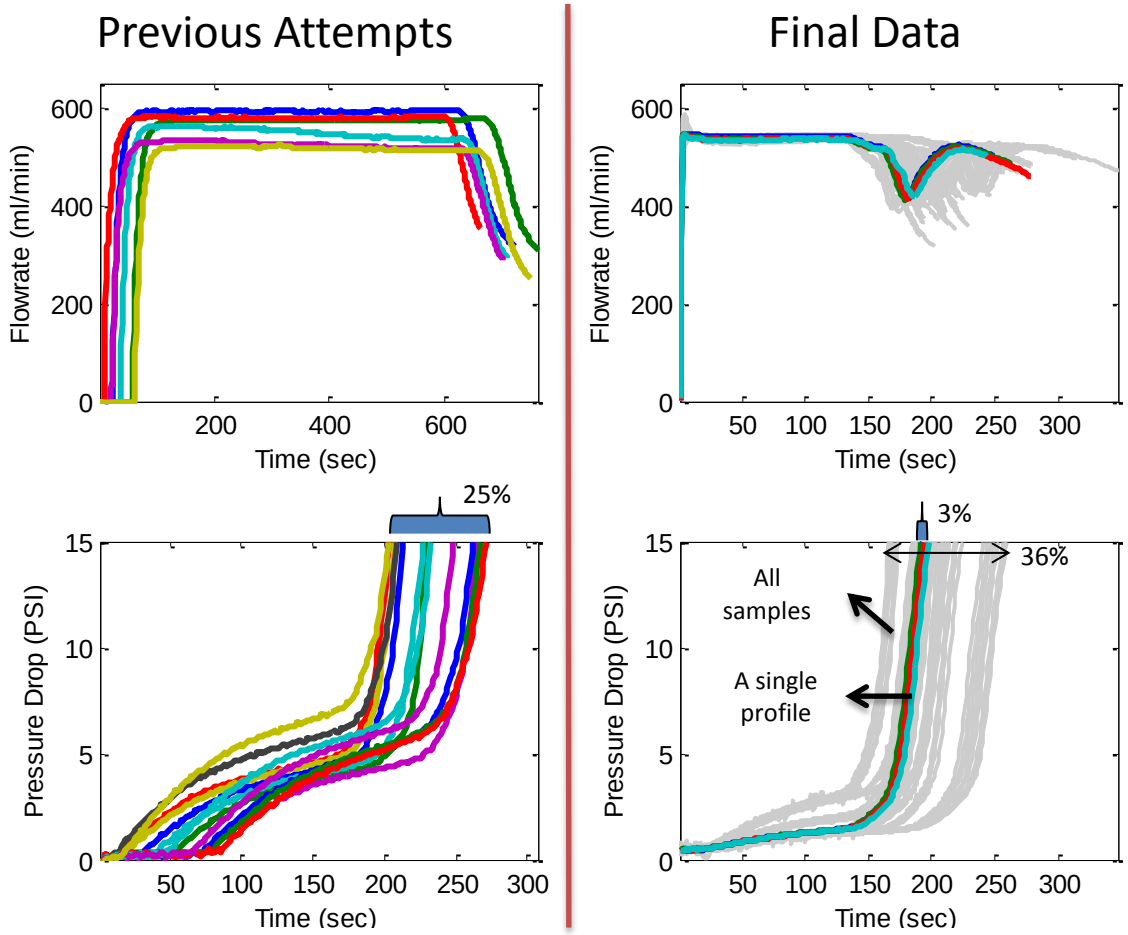

Figure 3.14. Improvements in pressure and flow rate values

The comparison of the previously collected and the final dataset is depicted in Figure 3.14. The previously attempted data represents the first and second data collection attempts where the life variation in the experiments stands 25%. In addition, a high variation in flow rates is also visible. Right column in the figure express the final data, where the entire dataset plotted with a grey colour. The different coloured trajectories in the right column exemplify the data from a single operational profile where the life spread is 3%. This shows the impact of the improvements in terms of reproducibility of the data. However, the complete dataset, comprising of sixteen operational profiles, have a variation of 36% which encompass higher variation of pressure drops compared to the previously attempted data

collections. Summary of the challenges and improvements are given in Table 3-7.

Table 3-7. Challenges & improvements

Challenge	Action	Goal
Picture quality & light reflection problem	Covering the filter area with a box	Image processing improvements
Keeping the operating condition same	Several enhancements done listed below	Reproducibility
Solid ratio variation	Putting another tank in the system	• Constant solid ratio • PbM enhancement
High variety in clogging EoL (22% - 30%)	Controlled test, pulsation dampening, fixing bubble problem, particle size narrowing	• Reproducibility • PbM improvement
High pulsations in pressure & flow rate measurements	Installing a pulsation dampener in the system	• Smoother data • Minimising the back and forth pressure effect
Accumulated bubbles in the filter container	Filling all the system with clean water prior to each test	• Avoiding the bubble effect on clogging of filter mesh • Reproducibility
High spread in the particle size distribution	Wet sieving the particles	• Narrower particle size distribution • PbM improvement

Chapter 4

Methodology

This chapter provides a list of prognostic methods to be practiced in the development of a hybrid approach for the selected two case studies. The details of each approach are given in each subsection. The approaches are discussed under two main categories: 1) Data-driven modelling, 2) Physics-based modelling.

4.1 Data-Driven Prognostic Modelling

Data-driven modelling details are discussed in the literature review chapter. In this section, the data-driven prognostic approach has been chosen for modelling of the two engineering case studies which are further elaborated.

4.1.1 Similarity-Based Prognostics

Similarity-based Prognostics (SBP) is a generic type of prognostic approach where the test specimen signal segments, consisting of sequential raw measurements or processed data are correlated to the previously collected data (i.e. historical data) segments by using a similarity concept. Unlike traditional data-driven models, in SBP, RUL is calculated by aggregating the weighted average of the training sample RUL values rather than extrapolating the test sample's current health level to a predefined threshold.

Similarity-based Prognostic approach is a powerful algorithm for RUL estimations, notably when the historical training sample size is relatively abundant. In addition, they are suitable for the cases where the degradation path is not necessarily exhibiting a monotonic propagation pattern which is difficult to model using parametric approaches (Wang, 2010). Wang et al. (2008) won the Prognostic and Health Management Society's data challenge competition in 2008 where they employed a similarity-based prognostic approach to predict the RUL of turbofan engines created by C-MAPSS simulation.

Zio and Di Maio (2010) developed a similarity-based prognostics methodology for estimating the remaining useful life of components in nuclear systems. Estimations of RUL implies evaluating the similarity between the test sample (i.e. 'q') and the training samples (i.e. '$r = 1{:}R$') as shown in Eq. (17). The similarity index is based on the calculated point wise Euclidean distances in between '$n - long$' sequences of observations. Distance score calculation in between training samples and the test sample at the 'i^{th}' time point formulated in Eq. (16). Final RUL estimation of a test sample at a time instance (i.e. 'I') is achieved by aggregating the weighted average of training samples' corresponding remaining useful life values as formulated in Eq. (18). To be more precise, 'rul_i^r' symbolises the remaining useful life of the 'r^{th}' training sample at 'i^{th}' time point which is obtained by calculating the difference between the training sample's end-of-life time and the 'i^{th}' time point. The most similar segment to the test segment is specified for each training sample whereas the RUL of the test sample is obtained by taking the weighted average of these training RUL values. In fact, the weights are obtained using the bell-shaped similarity functions which turns out to give credible results due to its gradual smoothness (Baraldi et al., 2013).

$$d_i^r = \sqrt{\sum_{j=1}^{n} \left\| z_{I-n+j}^{q} - z_{i-n+j}^{r} \right\|^2} \qquad (16)$$

$$s_i^r = e^{-\frac{(d_i^r)^2}{\lambda}} \tag{17}$$

$$RUL_I^q = \frac{\sum_{r=1}^{R} s_i^r rul_i^r}{\sum_{r=1}^{R} s_i^r} \tag{18}$$

'λ' is an arbitrary parameter which can be set to shape the desired interpretation of similarity, whereas 'n' defines the number of latest consecutive observations involved in similarity calculations. The smaller the 'λ' is, the stronger the definition of similarity. For instance, a small value for 'λ' signifies that the training segment should be very similar to the test segment so that it will be appointed with a similarity value reasonably higher than zero. However, when working with higher decimal point precision systems, this concept becomes trivial as the similarity ratio in between training samples remain the same.

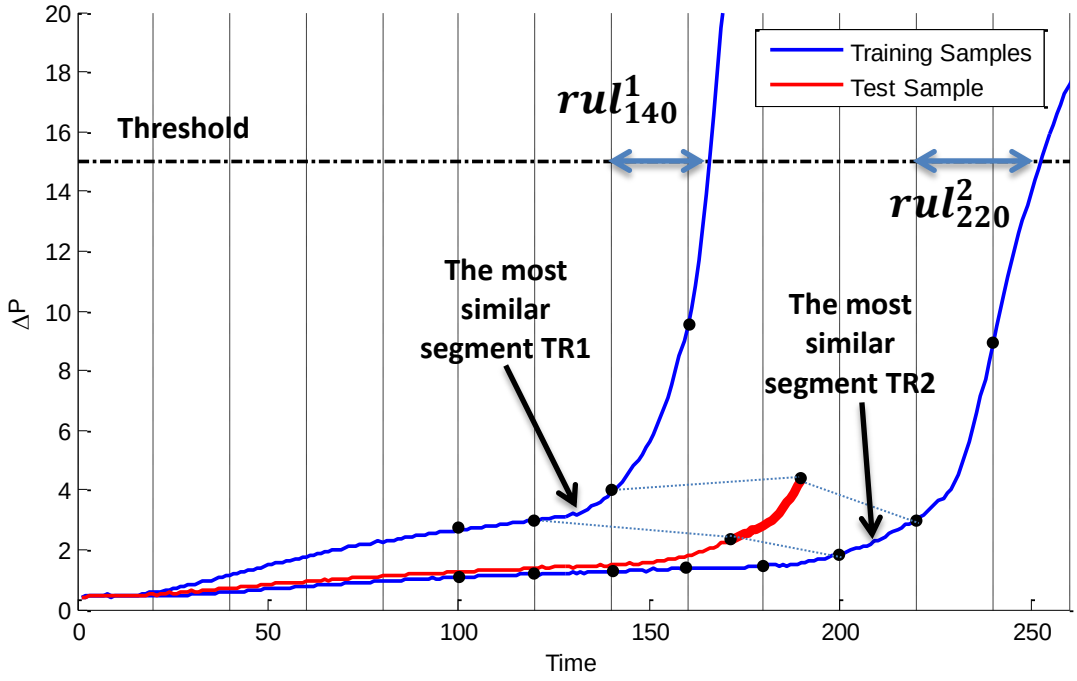

Figure 4.1. Similarity-based prognostic RUL calculation

Figure 4.1 demonstrates the calculation of a RUL for a test specimen at a specific time point. Vertical dashed lines divide the signals into '$n-long$' segments. The incomplete red line represents the test specimen signal trajectory whereas the blue complete signals stand for the two run-to-failure

training sample signals. It is assumed that the specimen is failed when it reaches the predefined threshold pictured in the black horizontal dashed line. Say, 'n' is chosen as 20, which denotes the latest 20 long test specimen segment will be our reference to be compared with the '$n - long$' segments within the training samples. Seventh segment of the first training sample comes forward as the most similar among the other segments. Similarly, eleventh segment is the most similar for training sample two as well. The corresponding RUL values for training samples (i.e. 'rul_{140}^{1}' and 'rul_{220}^{2}') are identified by subtracting the last points of the mentioned segments from the failure times as depicted in Figure 4.1. The final RUL assigned to the test specimen is calculated by aggregating the weighted average of the mentioned training RUL values.

4.1.1.1 Modified SBP

This subsection introduces the modifications that have been made on the similarity-based prognostic model discussed in the previous section.

The similarity-based model formulated in Equations. (16-18) achieve the RUL prediction by comparing the '$n - long$' train sample segments with the latest segment of the test specimen. However, as seen in Figure 4.1, the number of segments are limited to the '$train\ sample\ signal\ length/n$' which means only 8 and 12 comparisons have been made for the first and the second training samples respectively. Therefore, for the training signals, increasing the number of potential similar segments without decreasing the 'n' value, will broaden the search area, enabling to find more similar segments, hence better RUL representations within the training sample signal. In order to achieve this, instead of dividing the training signals into specific segments, all possible consecutive '$n - long$' segments are incorporated in the distance and similarity calculations using sliding window approach. Thus, each time point concatenated to its '$n - 1$' backward points form a new segment leading to the enrichment of segments up to the training sample's signal length. Therefore, for this specific case,

the numbers of segments to be used in comparisons are increased up to 166 and 253 for the training samples one and two respectively. It is important to note that, for the time points where it is impossible to go '$n-1$' backward points (e.g. the initial 18 time points when '$n=20$') are need to be treated differently.

Evidently, the first '$n-2$' time points in a training signal cannot form a '$n-long$' segment. For instance, when '$n=20$' one cannot calculate the similarity between the '$n-long$' test segment with the first 10-long train segment in this methodology. However, this can be solved by changing the static 'n' to a variable value as shown in Eq. (19). Moreover, similarity calculation measure should be modified in order to equally treat the varying segment lengths, as lower length segments will produce less distance values. In the modified similarity calculation, variable segment length (i.e. 'n_i') is added in the equation to fix the mentioned bias. Equations (20, 21) are the modified version of the original distance and similarity calculations (i.e. Equations (16, 17)) shown below.

$$n_i = min(i, n) \tag{19}$$

$$d_i^r = \sqrt{\sum_{j=1}^{n_i} \left\| z_{I-n_i+j}^q - z_{i-n_i+j}^r \right\|^2} \tag{20}$$

$$s_i^r = e^{-\frac{(d_i^r)^2}{\lambda n_i}} \tag{21}$$

It has been found that the modifications in the distance and similarity calculations have enhanced the capability of the model for both case studies. Corresponding results of the modifications will be discussed in the Results Chapter.

4.2 Physics-Based Prognostic Modelling

This section starts with introducing the renowned Particle Filters which is widely used in the prognostics community followed by discussion on details

of the physics-based approaches, developed for the modelling of the two different engineering studies.

4.2.1 Particle Filters

"The probability of any event is the ratio between the value at which an expectation depending on the happening of the event ought to be computed, and the value of the thing expected upon its happening"

-Thomas Bayes (1701-1761)

Kalman and particle filters are two of the most known Bayesian stochastic filtering techniques, which have been widely used in prognostics, object tracking, computer vision and robotics, speech recognition; and in general, machine learning. Kalman filters (KF) are limited to the occasions where the degradation of an asset exhibit linear characteristics. KF estimators approximate the parameters distributions of the model, deterministically. On the other hand, in particle filters (PF), model parameter distributions are represented by means of significant amount of weighted particles rather than an analytic probability distribution function (PDF) (Chen, 2003). This means that each particle contributes to the parameter probability distribution and evolves through time. In addition, PFs are more generic compared to KFs, hence they are applicable to non-linear degradation profiles and also are not limited the Gaussian noise. Therefore, in this study, we have selected PFs over KFs as they provide wider application space for both filter clogging and crack propagation modelling. A brief literature review on PF applications in prognostics and the mathematical background are provided as follows.

Particle filters, also called as 'Sequential Monte Carlo Estimation', have been used widely in prognostics, peculiarly integrated in physics-based models. Some of the examples found in the literature are; fatigue crack propagation modelling for various engineering structures (Zio and Peloni, 2011; An et al., 2013; Baraldi et al., 2012; Cadini et al., 2009; Bechhoefer,

2008; Orchard et al., 2008), battery capacity modelling (An et al., 2013; Abbas et al., 2007; Weiming Xian et al., 2014), centrifugal pump degradation modelling (Daigle and Goebel, 2013), thermal processing unit degradation (Butler and Ringwood, 2010), pneumatic valve modelling (Daigle and Goebel, 2010), DC-DC converter system level degradation modelling (Samie et al., 2014), Isolated Gate Bipolar Transistor (IGBT) degradation modelling (Saha et al., 2009), Proton Exchange Membrane Fuel Cells (PEMFC) life modelling (Jouin et al., 2014), Lumen degradation modelling for LED light sources (Fan et al., 2015). The list can be expanded to various engineering prognostic applications.

In general, dynamic systems can be modelled in the form of state transition equation, which describes the evolution of its state through time (Cadini et al., 2009). The system state and measurement models underpinning Particle Filter process are given in Equations (22, 23).

$$x_k = g_k(x_{k-1}, \theta_{k-1}, w_{k-1}) \quad (22)$$

$$z_k = h_k(x_k, v_k) \quad (23)$$

Where:

$g_k: R^{n_x} \times R^{n_\theta} \times R^{n_w} \rightarrow R^{n_x}$	*: Dynamic state transition equation*
x_k - x_{k-1}	*: State vector at discrete time points k and k-1*
θ_k	*: Model parameter vector*
w_k	*: Process noise*
$h_k: R^{n_x} \times R^{n_v} \rightarrow R^{n_z}$	*: Measurement equation*
z_k	*: Measurement at time point k*
v_k	*: Measurement noise*

Particles, evolving in the system, can be represented as: '$\{x_k^i, \theta_k^i, w_k^i\}_{i=1}^N$', where '$N$' symbolises the total number of particles and 'i' is the particle number. This means that, each particle accommodates a state, model

parameters, and a process noise value, which evolves through time. Generally, the higher number of particles used in the construction of parameter distribution, the better representativeness of the system. Therefore, we selected a high number for 'N' in the modelling of both filter clogging and crack propagation scenarios. However, higher numbers for 'N' will increase the computational complexity, which may be burdensome when dealing with higher numbers of system parameters.

In particle filters, the posterior distribution filtering process usually comprises three recursive steps: 1) Prediction, 2) Update, 3) Resampling. In the prediction step, system state is predicted using previous step's the updated parameters via state transition equation. Then the predictions are updated for the current time step by using a likelihood function. Likelihood function assigns weights to particles according to the closeness to the measurement at each time point. In the resampling step, the particles with lower and higher weights are eliminated or duplicated, respectively, which is called inverse CDF (cumulative density function) method (An et al., 2013). This filtering process is entitled as Sequential Importance Resampling (SIR) particle filters.

This parameter learning process is continued until no measurements have left where the extrapolation step commences (i.e. actual RUL calculation step). In the extrapolation phase, the state parameter vector (i.e. 'x_k') is projected continuously by using the state transition equation until it reaches the failure threshold. In this way, 'N' number of trajectories also entails the distribution of RUL estimations. Mean or median of the RUL distribution is generally used for visualisation of the estimated RULs.

Next two sections describe the physics-based modelling for the two specific case studies where both models are incorporated with particle filters.

4.2.2 Fatigue Crack Propagation Modelling

Fatigue crack propagation modelling is studied under the structural health monitoring (SHM) damage detection and characterisation strategy. SHM is specified as the process of implementing damage identification for engineering structures such as civil, aerospace and mechanical engineering infrastructures (Farrar and Worden, 2007). The damage term in the definition is understood as the adversely affecting changes to the material or its geometric properties. Fatigue and corrosion damage accumulations are two of the most common examples in SHM literature. In SHM, health status of an asset is monitored periodically. Scheduled (e.g. aircraft landings) or unscheduled (e.g. earthquake) events which result in accumulation of degradation leading to the failure of systems are also taken into consideration.

Damage identification is carried out with five disciplines including SHM:

1. Structural Health Monitoring (SHM)
2. Condition Monitoring (CM)
3. Damage Prognosis (DP)
4. Statistical Process Control (SPC)
5. Non-Destructive Evaluation (NDE)

Typically, SHM is applied online in aircraft and building structure for damage identification, whereas CM application areas described are mostly rotating machines. On the other hand, NDE, carried out for offline damage characterisation, is performed after the localisation of the damage. SPC focuses on the detection of the causes of damage results. As the name suggests, damage prognosis is employed for predicting the remaining useful life of a structural system. DP attempts to forecast the system performance by assessing the current damage state of the system (i.e. SHM), estimating the future loading environments, and predicting the remaining useful life of the system through simulation and the past experience (Farrar and Lieven,

2007). However, the damage prognosis is in development phase and still relatively immature compared to the other disciplines.

Typically, by implementing the SHM technology in maintenance planning, the maintenance cycles (i.e. mean time to repair) are anticipated to be extended leading to more cost effective maintenance activities. SHM process steps can be lined up as follows:

1. Operational evaluation
2. Data acquisition, normalisation, and cleansing
3. Feature extraction and information condensation
4. Statistical model development for feature discrimination

Operational evaluation step is the decision making process where failure types and possible scenarios are analysed before the data collection step. Sensors are installed in the system to carry out monitoring and data acquisition. Normalisation is performed in order to evaluate all sensory information under equal terms. Data cleansing stands for the feature selection and removing useless data from the database. Feature extraction performs transforming input data into the feature space. Enormous amount of raw data is replaced by the features which are significantly lower in size. These meaningful features are extracted and passed on to the next stages. Next step is the statistical model development in which the extracted features are evaluated and separated. Supervised and unsupervised techniques form the basis for classifying features, assessing the severity of the damage, and eventually predicting the remaining useful life of system.

Several different techniques including eddy current testing, ultrasonic inspection, acoustic emission (AE), and vibration based methods used in SHM are discussed in (Diamanti and Soutis, 2010). They have examined the methods on determining the critical crack size and the effects of defects on composite structures' life and strength. They have worked more on finding

the most reliable non-destructive evaluation (NDE) technique for detecting, characterising and locating the damage on composite materials.

In fatigue crack propagation modelling, fatigue is defined as a progressive type of structural damage. It occurs when the material is exposed to a cyclic loading and unloading. In earlier steps of the fatigue damage, cyclic loadings provoke micro scale cracks on the material surface. The cracks will eventually reach to a crucial length leading to a sudden fracture within material. The fatigue damages are cumulative and irreversible unless a crack retardation technique is taken into consideration. Thus, resting the material does not imply a recovery process. In addition, the applied stress range is indirectly proportional to the total life of a structure before occurrence of a fracture. Ritchie (1999) reports that over 80% of all service failures can be related to fatigue concept.

The detection and prediction of fatigue crack progression is of great importance as the consequences due to a sudden fracture in a structure may be catastrophic. Several catastrophic fatigue failures can be listed to remark the importance of fatigue modelling. Some of those failures are listed as follows.

In 1842, a train was derailed and crashed in Paris, due to an excessive crack propagation leading to a broken locomotive axle, causing the death of 55 passengers (Gray, 1845). Another disaster, caused by metal fatigue failure, occurred in 1954. A de Havilland DH-106 Comet passenger jet broke up in mid-air and crashed into the Mediterranean Sea while resulting with 35 fatalities (Job, 1994). In 1980, a drilling rig located in Norwegian waters capsized due to an enormous fatigue crack in one of its six bracings, killing 123. This was due to cyclic stresses aroused from the sea waves up to 12m (Norwegian Public Reports, 1981). In 2005, a twin engine G-73 Mallard seaplane crashed, killing all the passengers and crew. The crash was caused

by separation of the right wing from the fuselage which was due to metal fatigue (Goodnough, 2005).

Physics-based modelling of fatigue crack propagation is a widely studied research area. The simplest and the most commonly used fatigue crack propagation model is developed by (Paris and Erdogan, 1963). Paris & Erdogan Law, as shown in Eq. (24), expresses the relationship between the crack growth rate per cycle 'da/dN'; and previous crack length 'a' (Paris and Erdogan, 1963; Cross et al., 2006).

$$\frac{da}{dN} = C(\Delta K)^m \qquad (24)$$

Where:

$$\Delta K = \Delta\sigma\sqrt{\pi a} \qquad (25)$$

The Paris & Erdogan crack propagation equation consists of the two material specific constants 'C' and 'm', and the stress range intensity factor '$\Delta K = K_{max} - K_{min}$', where '$\Delta\sigma$' is the range of cyclic stress amplitude, and 'a' symbolises the crack length. Derivatives of this well-known equation are widely used in prediction of fatigue life (An et al., 2013; Luo and Bowen, 2003; Wu and Ni, 2003; Righiniotis and Chryssanthopoulos, 2003; Liu et al., 2015; Bigerelle et al., 2006; Kotulski, 1998).

In this particular research, the renowned Paris Law, shown in Equations (24, 25), is incorporated with particle filters to establish a complete stochastic physics-based prognostic model. PF is employed for estimation of the parameters within the state transition function as well as in RUL predictions. Therefore, a system degradation model is required to be incorporated with PF. For sufficiently small 'dN', Paris law can be approximated into a discretised state transition function given in Eq. (26).

$$a_t = C_t(\Delta\sigma\sqrt{\pi a_{t-1}})^{m_t} e^{w_t} dN + a_{t-1} \qquad (26)$$

$$w_t \sim N(0, \sigma_w^2) \qquad (27)$$

In the equation, the dynamic current state parameter (i.e. crack length) is symbolised as 'a_t', whereas 'a_{t-1}' represents the previous cycle crack length. 'C_t' and 'm_t' are the model parameters pertain to material characteristics, which are updated continuously in the PF mechanism. 'w_t' exemplifies the process noise following a normal distribution shown in Eq. (27).

Details of the crack propagation modelling results will be discussed in section 5.2. Next section describes the development of a physics-based prognostic model for filter clogging failure scenario.

4.2.3 Filter Clogging Modelling

Separation of solids from fluid is a vital process to achieve the desired level of purification in industry, where the contaminant filtration is a common process in a variety of applications. Clogging of filter phenomena is the primary failure mode leading to replacement or cleansing of filter. Reduced performance and efficiency, and cascading failures are the unfortunate outcomes of a clogged filter. For instance, solid contaminants in fuel may lead to performance reduction in the engine and rapid wear in the fuel pump.

Filtration is basically described as a unit operation that is separation of suspended particles from the fluid, utilising a filtering medium, where only the fluid can pass (Cheremisinoff, 1998). Driving force for the filtration is the pressure gradient generated across the filter.

Solid-liquid filtration processes can be classified into three categories:

1) Deep-bed filtration
2) Cross-flow filtration
3) Cake filtration

Deep-bed filtration can be performed using depth-filters. Depth filters retain the particulate through a porous packed bed. Sand filters are the common

examples of depth filtration. In cross-flow filtration mechanism, slurry flows parallel to the filter medium where only clean liquid can pass to the other side, leaving the particulate inside the filter.

In cake filtration, solid particles in a suspension, flowing through a filter media, are retained on a filter medium, building up an increasing thicker cake as shown in Figure 4.2. As the cake layer becomes thicker, the cake structure becomes the main filtration component, leading to an excessively flow resistance in the final stages of filtration process. Eventually the flow rate drops to a certain level due to filter plugging, creating a need for cleansing or replacement of the filter. Ni et al. (2006) reports that the cake filtration process can be found in many industries including; mineral, chemical, pharmaceutical, food, and petroleum. From now onwards this section, we elaborate the cake filtration mechanism as our experimental filtration mechanism involves cake filtration.

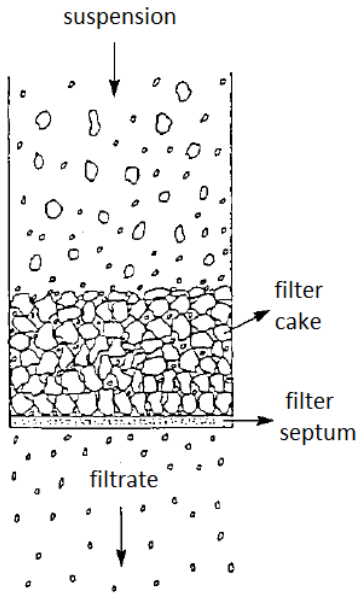

Figure 4.2. Schematic representation of cake build-up on filter medium (Abboud and Corapcioglu, 1993)

Cake filtration processes are in the form of two: 1) constant rate filtration and 2) constant pressure filtration. Figure 4.3 depicts the flow rate and

pressure behaviours in each operating regime. Regime A exemplifies the constant rate filtration where the fluid flow rate of the system remains constant. Pressure drop across the filter increases as the cake builds up. Pressure build-up process may exhibit a stochastic logarithmic or exponential character. In most cases cake becomes compressed and more compact as the pressure increases, leading to higher cake resistance. Regime B represents constant pressure filtration where the flow rate of the system declines as the cake builds up.

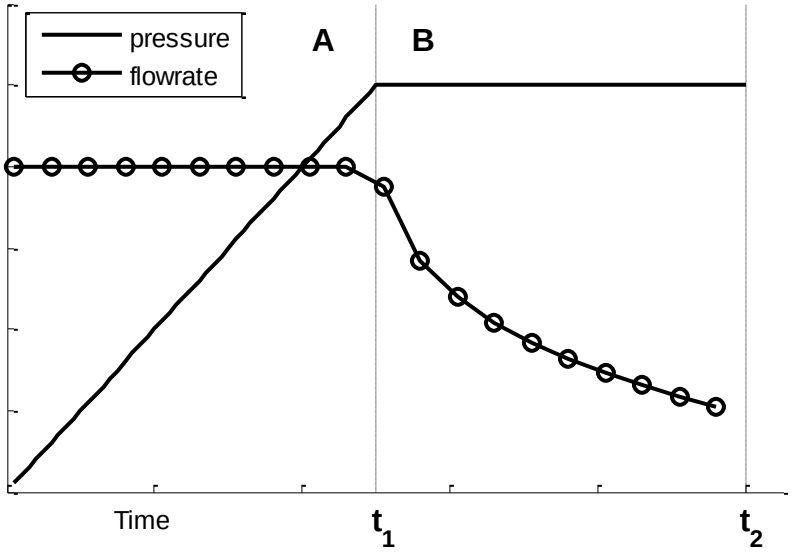

Figure 4.3. Constant rate vs. constant pressure filtration

In our experiments, both regime A and B are experienced. However, we only modelled the constant rate regime as our threshold (i.e. 15 PSI) restricts the experiment life to only regime A. Note that, regime A can be divided into three stages. First stage, illustrated in Figure 4.4, represents so called *'clean filter filtration regime'* which is the predecessor stage of the actual cake filtration (Endo et al., 1998). In this stage, majority of the particles passes through the filter mesh without being retained, however bridges appear to form by jamming of the particles gradually. During this stage, pressure and flow rate values remain relatively constant. At the end of this stage filter medium pores are blocked which led to dramatic increase in the retention of

particles. Second stage can be called *'actual cake filtration'* as the captured particles form and build up the layers of cake which is significantly prolonged step than the initial one. The pressure drop increases steadily while flow rate remains constant. When the cake thickness reaches the filter container interior level height, a sudden drop occurs in flow rate measurement whereas the pressure drop values enter to an exponentially growing region. This dramatic increase in pressure drop is thought to be by virtue of the restriction of cake thickness by the filter chamber which led to raise different type of forces (e.g. reduction in effective filtration area). However, the growth in pressure drop turns into logarithmic characteristics as the pump approaches its maximum pressure levels.

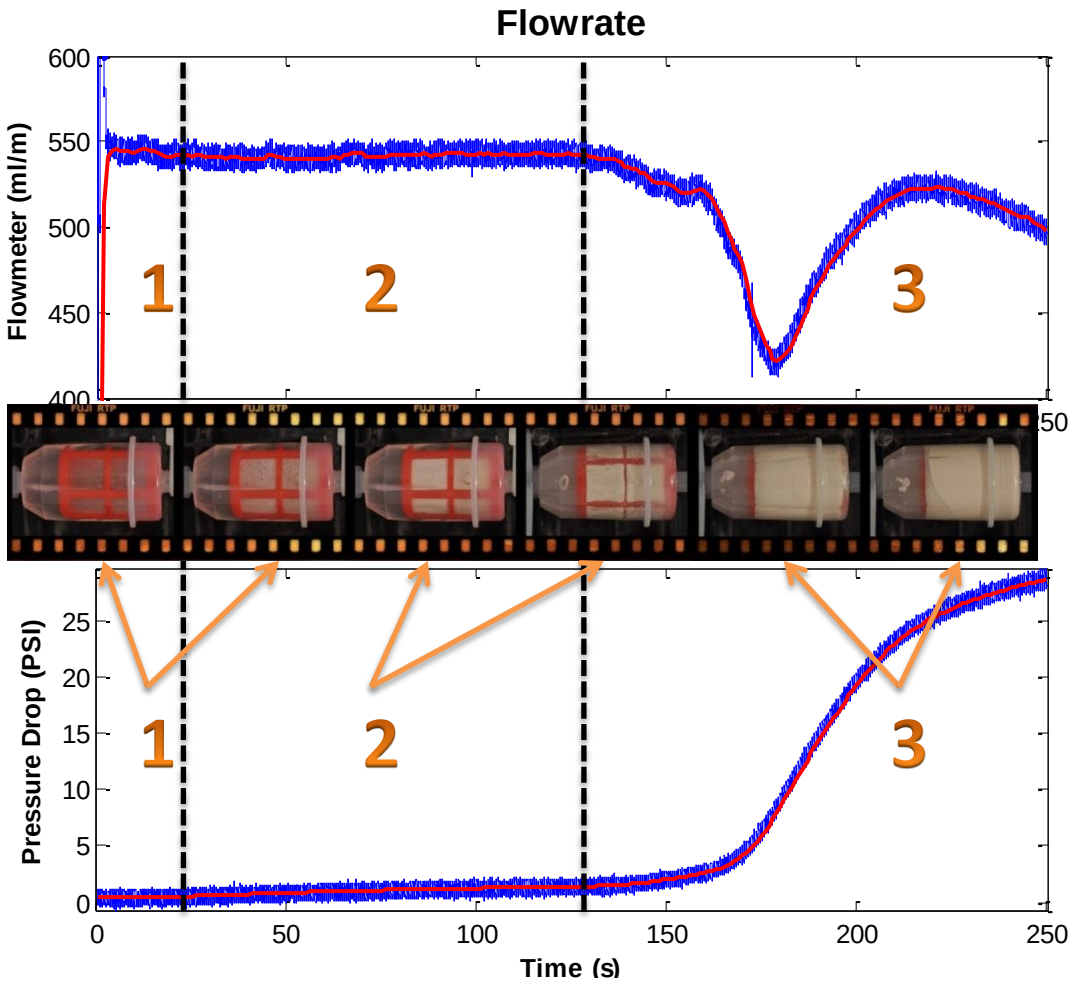

Figure 4.4. Filtration stages

Several studies on modelling of filtration process and fuel system exist in the literature. Park (2002) has investigated F-5F aircraft engine failure caused by erosion-corrosion of a fuel manifold, claiming the engine failures are caused by sudden pressure drop due to particles (e.g. mostly steel and iron) from the welding beads of fuel manifold. Internal welding beads are corroded and metal particles spread out which makes the fuel pump failed. The results are obtained by using energy-dispersive X-ray spectroscopy (EDX) analysis of related surfaces.

A comprehensive investigation of unmanned aerial vehicle (UAV) fuel systems has been conducted in IVHM Centre, Cranfield University, UK (Niculita et al., 2012; Niculita et al., 2013). Several failure scenarios including clogged filter and faulty gear pump are investigated; particularly diagnostics-based studies are conducted.

Clogging process of different types of filtration mechanisms has been studied in the literature. Roussel et al. (2007) presented a particle level filtration case study; stating that the general clogging process can be considered as a function of: ratio of particle to mesh pore size, solid fraction, and the number of grains arriving at each mesh hole during one test. The group conducted several clogging experiments and optimised the clogging parameters in their model. Their studies may help to model the first regime of cake filtration clogging process. Sappok et al. (2010) worked on the effects of ash accumulation in diesel particulate filters (DPF). They presented detailed measurement results with formulated lubricants, correlating ash properties to individual lubricant additives and their effects on filter pressure build-up. Pontikakis et al. (2001) developed a mathematical model for dynamic behaviour of filtering process for ceramic foam filters. The model is capable of estimation of the filtration efficiency, accumulation of particle mass in the filter, and the pressure drop throughout the filter. Roychoudhury et al. (2013) presented a diagnostic and prognostic solution for water recycling system for next generation spacecrafts. They simulated

several failure scenarios including clogging of membranes and filters. Baraldi et al. (2013) and Baraldi et al. (2015) developed a similarity-based and Gaussian process regression (GPR) prognostic approach to estimate the remaining useful life (RUL) of sea water filters. Saarela et al. (2014) presented a nuclear research reactor air filter pressure drop modelling scheme which utilises gamma processes. However, no physics-based or hybrid prognostic results are found in the literature for filter clogging scenario.

Researches have been attracted to model the fluid flow through a porous media since early 1900s. One of the earliest models for this type of flow is hypnotised by Forchheimer (Tien and Ramarao, 2013). His simple model associates pressure drop to fluid flow, given in Eq. (28) where 'Δp' is the pressure drop across the porous medium, 'V_s' is the flow velocity, 'A' and 'B' are the constants characteristic to the filter medium. This model has served a basis for several complex models in the future (e.g. Kozeny-Carman, Ergun, and Endo equations).

$$\Delta p = AV_s + BV_s^2 \qquad (28)$$

Darcy's Law is another initial model which has been used for calculating the permeability of a filter septum (Wakeman, 2007). Darcy described the volumetric flow rate 'Q' of a system as a function of pressure drop 'Δp', permeability 'K', cross sectional area to flow 'A', viscosity 'μ' of the fluid, and the thickness 'L' as shown in Eq. (29).

$$Q = \frac{KA}{\mu L}\Delta p \qquad (29)$$

Kozeny-Carman (Carman, 1997) and Ergun (Ergun, 1952) equations are two of the commonly used formulations applied in fluid dynamics to model the pressure drop of a fluid flowing through a porous medium (e.g. packed bed, filter mesh). Tien and Ramarao (2013) brought an issue that Kozeny-Carman equations are questionable when it comes to *'porosity'* (i.e. void

fraction of the filtration medium) modelling of compressible and randomly packed filter cakes in gas-solid separation processes. They claimed that Kozeny-Carman is appropriate when it is used only for pressure drop-flow rate correlations.

Endo et al. (1998) reports that Kozeny-Carman or the extended version (e.g. Ergun equation) can only be applied to the particles with a narrow size distribution. They developed a novel pressure drop model incorporating the particle size distribution and particle shape factor.

Conventional cake filtration theory has the capability of estimating the cake thickness, cake resistance, porosity, and pressure drop in the system. Tien and Bai (2003) discussed a more accurate procedure applying of the conventional cake filtration theory. They reported that the cake thickness and compressibility of the cake have the highest influence on pressure drop across the filter.

Several methods have been implemented to measure the cake thickness depending on the filter geometry including ultrasonic, electrical conductivity techniques, nuclear magnetic resonance micro-imaging, optical observation, and cathetometer measuring (Hamachi and Mietton-Peuchot, 2001). Ni et al. (2006) have modelled cake formation and pressure drop of a filtration mechanism in particle level (i.e. micro level) where majority of the studies in literature are conducted in macro level. They simulated the cake filtration process in both constant pressure and constant rate stages. Liu et al. (2013) implemented pressure drop modelling on the impact of membrane diesel particulate filter based on Endo's extended version of Kozeny-Carman equations. In their model, they correlated the pressure drop across a type of membrane filters to diesel exhaust gas particulate retention parameters.

In this research, the experimental rig is designed so that no other component is failed but the filter. Therefore, the modelling of differential pressure phenomena will pinpoint the system health. Pressure drop across

the filter, volumetric flow rate, cake thickness, and porosity parameters are the main dynamic indicators revealing the clogging severity of the filter. These parameters are required to be measured or derived from other parameters. In this study, correlation between the pressure drop and the other clogging parameters are modelled based on Ergun equation given in Eq. (30).

$$\Delta P = \frac{AV_s\mu(1-\epsilon)v(\epsilon)L}{D_p^2\epsilon^2} + \frac{B(1-\epsilon)\rho {V_s}^2 L}{\epsilon^3 D_p} \quad (30)$$

$$v(\epsilon) = \frac{10(1-\epsilon)}{\epsilon} \quad (31)$$

Where:

ΔP : *Pressure drop=upstream pressure-downstream pressure*

$v(\epsilon)$: *Void function of porosity*

L : *Total height of the bed (e.g. cake thickness)*

ϵ : *Porosity of the bed (or cake)*

V_s : *Superficial (empty-tower) velocity*

μ : *Viscosity of the fluid*

D_p : *Diameter of the spherical particle*

ρ : *Liquid density*

A, B : *Constants*

According to the equation; viscosity and velocity of fluid and thickness of cake are the parameters which raise the pressure drop across cake when they increase, in contrast to particle diameter and porosity parameters. The Ergun equation is a detailed version of the renowned Kozeny-Carman equation. Tien and Ramarao (2013) claimed that the Ergun equation is the most commonly used model which is capable of describing the pressure drop and flow rate correlation. The first term in the Ergun equation represents viscous effect whereas the second term associates with the inertial effect which is not taken into account in Kozeny-Carman model. Therefore Ergun

equation is chosen for the pressure drop modelling for our second case study.

The void function of porosity (i.e. '$v(\epsilon)$') has other complex forms for different type of applications (Liu et al., 2013). However a simpler version is used for Ergun and Kozeny-Carman equations, given in Eq. (31). Void function is substituted in the main equation and another parameter (i.e. 'a') was added by the author to put the equation into the final form, given in Eq. (32).

$$\Delta P = \frac{10AV_s\mu(1-\epsilon)^2L}{D_p^2\epsilon^3 a} + \frac{B(1-\epsilon)\rho{V_s}^2L}{\epsilon^3 D_p a} \qquad (32)$$

The parameter 'a' represents the effective filtration area rate which assist in modelling final stage of the filtration process (i.e. the third regime depicted in Figure 4.4) where the cake height is restricted to grow by the filter container leading to other type of forces to be concerned. However, these forces are not captured in the Ergun equation. Therefore, we linked these forces to the deviation within effective filtration area which led to favourably modelling of the final stage of filtration.

The parameter 'a' is a dynamic variable, driven by the sphere packing simulation modelling. The effective filtration area rate is defined as the rate of the filtration area of the particle deposit cake inside the filter chamber where fluid can pass. However this rate reduces dramatically when the deposited particles start reaching the filter container. Figure 4.5 depicts the progress in the adapted parameter. As seen in the figure, effective filtration area remains 100% during the first two stages defined before. However it drops dramatically as it enters the third regime where the cake height is restricted to grow by the filter container.

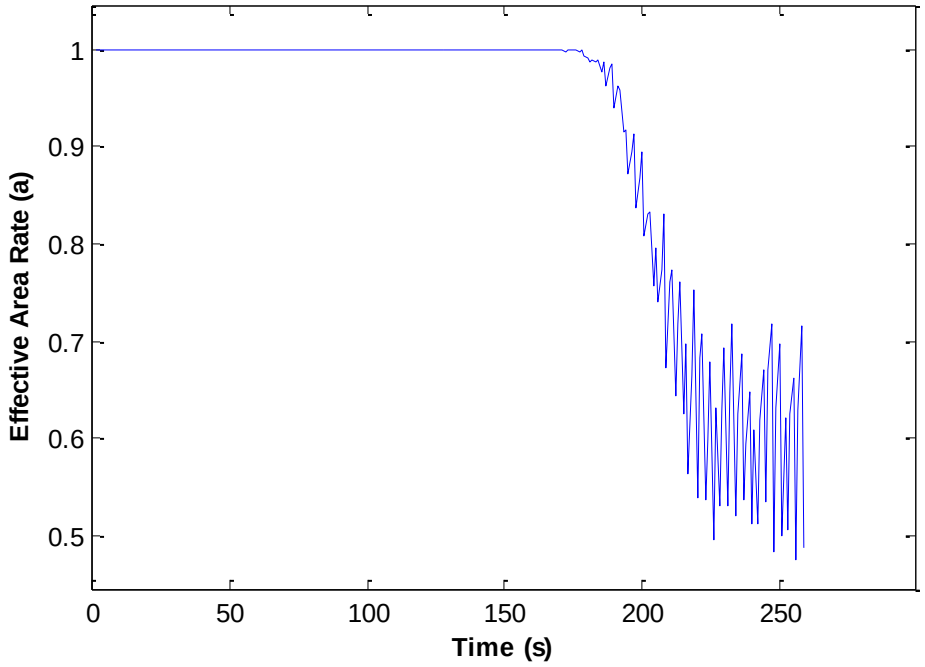

Figure 4.5. Sphere packing simulation results of the adapted parameter

The modified Ergun equation is transformed into a dynamic state transition equation in order to be integrated with Particle Filters. For sufficiently small 'dt' intervals, the state space model can be discretised to give:

$$\Delta P_{t+dt} \cong \Delta P_t + \Delta P_t' dt + w_t \tag{33}$$

Eq. (33) represents a nonlinear pressure drop increment steps. '$\Delta P_t'$' term can be obtained by taking the first derivative of the modified Ergun equation given in Eq. (32). A MatLab program is written to solve the discretised version of pressure drop model equations, simulate the dynamic parameters and integrate with Particle Filters.

In Eq. (32), cake thickness 'L', porosity of the cake 'ϵ', effective filtration area rate 'a', and the fluid velocity 'V_s' are the dynamic parameters while rest of the parameters remain constant as the filtration process proceeds. In this regard, these dynamic parameters are required to be modelled separately for prognostic goals. It is important to note that, even though the fluid velocity changes over time, we have not modelled the velocity and assumed

it to be constant, for simplicity. However, this study can be extended by modelling the flow rate or fluid velocity in the future.

Next section elaborates the dynamic parameter simulation process and proposes an image processing technique for an indirect cake thickness measurement method.

4.2.3.1 Cake Thickness and Porosity Modelling

Cake thickness and porosity are the dynamic cake structure parameters required to be measured or simulated separately when modelling the pressure drop in the system.

In general, the cake structure is assumed to be uniform, which means that the particles disperse equally in the filter container leading to a minor spread in cake thickness distribution. In this research, we propose an indirect way of obtaining the cake thickness information rather than using the cake thickness measuring techniques mentioned in the previous section. High quality, continuously captured filter mesh pictures are used in an image processing technique to correlate the particle deposition with the cake thickness phenomena.

Figure 4.6 demonstrates the cake thickness approximation method. Original and the black & white transformation of the filter picture are depicted. Image processing was performed on the orange rectangular area covering one of the filter mesh areas. An image processing program is developed to capture the biggest white area within the orange zone shown in green lines. The reference line is located in the far left of the mesh area. It is found out that the cake thickness is directly proportional to the expansion of particles to the left, starting from the reference point. Therefore, the mean expansion rate is calculated during the experiments, illustrated in Figure 4.7.

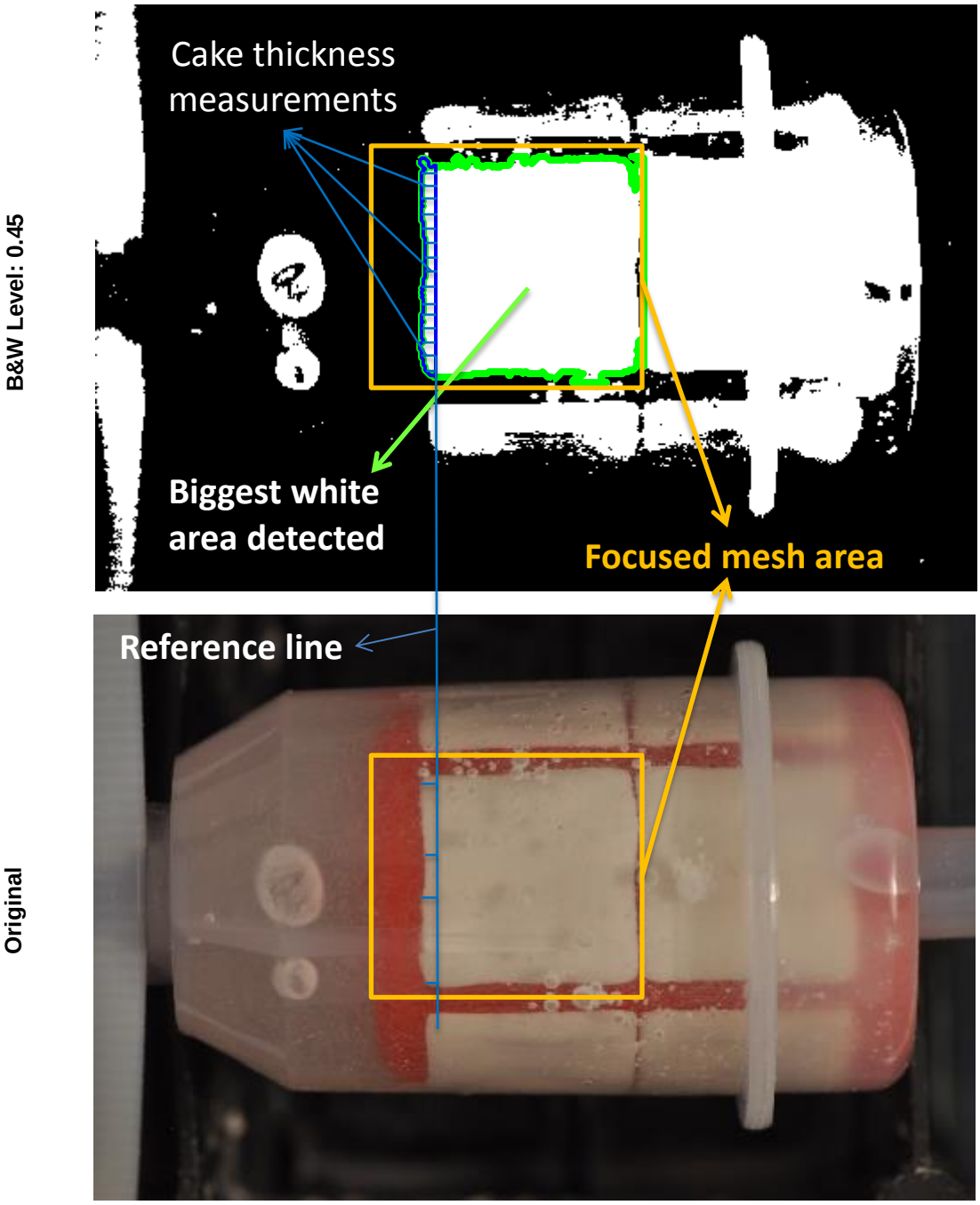

Figure 4.6. Cake thickness calculation using filter images

In Figure 4.7, blue dotted line represents the average cake thickness values obtained from the picture data via the image processing program. Black solid line stands for the maximum cake thickness level restricted by the filter container. In addition, the logarithmic cake thickness measurement model is shown in solid red line. The measurement model is obtained by

fitting a logarithmic growth trajectory to the indirect cake thickness measurement points obtained from image processing technique. The pressure drop data is also utilised to define the minimum and maximum cake thickness time point detection. Cake thickness growth exhibits a reciprocal trajectory to the pressure drop values as it is confirmed by several studies in the literature. The logarithmic cake thickness model is determined as the final indirect cake thickness measurement and used as auxiliary information in pressure drop modelling.

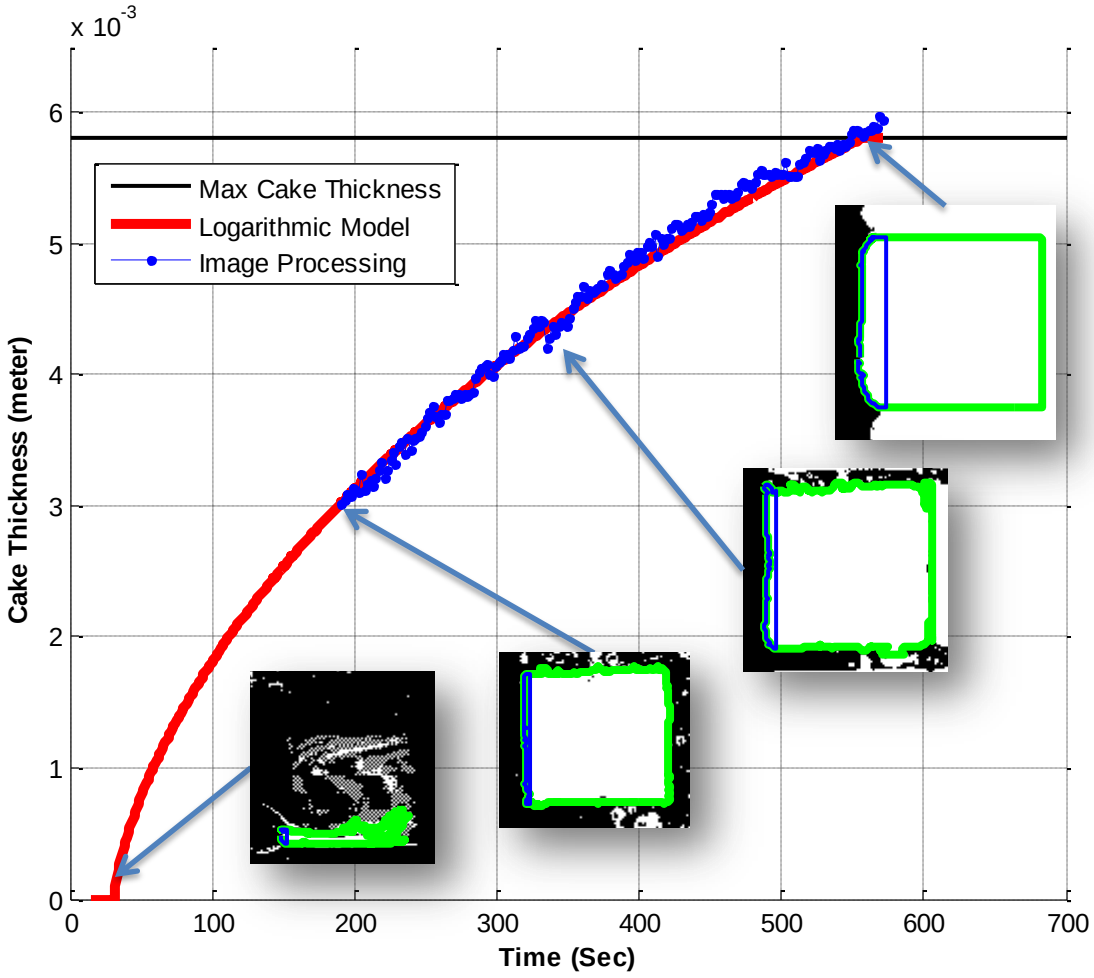

Figure 4.7. Cake thickness modelling demonstration

Moving onwards from the cake thickness modelling to porosity modelling, porosity 'ϵ' is defined as the void fraction of the cake. The porosity calculation model is provided in Eq. (34) where 'M_c' is the loaded mass of

particles, 'ρ' is the particle density, and 'A_f' is the cake area. The term 'M_c/ρ' outlines the loaded cumulative particle volume for each time instance whereas 'LA_f' stands for the cake volume. Loaded particle volume is calculated by multiplying the flow rate (i.e. 'Q') of the system by the solid fraction (i.e. 'x') of the suspension.

$$\epsilon = \frac{void\ volume}{total\ cake\ volume} = 1 - \frac{M_c/\rho}{LA_f} \qquad (34)$$

The dynamic parameters 'M_c', 'LA_f' hence the porosity values are simulated to imitate the clogging process of the filter. The simulation results including cake thickness, porosity and pressure drop will be provided in section 5.2. Next section elaborates the hybrid prognostic modelling integration methodology.

4.3 Hybrid Prognostic Modelling

In the previous sections, data-driven and physics-based modelling of the filter clogging and fatigue crack propagation case studies is discussed. In this section, we describe the proposed hybrid prognostic integration scheme.

The motivation for the hybrid prognostic modelling is discussed in Chapter 0. The proposed hybrid methodology aims to integrate a physics-based model (PbM) with a data-driven model (DDM) to enhance the prognostic capabilities. As discussed in the literature review chapter, majority of the hybrid prognostic models consist of two different models, where one performs the health state assessment while another performs the state projection and RUL calculation. Unlike those methodologies, we propose a generic integration scheme which appears in remaining useful life calculation phase of the prognostic process.

The integration scheme can be analysed in the five different scenarios displayed in Figure 4.8. First two scenarios represent cases where the RUL results (i.e. '*RUL1'* and '*RUL2*') are obtained from single complete models

which produce highly accurate estimations. These two cases are representative of the conditions where the sources feeding the models and the prognostic models are exceptionally rich to provide remarkably precise prognostic outputs. However, as mentioned in section 2.3.5, it is often difficult to model system/component degradation profile completely due to many reasons which have been discussed in previous sections. Therefore we call these perfect modelling cases as *'unrealistic'*. Moreover, the first four cases represent the unrealistic cases where one of the models contributing to the hybrid scheme can capture the system degradation profile perfectly, which is not really the case in real life maintenance.

However, we can investigate such unrealistic scenarios by dealing with simpler systems/components to capture the degradation profile perfectly. Therefore, we have worked on the Virkler crack propagation dataset and the filter clogging experimental studies which are relatively less complex assets and providing rich data sources. These two case studies can be modelled and their samples' remaining useful lives can be estimated with significantly high accuracy levels. First two scenarios exemplify these accurate modelling cases for physics-based and data-driven modelling cases.

Solid line arrows in the diagram represent the input/output for the complete modelling cases. On the other hand, the dashed arrows which symbolise the imperfect inputs/outputs represent real life conditions where the prognostic models often do not produce robust results linked to their weaknesses. The immaturity of a model may stem from many sources such as the lack of enough historical failure data or poor analysis of the degradation physics.

Third and fourth scenarios represent the mixture models where a mature model integrated with an incomplete model. In these scenarios, the integration scheme is biased towards a model to compare and investigate the bias effectiveness. Therefore, third and fourth scenarios assist to reveal

the integration effectiveness for both physics-based and data-driven modelling cases.

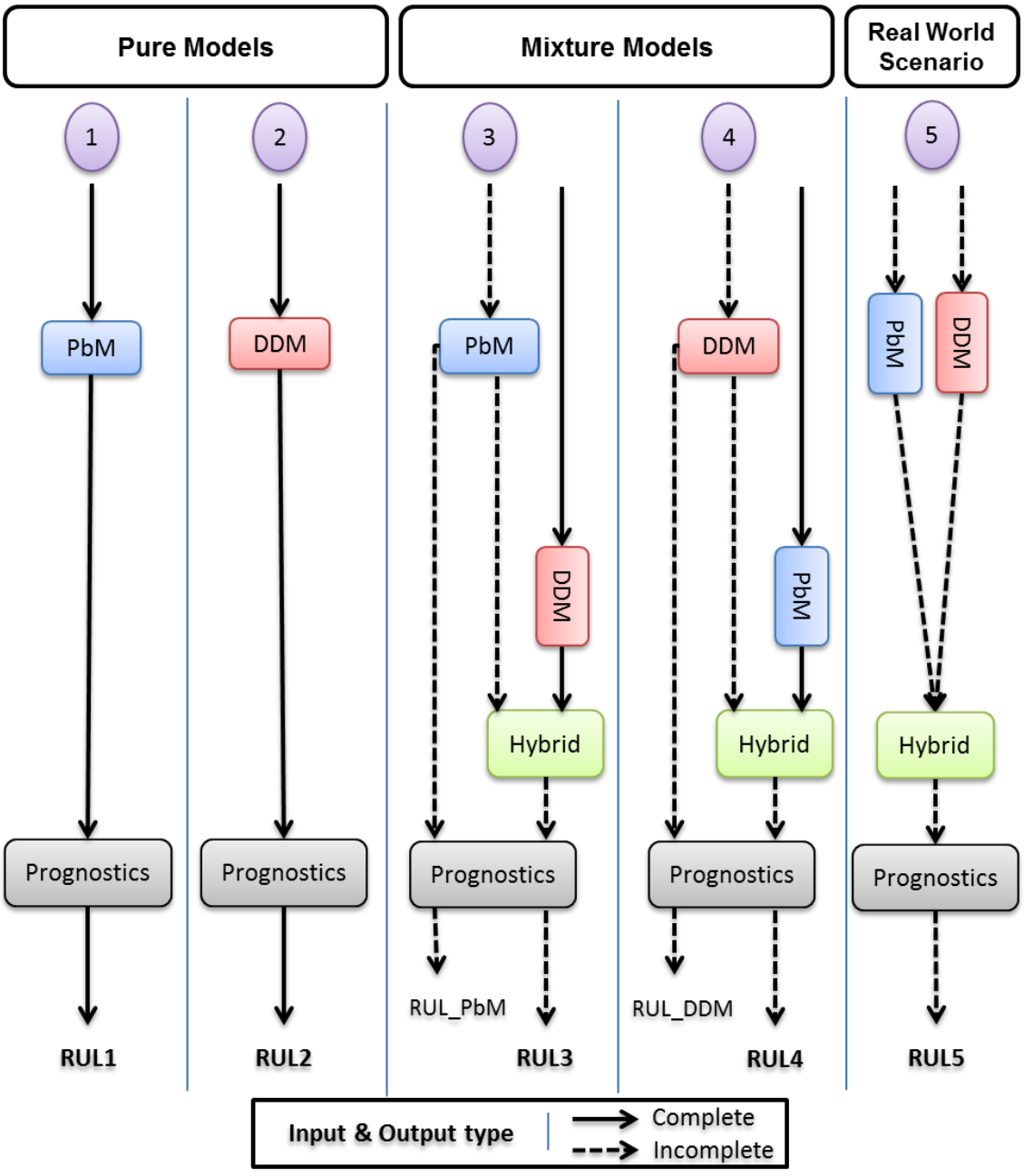

Figure 4.8. Hybrid integration scenarios

The bias effect is also exemplified in the results chapter (i.e. Figure 5.4). The effect of changing the bias ratio is investigated and the results are illustrated in the figure.

In third scenario, the data-driven model (DDM) is identical to the second case whereas the physics-based model is weakened on purpose to observe the compensation effects on the hybrid results. The physics-based model is crippled by starting with poor initial parameters used in the particle filter modelling. In addition, the cake thickness simulation is also weakened by adding randomly shifted errors specifically for the filter clogging case study. These modifications are anticipated to be resulted in narrowed prognostic capability of the physics-based model. In Figure 4.8, *'RUL_PbM'* represents the poor prognostic results obtained from incomplete physics-based model, whereas '*RUL3'* can be considered as the physics-based results enriched with data-driven model inputs. In this scenario the integration mechanism is biased towards the DDM, which means that the data-driven model output weight is relatively higher than the physics-based model output.

Similarly, in fourth scenario, for once the DDM is weakened by reducing the number of training samples. Training samples are the historical run-to-failure data observations to be used in the training of the data-driven model. The less data imply insufficient training of the model resulting with inadequate prognostic results. The enhanced prognostic output (i.e. '*RUL4*') is compared with the '*RUL_DDM*' to assess the improvement rate.

Lastly, the fifth scenario represents a real world prognostic application case where both models are incomplete; hence they are foreseen to produce relatively inaccurate results. However, even though these models are incomplete, each model can contribute to the final hybrid model when they are integrated to establish a hybrid model. Results of this final model are labelled as 'RUL5' in Figure 4.8.

It is important to note that the highest accuracy in RUL estimations will obviously be achieved from the first two scenarios (i.e. '*RUL1*' and '*RUL2*') as both models are complete and fed by rich information sources. '*RUL3*' and '*RUL4*' result are still obtained under unrealistic conditions where half of

the sources are rich. Therefore, the '*RUL5*' results are required to be compared with the results '*RUL_PbM*' and '*RUL_DDM*' which are fed by the same incomplete information sources. The third and the fourth cases are designed to investigate the effects of bias ratio to serve a basis for the fifth and the final scenario.

The details of the proposed integration scheme are discussed in next section.

4.3.1 Proposed Hybrid Prognostic Methodology

In Figure 4.8, the light green boxes represent the hybrid integration scheme where the physics-based model is integrated in the data-driven model. The PbM and DDM integration scheme is based upon the similarity-based prognostic methodology discussed in section 4.1.1.

Typically for the similarity-based models, the latest '$n - long$' segment of the test specimen is compared with the same lengths of segments within the training sample signals. In the proposed approach, similarity comparison is performed using '$n_0 + n_1\ long$' segment. The former part, '$n_0 - long$' segment, is obtained from the data from previous time units; whereas the latter part, '$n_1 - long$' segment is obtained from the forecasted data obtained from the physics based model. Hence, the similarity is obtained not only using the past, but also with model based future predictions. The forecasted values bring the failure point closer, which is expected to increase the estimation accuracy. The accuracy of the physics based model, selection of the number of forecasted points (n_1) and the number of past data to be used (n_0) are crucial.

After the segment has been defined, the distance (i.e. Eq. (20)) and similarity (i.e. Eq. (21)) values for each training segment are calculated as it is discussed thoroughly in the modified SBP section (i.e. section 4.1.1.1). RUL value for the test specimen for the current time point is assigned by aggregating the weighted average of the training samples' RUL values, given in Eq. (18) in section 4.1.1.

A demonstration of the RUL estimation integration mechanism is shown in Figure 4.9. In the figure, RUL calculation is performed for a test specimen at 140th second of its clogging process, shown in a red line where the future measurements are not known. The other two blue run-to-failure trajectories represent the training samples. Note that, for simplicity in the illustration, two out of 56 training signals are shown. It is assumed that the sample is failed when it reaches the predefined threshold shown in the black horizontal dashed line. Light green line extension is the 'n_1' number of time point estimations to the future, obtained from the physics-based model (e.g. Particle Filter & Ergun integration).

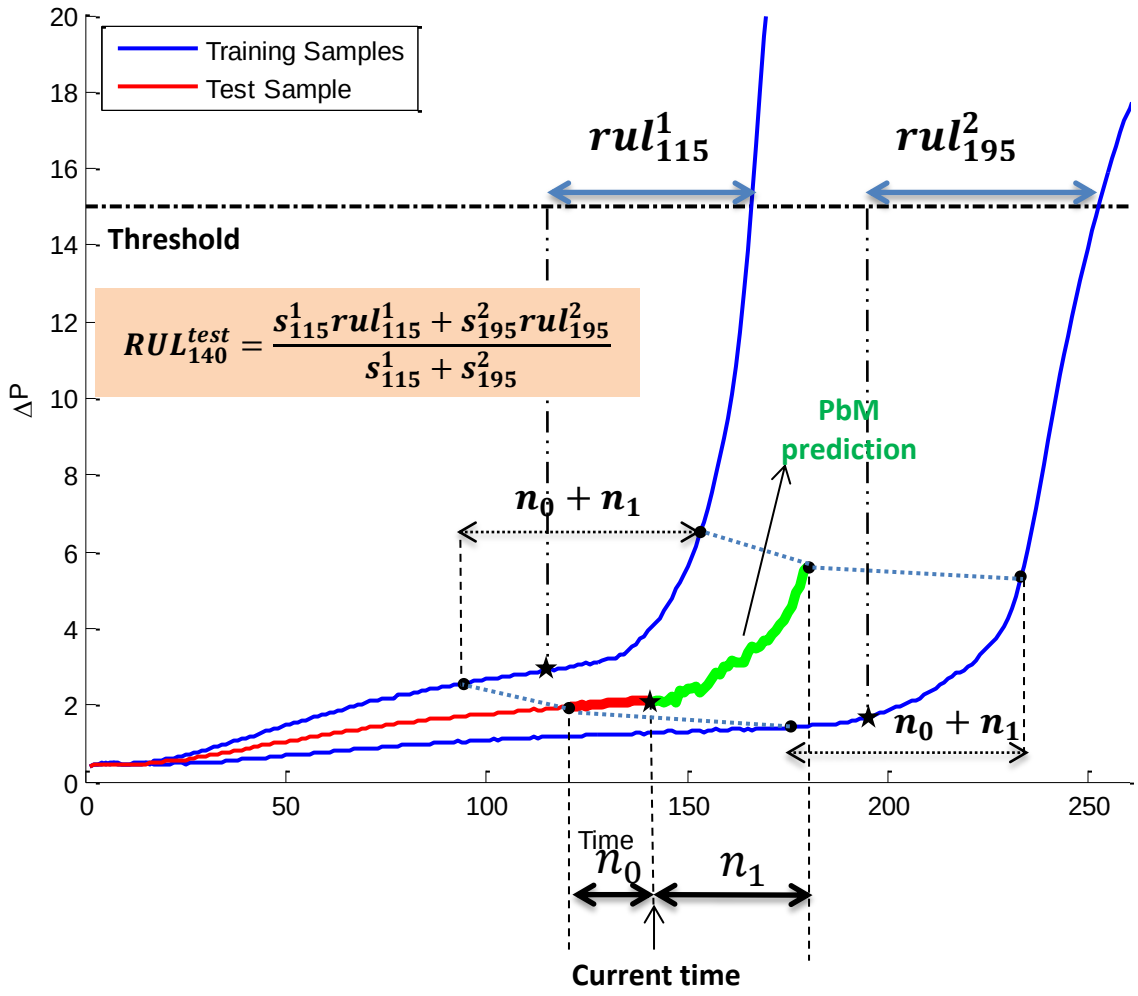

Figure 4.9. Hybrid integration scheme demonstration

Similarly, for the crack propagation case study, future crack levels are predicted using discretised Paris Law and particle filter combination model. The current time is indicated with a black star marker for the test signal. Every possible '$n_0 + n_1\ long$' segment for each training is got involved in the similarity calculation and similarity values are assigned to each segment. The most similar segment for each training segment is detected and its RUL and similarity values are used in the final RUL calculation shown in Figure 4.9. For instance 's_{115}^1' and 'rul_{115}^1' represents the similarity and RUL values of the most similar segment for training sample one. This means that the first training sample's 115th second reference point is the most similar point to the current time of test specimen. Similarly, for the second training specimen, 195th second time point stand out as the reference point representing its '$n_0 + n_1\ long$' segment.

In this way, by conjoining the future estimations in the similarity calculation, it is anticipated to enhance the prognostic results compared to the original definition of the similarity-based prognostic model. The results of the proposed integration scheme as well as the other models mentioned will be discussed in next chapter.

Chapter 5

Results

This chapter presents the results obtained from the models mentioned in the previous chapter. Data-driven, physics-based and the hybrid modelling prognostic results are analysed for two different engineering case studies: 1) Fatigue crack propagation 2) Filter clogging. Furthermore, prognostic performance metrics are discussed and the results are evaluated according to the metrics. The chapter is concluded with a discussion section.

5.1 Prognostic Performance Evaluation Metrics

It is necessary to introduce the prognostic evaluation metrics before discussion of the prognostic results. These metrics can be of generic use in many fields such as weather, aerospace, finance, medicine, automotive; which involve forecasting or prediction applications. Typically, prediction accuracy and precision levels are measured to evaluate the performance of algorithms. Mean squared error (MSE) and Root mean squared error (RMSE) are two of the most commonly used accuracy measure for prediction analysis. In addition, mean absolute deviation (MAD) and mean absolute percentage error (MAPE) are also widely used metrics for accuracy and precision evaluation (Saxena et al., 2010). RMSE and MAPE calculation equations are given in Equations (35-36).

$$RMSE = \sqrt{\frac{\sum_{i=1}^{n}(y_i - f_i)^2}{n}} \quad (35)$$

$$MAPE = \sum_{i=1}^{n} \left| \frac{100(y_i - f_i)}{n y_i} \right| \quad (36)$$

Where:

y_i : *Actual RUL value at time point 'i'*

f_i : *Predicted RUL value at time point 'i'*

n : *The number of prediction time points*

As it is evident from the name, RMSE gives the root mean squared error of the predictions based on the actual RUL values for test signals. However, the outliers in the predictions will greatly affect the averaged result of RMSE. Unlike the RMSE metric, MAPE is a unit-free measure where the results make sense in percentage levels. In MAPE calculation mechanism, the error values are weighed via the actual RUL values which capture the time varying aspects relatively more compared to RMSE.

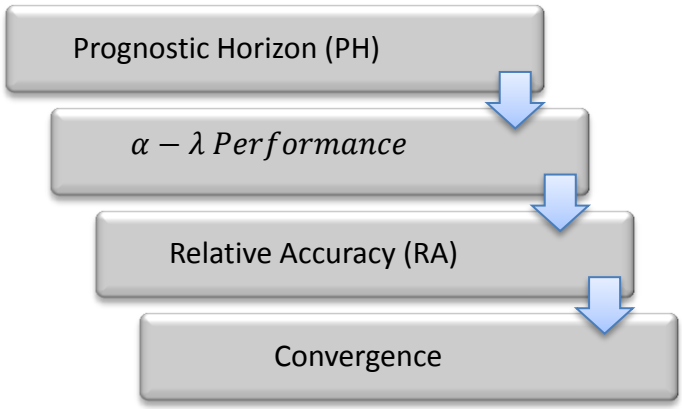

Figure 5.1. Hierarchical design of the prognostic metrics (Saxena et al., 2009)

Saxena et al. (2008) claims that these traditional forecasting performance metrics do not perfectly accommodate prognostic model performance requirements. For instance these metrics are not designed for applications where the predictions are updated continuously as more data become available. Typically, prognostic prediction performance tends to improve as

time progresses where the asset nears its end-of-life. In the early stages of an equipment degradation process, predictions are anticipated to be less accurate since there are not enough measurements fed to update the model parameters. Therefore, penalty rates of the crucial time points for errors should be higher than the earlier stages. Certainly, it is found to be necessary to tailor these traditional prediction performance metrics for prognostic algorithm performance evaluation.

A research group from NASA have been conducting a comprehensive research on the standardisation of prognostic evaluation metrics (Saxena et al., 2010; Saxena et al., 2008; Saxena et al., 2009; Saxena et al., 2009; Saxena et al., 2010). They have introduced a hierarchical group of prognostic evaluation metrics. The hierarchical design of the proposed new metrics is illustrated in Figure 5.1. In this hierarchical design, a prognostic algorithm is tested and passed to the next metric if the metric condition is satisfied. These metrics follow a systematic progression in the sense of the data they seek. The evaluation metrics will be discussed briefly before passing on the prognostic modelling results.

5.1.1 Prognostic Horizon (PH)

PH is defined as the range in between the point where the predictions fall under the allowable error bound (defined by 'α') for the first time and the end-of-life time point, given in Eq. (37). In other words, PH determines how far in advance an algorithm can provide estimations within the predefined accuracy bounds. Higher PH values imply longer prognostic horizon, hence better prognostic results.

$$PH = EoL - i \qquad (37)$$

Where:

$$i = min\{j|(j \in \ell) \wedge (r_* - EoL * \alpha) \leq r^l(j) \leq (r_* + EoL * \alpha))\} \qquad (38)$$

i *: The first time index when predictions satisfy* α*-bounds*

α : *Accuracy modifier*

EoL : *The ground truth end-of-life*

ℓ : *Set of all RUL estimation point time indexes*

l : *Test sample or specimen number*

r_* : *Actual RUL*

$r^l(j)$: *Predicted RUL at time instance 'j' for the test sample number 'l' (i.e. can be mean or median of prediction RUL distribution).*

Best possible score for the PH is that the predictions always stay within the error bound whereas the worst score indicates it has never entered the accuracy zone. PH ranges can be described in percentage levels too. We prefer to present PH results as the percentage of actual life of test specimens.

5.1.2 $\alpha - \lambda$ Performance

This metric determines whether the predictions fall within the shrinking accuracy cone (defined by 'α') around the actual RUL values. The output of the metric is binary; however, it can be converted to percentage values if the metric is implemented at multiple time instances. Shrinking cone boundaries are determined by the accuracy modifier 'α'. On the other hand, the parameter 'λ' specifies the rate of actual RUL over full life at time of the first predictions made within the allowable range. For instance, using this metric with '$\lambda = 0.5$' determines if a prediction falls within the accuracy bounds halfway through the failure from the time where first prediction made. Higher percentages of this metric result signify better prognostic ability.

$$\alpha - \lambda = \begin{cases} 1 & if \quad the\ condition\ is\ met \\ 0 & otherwise \end{cases} \tag{39}$$

Where:

$Condition$: $r_*(1-\alpha) \leq r^l(t_\lambda) \leq r_*(1+\alpha)$

$$t_\lambda = t_P + \lambda(EoL - t_P)$$

λ : *Time window modifier*

t_P : *Prediction time*

5.1.3 Relative Accuracy (RA)

This metric is similar to the alpha-lambda accuracy measure. Instead of inspecting whether the predictions fall within the boundaries, RA measures the accuracy level utilising absolute percentage error. Cumulative relative accuracy (CRA) is the weighted average of the RA values for the time instances of prediction points. RA and CRA equations are given in equations (40, 41) respectively. It is desirable getting higher RA and CRA scores for improved prognostics. Saxena et al. (2009) states that it is desirable to assign higher weights to RAs at final stages of predictions as it gets closer to EoL.

$$RA_\lambda = 1 - \frac{|{r_*}^l(t_\lambda) - r^l(t_\lambda)|}{{r_*}^l(t_\lambda)} \qquad (40)$$

$$CRA_\lambda = \frac{1}{\ell}\sum_{i=1}^{\ell} w(r^l) RA_\lambda \qquad (41)$$

Where:

w : *Weight factor as a function of RUL at all-time indices*

5.1.4 Convergence

Convergence is the final metric to be verified in the hierarchical design. Firstly, an accuracy or a precision metric (i.e. '$M(i)$') such as RA or MAPE is selected. Formerly, the algorithm is quantified whether it improves over time to converge the true RUL path. The convergence calculation is given below:

$$C_M = \sqrt{(x_c - t_P)^2 + {y_c}^2} \qquad (42)$$

Where:

$$x_c = \frac{{}^1\!/_2 \sum_{i=P}^{EoP} ({t_{i+1}}^2 - {t_i}^2) M(i)}{\sum_{i=P}^{EoP} (t_{i+1} - t_i) M(i)} \qquad (43)$$

$$y_c = \frac{{}^1/_2 \sum_{i=P}^{EoP}(t_{i+1}-t_i)M(i)^2}{\sum_{i=P}^{EoP}(t_{i+1}-t_i)M(i)} \qquad (44)$$

The terms 'x_c' and 'y_c' symbolise coordinates of the centre mass of the area under the curve '$M(i)$'. Therefore, Eq. (42) provides the Euclidean distance (i.e. 'C_M') from the origin defined as '$(t_P, 0)$'. Lower convergence distances reveal that the algorithm converges faster, which is desired for prognostics.

5.2 Crack Propagation Modelling

The detailed discussion on the fatigue crack propagation modelling is provided in the methodology chapter at section 4.2.2. This section provides the remaining useful life estimation results of the physics-based, data-driven, and hybrid modelling approaches. This section also entails the investigation of model performance evaluation. The entire prognostic models mentioned in the methodology chapter are implemented on the Virkler fatigue crack propagation dataset.

The Virkler dataset (Virkler et al., 1979) consist of 68 crack growth trajectories collected upon well-controlled fatigue loading experiments. The experiments were conducted under the identical constant amplitude fatigue loading and controlled environmental conditions. Several preliminary tests were conducted for determining the actual load levels for the material type. The specimens aged in the experiments were the 2024-T3 aluminium alloy plates which are drilled in the centre to form a 2.54mm initial notch, illustrated in Figure 5.2. Test specimen geometry details are also shown in the figure. They reported that the dataset do not contain measurements until 9mm of half crack lengths as the steady state conditions would not met up to that level.

During the aging process, samples were subjected to cyclic tensile loading at '$R = 0.2$' stress ratio with '$\Delta\sigma = 48.28\,MPa$' stress range levels. Throughout the experiments, cycle numbers are recorded at fixed increments in crack lengths (i.e. '$\Delta a = 0.2mm$') until it reaches the predefined final length;

49.8mm. Note that, in the final stages of data collection, cycles were recorded at 0.4mm and 0.8mm increment levels as well. Each signal in the dataset contains 164 measurement points throughout its degradation path.

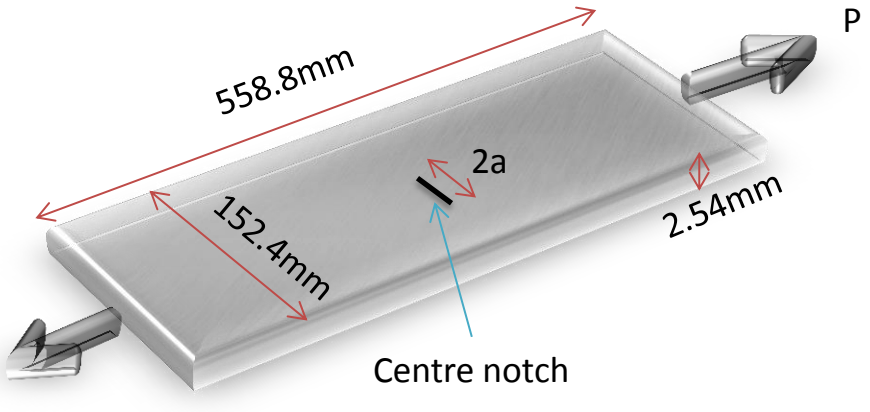

Figure 5.2. Test specimen geometry

As mentioned in the methodology chapter, the dataset is investigated by comparing the prognostic results from the integration scenarios discussed in section 4.3. The first scenario represents obtaining RUL from the particular physics-based model. The physics-based model implemented on the Virkler dataset is the distinguished Paris Law combined with particle filters. A demonstration of obtaining a RUL distribution result is shown in Figure 5.3. The top two subplots visualise the model parameter learning processes until the RUL prediction starting point at 150 thousand's cycle. During this learning process PF is used to track and update the main parameter (i.e. crack length) and also the auxiliary parameters (i.e. C and m). Starting from the RUL estimation point, where the measurement input feed is terminated, the model parameters are extrapolated into the future up to the maximum crack length threshold using the discretised Paris Law equation via Monte Carlo simulation. Thus, the RUL distribution at this specific point is obtained by calculating the differences between the RUL estimation starting point time and the times where trajectories (i.e. the number of trajectories is equal to the number of particles) hit the threshold. In the figure, red lines

represent the mean values of the distribution whereas the green curves encapsulate the 95% of the distribution (i.e. confidence bounds).

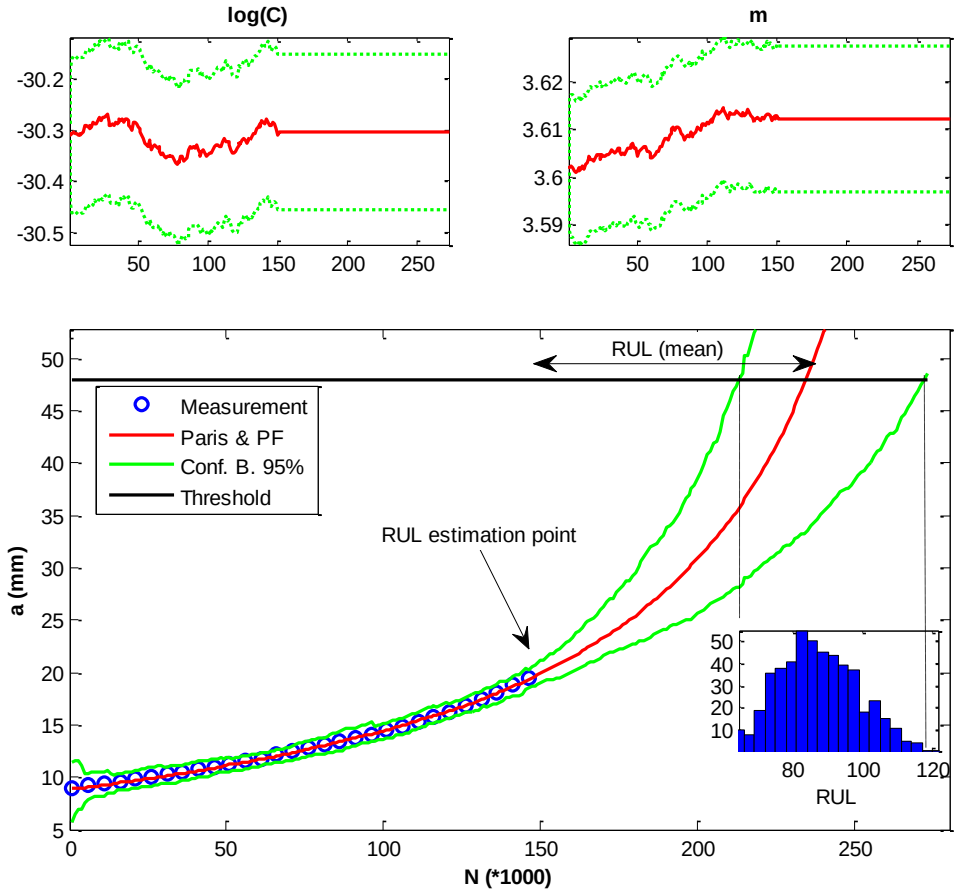

Figure 5.3. Paris Law and particle filter integration

For each test specimen, the RUL estimations are set to perform at every ten thousand cycles. RUL results of the individual physics-based modelling is analysed along with the fourth scenario.

For the second scenario, the RUL results are obtained from a singular and complete data-driven model (i.e. modified SBP). The complete data-driven model refers to a model where the sources feeding the algorithm are rich enough to produce immensely accurate RUL estimates. A visualised comparison of the data-driven model (i.e. modified SBP) against the physics-based model (i.e. Paris & PF) is depicted in Figure 5.5. X-axis scales the life period of the specific sample whereas y-axis stands for the corresponding

RUL values. In this figure, the dashed linear black lines represent the actual RUL values. Actual RUL values for a specimen are calculated by subtracting the current cycle from the EoL value specific to the specimen. The blue line represents the complete SBP model RUL estimation results (i.e. data-driven model results from the second scenario) where all training samples are used in the similarity calculations. The red curve serves as the complete physics-based model results (i.e. physics-based model results from the first scenario). The discretised Paris Law integrated with particle filters is the physics-based model which is selected for modelling the Virkler dataset signals. The physics-based modelling methodology is given in section 4.2.2.

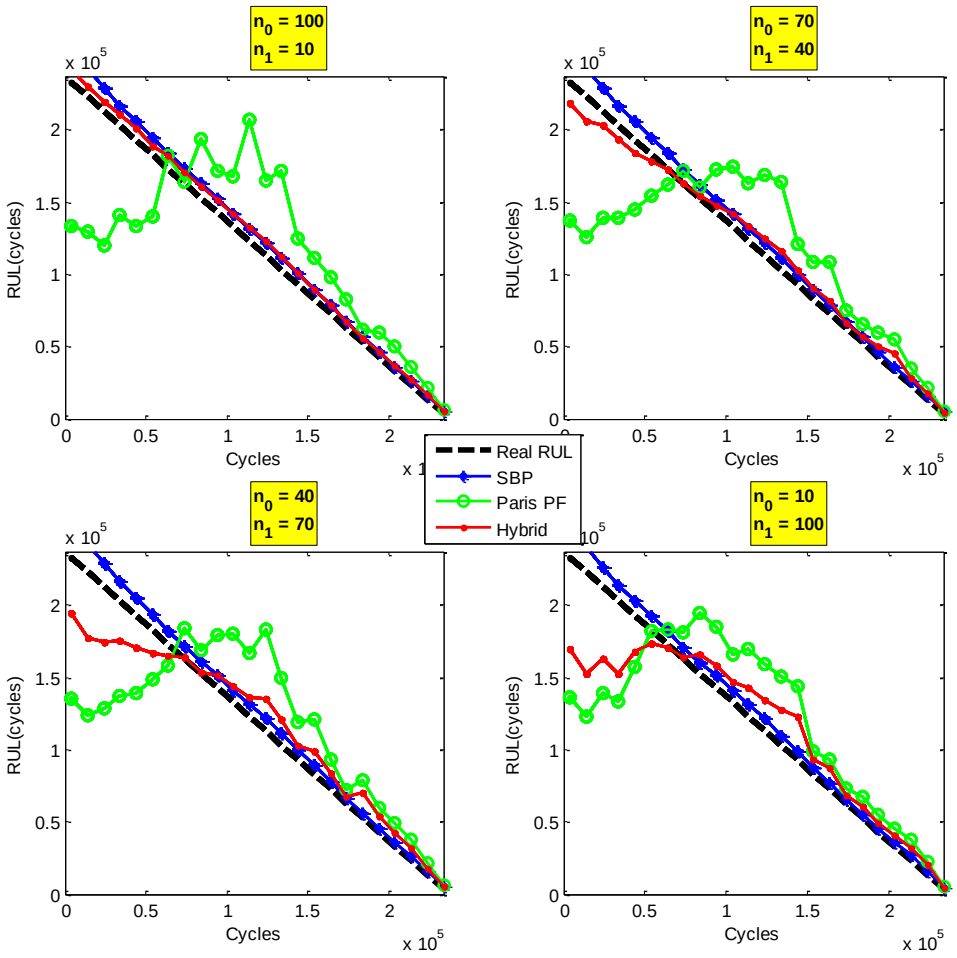

Figure 5.4. System bias comparison

The RUL estimation results presented in Figure 5.5 are obtained from the first two scenarios where the models are highly accurate. Shrinking alpha cone visual comparison, recommended by (Saxena et al., 2010), is used for visualisation of the complete models, hence the results from a single test specimen show that both models stay within the 10% error bound predominantly throughout the degradation process. Henceforward the results obtained from all test samples for these two scenarios are investigated along with the third and fourth scenarios.

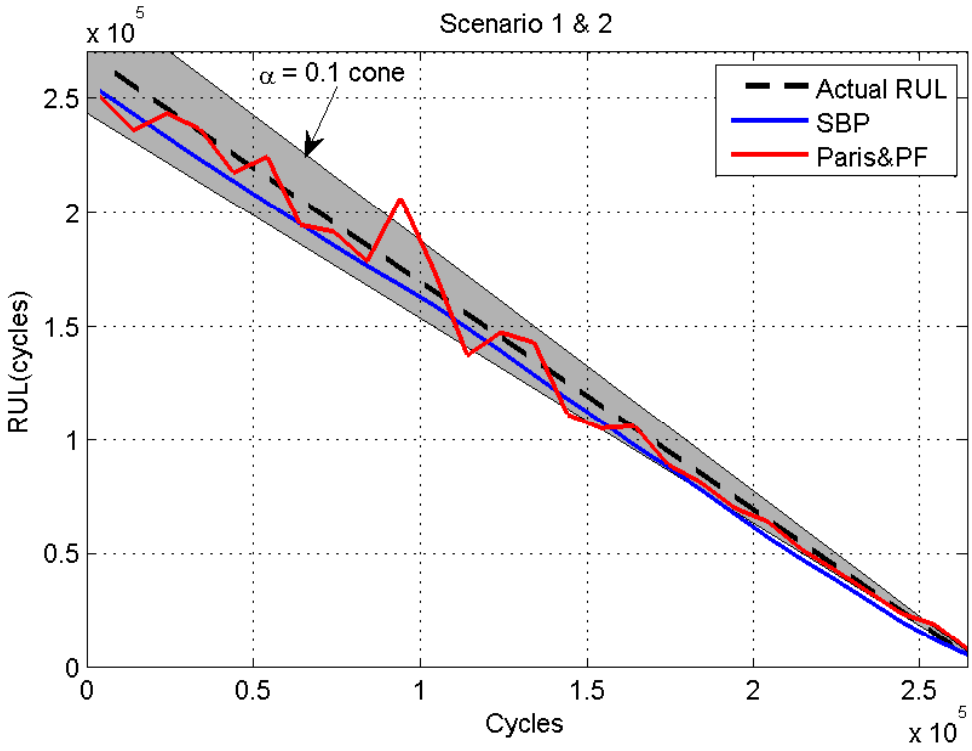

Figure 5.5. PbM vs DDM RUL visualisation on a Virkler dataset sample

The use of 'n_0' and 'n_1' for the models is summarised in Table 5-1. Recall that 'n_0' stands for the number of latest data points within the signal to be used in similarity calculations for SBP and hybrid modelling. On the other hand, 'n_1' symbolise the number of estimations towards the future by the physics-based model. Therefore the numbers 'n_0' and 'n_1' can be used as a bias between the models. For instance, increasing 'n_0' means involving more data points from the past monitoring data into the similarity calculations

which imply the hybrid integration system is biased towards the data-driven model. Contrarily, where the system is biased of physics-based modelling, can be achieved by increasing the 'n_1/n_0' ratio.

In Figure 5.4, we exemplify the effect of bias on the hybrid modelling results with four different 'n_0/n_1' ratios. The top left plot in the figure represents the highest bias towards the data-driven models with '$n_0/n_1 = 10$' bias rate. The rate is decreased moving through the bottom right down to 0.1 levels. Note that, for this figure, the DDM is complete and the PbM is incomplete model (i.e. Scenario 3). Therefore the degeneration in the hybrid model results is apparent as the bias towards the complete model disappears. The hybrid curves remain significantly close to actual RUL values when the bias is directed to the matured model. The integration mechanism gives user the flexibility to play with the bias values as they desire.

In addition, the standard deviation values selected for the measurement 'σ_v' and process noise 'σ_w' are selected 1 and 0.5 respectively. Similarly, for the parameters *'log(C)'* and *'m'*, the error terms for the particle filtering are constructed with standard deviation values of 0.1 and 0.01 respectively. Five hundred numbers of particles are employed for PF for all scenarios.

Figure 5.6 displays the remaining useful life results obtained from the scenario three, where the physics-based and data-driven models are incomplete and complete respectively. The modified similarity-based prognostic (SBP) model, discussed in section in 4.1.1, is selected to be used as data-driven model for the Virkler dataset modelling. The dataset samples are divided into training and testing parts. 59 out of 68 samples (i.e. ~85%) are selected to be used in the training of the modified SBP model while the remaining nine samples are (i.e. ~15%) left for testing the algorithm.

The crack propagation physics-based model is crippled by initialising the model parameters poorly, which are learned by the particle filter as more data becomes available. However, ideally for physics-based models, the

model parameters are initialised wisely by calibrating the physics principles empirically. Moreover, parameter initialisation can be improved by learning the parameter variation from the training dataset.

Table 5-1. Segment size construction for different scenarios

	Scenario				
	1	**2**	**3**	**4**	**5**
n_0	-	100	100	10	100
n_1	-	-	10	100	100

The RUL results obtained from the nine test samples at every ten thousand cycles are depicted in Figure 5.6. As seen in the figure, SBP prediction accuracy is almost ideal; accordingly, the blue curves stayed significantly close to the actual RUL lines. This is due the training sample population that is rich enough to encapsulate the spread within the entire dataset.

On the other hand, the physics-based model, represented in green curves, struggles to adapt its parameters yielding poor results for the initial periods. However, in the virtue of particle filter uncertainty handling, significant enhancement appears in the further stages as more data become available. The hybrid model, shown by the red lines, integrates the complete SBP with the incomplete physics-based model, (i.e. 'RUL3 in Figure 4.8). The hybrid prognostic results stay as almost close as the SBP results to the actual RULs.

Accuracy of the RUL estimations is measured by the performance metrics which are investigated in the previous section. Figure 5.7 visualises the comparison of the RUL prediction performances for the third hybrid scenario. X-axis for the plots signifies the test sample number, whereas the y-axis scales are specific to the performance metric. It is important to note that, the SBP results in Figure 5.6 and Figure 5.7 represent the second scenario. Figure 5.7 reveals that the hybrid model outperforms the incomplete physics-based model. Higher percentages indicate better

prognostic accuracy in prognostic horizon (PH), '$\alpha - \lambda$' performance, and cumulative relative accuracy (CRA) metrics. For all metrics 'α' and 'λ' values are selected as 0.1 and 0 respectively. Unlike other metrics, lower convergence distances signify improved prognostics, displayed in bottom right of the figure. According to the figure, for each metric, the hybrid and SBP models outperform the incomplete physics-based model as expected.

The average results of all test specimens are displayed in each metric legend entries. For instance, the hybrid and data-driven models provide results at an average 88% band for the cumulative relative accuracy, whereas PbM stays in 61% accuracy levels. In this regard, these results manifest that the integration scheme favourably improves the prognostic results of the singular incomplete model.

Moving on the fourth scenario; where the data-driven model is incomplete, whereas the physics-based model is complete. The data driven model is immatured by restricting the training data source significantly. Recall that the number of training samples was 59 out of 68 (~85%) for the previous scenarios. In order to limit the capabilities of the data-driven model, the number of training samples is significantly reduced (e.g. 2%). As mentioned in previous sections, in most industries, the number of run-to-failure data is notably limited; sometimes there is even no historical data available. Therefore, reducing the training sample size down to 2% may well be more representative of the real life scenario than the complete dataset usage cases.

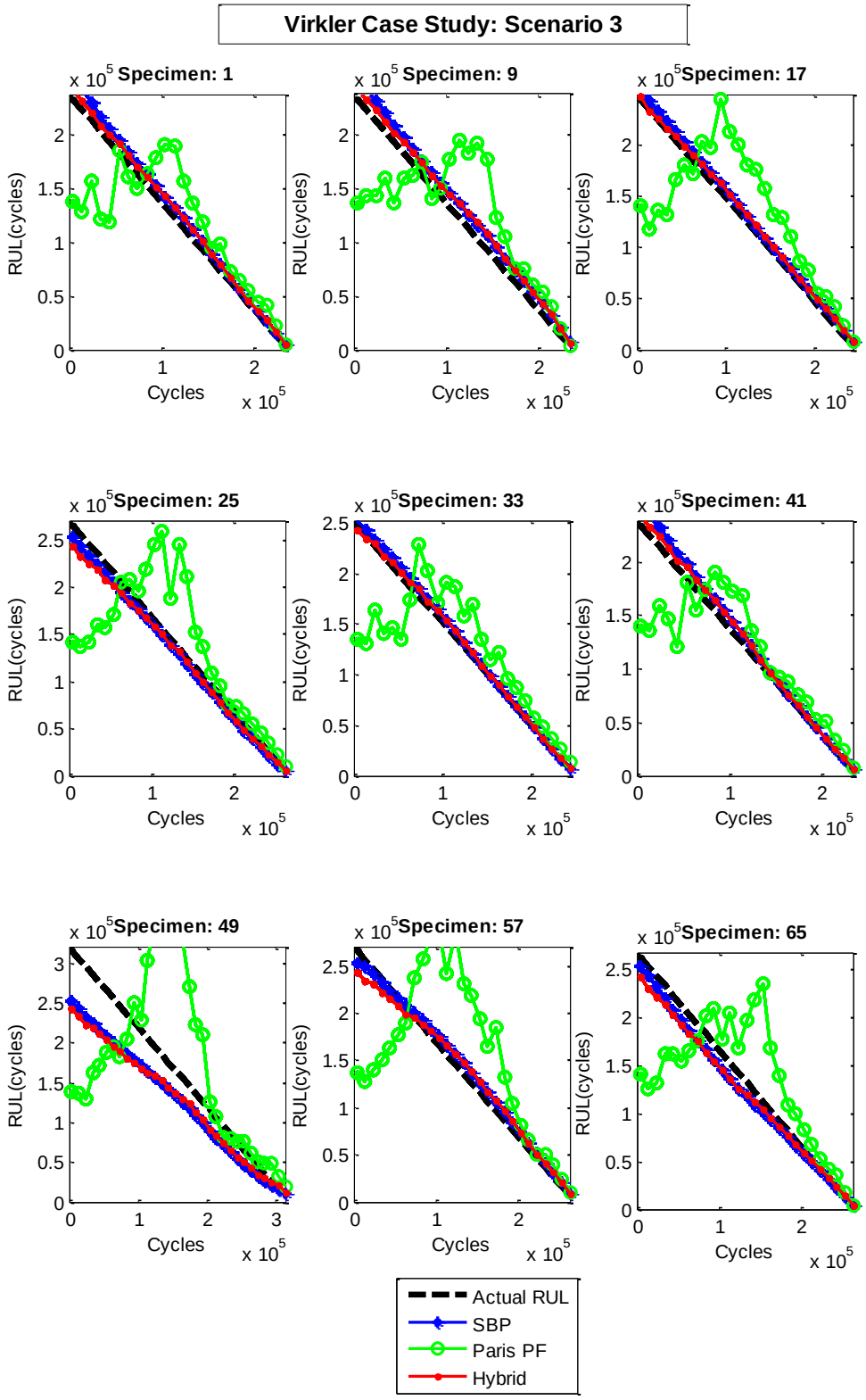

Figure 5.6. RUL results for Virkler dataset scenario 3

Figure 5.8 depicts the prognostic results for the fourth (i.e. the results labelled as 'SBP' and 'Hybrid') and the first (i.e. 'PbM') scenarios. In this figure, it is evident that the SBP model performance is greatly reduced after disregarding considerable amount of training samples. This performance drop in the RUL predictions is visually apparent that the predictions stay fairly beyond from the actual RUL values. Furthermore, the improvement in the physics-based model predictions when it is complete is noticeable as well.

The hybrid results, represented as in red curves, remain close to the SBP trajectories in the early stages of crack propagation. However, the predictions tend to follow the Paris Law & Particle Filter model starting approximately halfway through the failure. This trend can be linked to the high numbers of similarity segment sizes ($n_0 + n_1 = 200$).

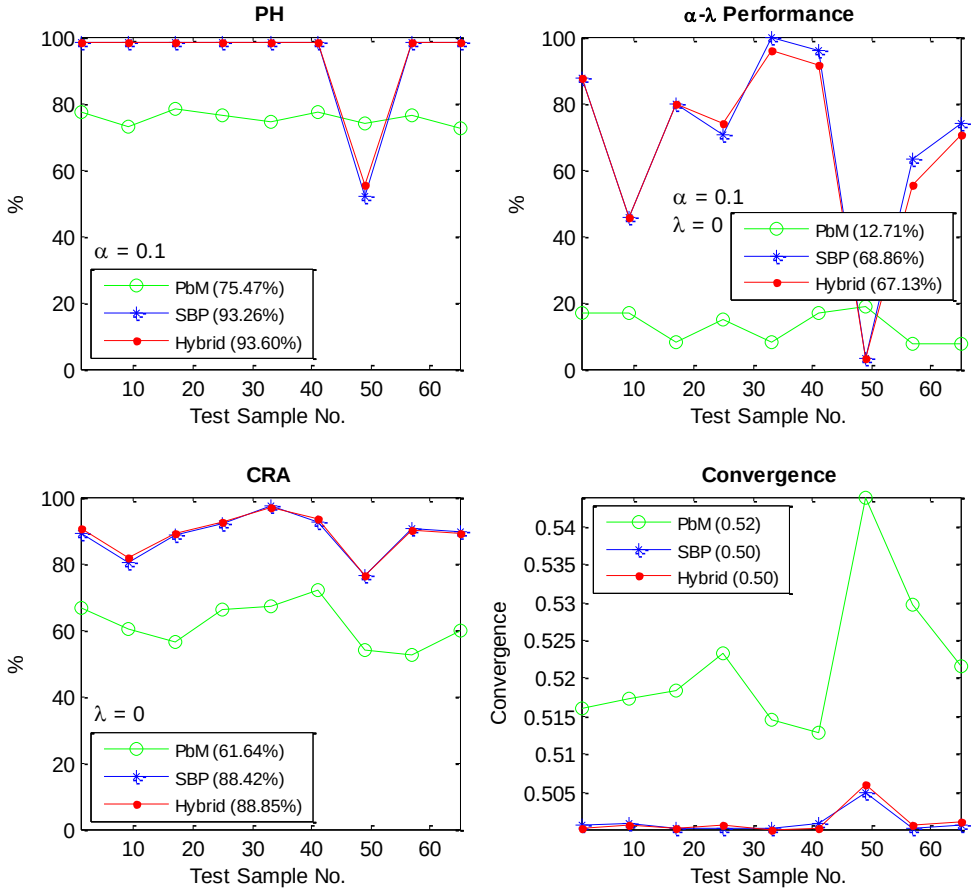

Figure 5.7. Performance results for Virkler dataset scenario 3

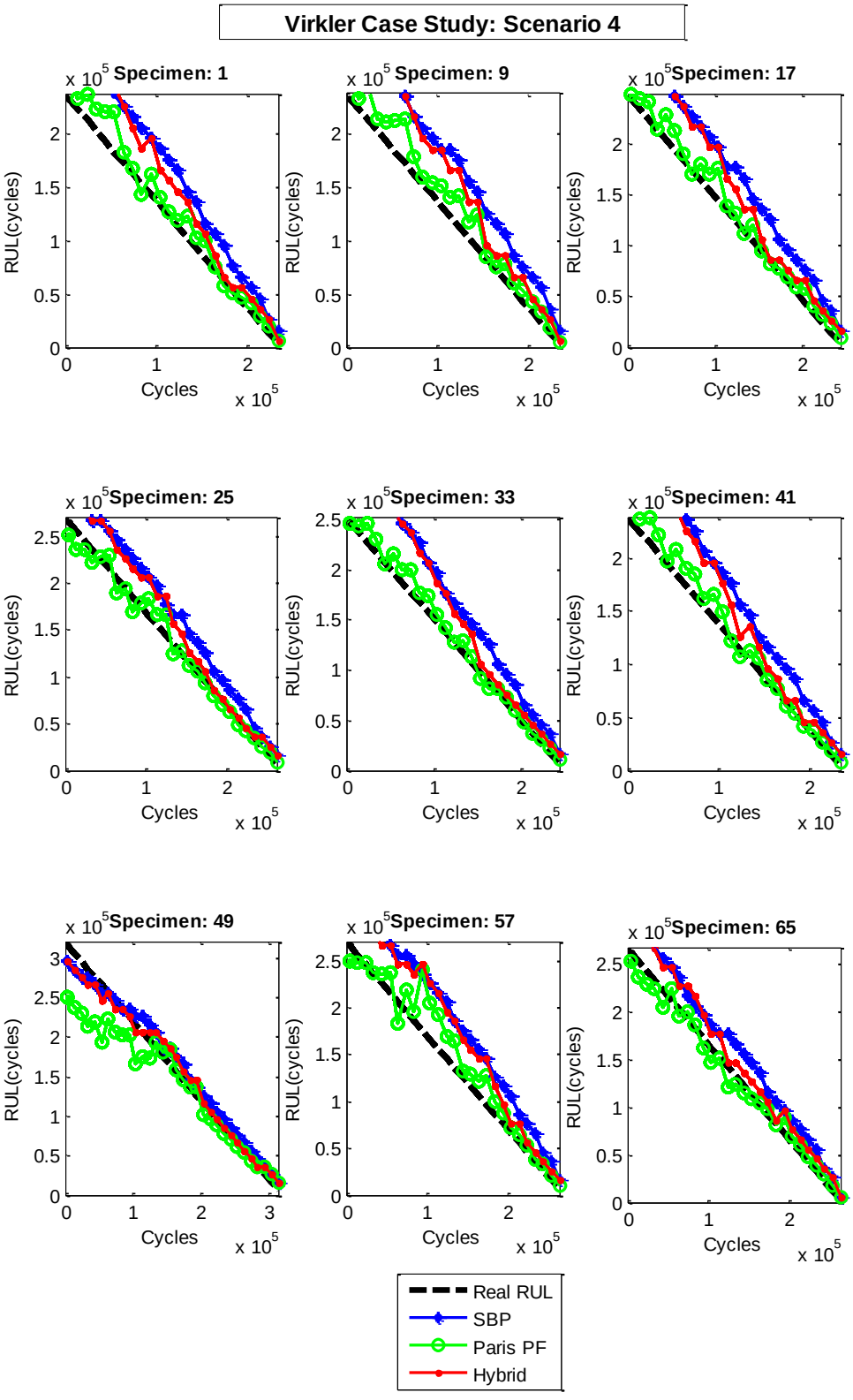

Figure 5.8. RUL results for Virkler dataset scenario 4

As seen in Figure 5.9, not surprisingly the complete PbM provides the highest prognostic performance. Aside from the complete PbM, one needs to focus on the comparison of the hybrid and the incomplete SBP results which reveal the hybrid prognostic efficiency levels. The hybrid model outperforms the SBP; however, the performance differences between the hybrid and incomplete model is not as high as the third scenario performance increase. Nevertheless, the performance increase is an indicator of hybrid integration scheme efficiency.

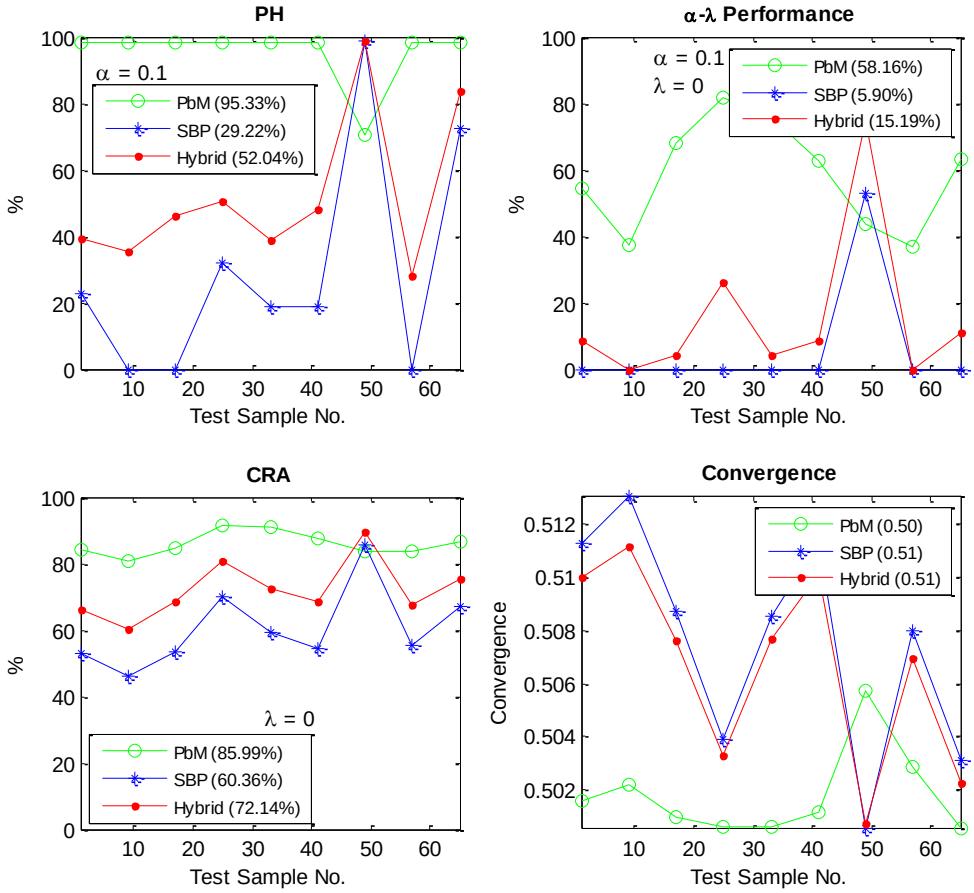

Figure 5.9. Performance results for Virkler dataset scenario 4

Lastly, the fifth scenario, which is thought to be the representative of a real world prognostic scenario results are displayed in Figure 5.10 and Figure 5.11. In this scenario the 'n_1/n_0' ratio is chosen as equal to one where '$n_0 = n_1 = 100$'. This means that the hybrid mechanism is neither biased

towards PbM nor DDM. In addition, in this scenario, both DDM and PbM are incomplete.

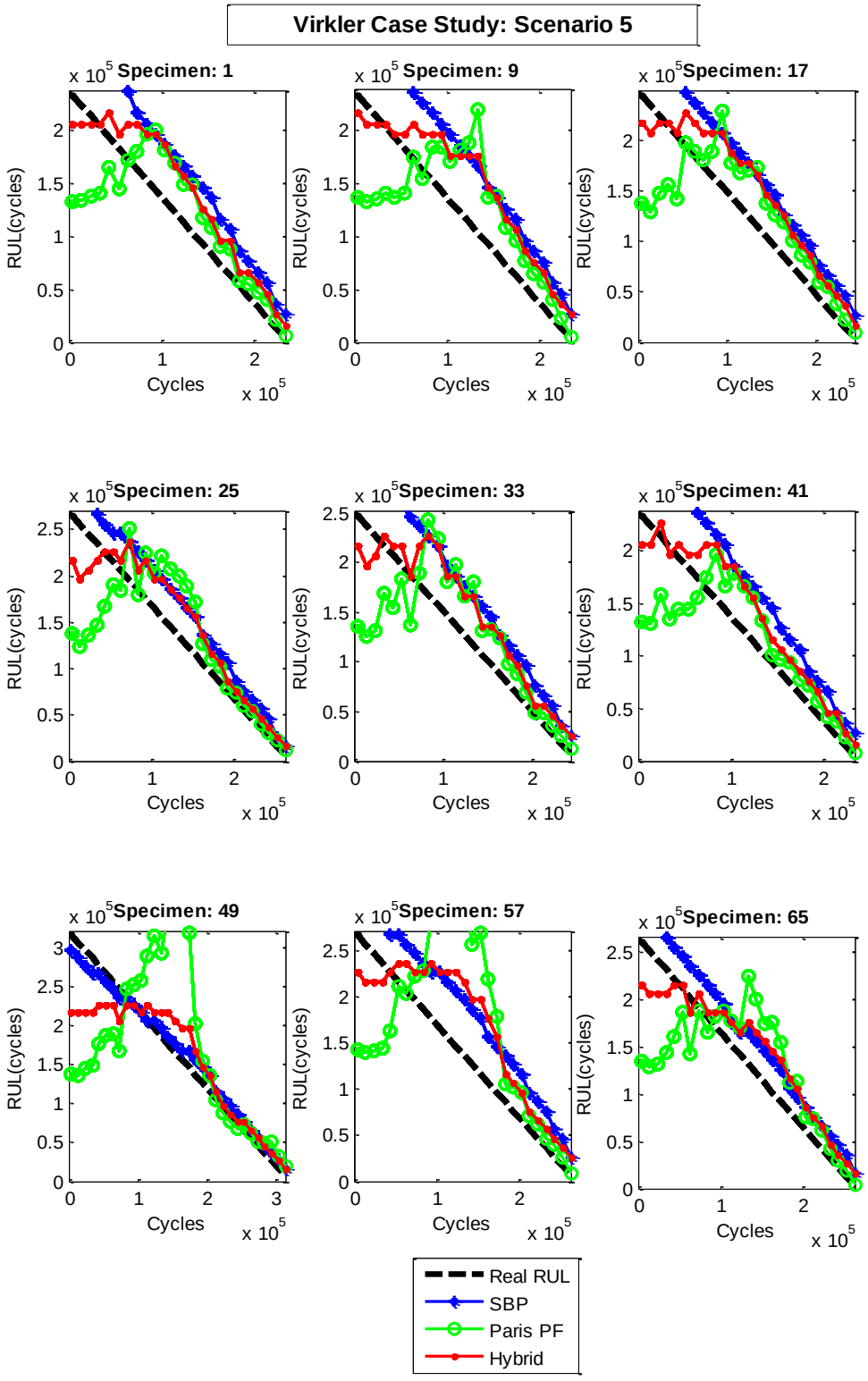

Figure 5.10. RUL results for Virkler dataset scenario 5

However, the results show that the prognostic performance increases when they are integrated together. The performance metric results are shown in Figure 5.11. After the integration, the prognostic horizon of the model increases up to 90% levels in average. The other accuracy metrics (i.e. '$\alpha - \lambda$' performance and cumulative relative accuracy) also indicate that the accuracy escalates after the integration. Noticeably, the model converges faster than the other two, which is also an indicator for performance improvement.

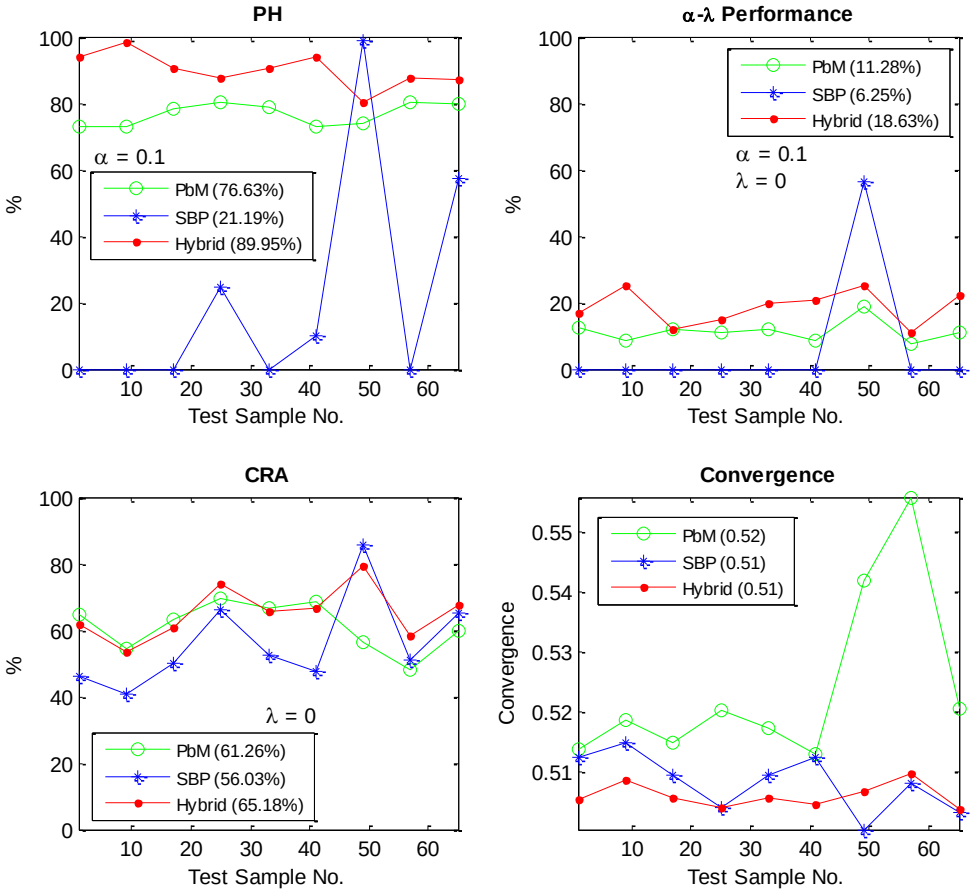

Figure 5.11. Performance results for Virkler dataset scenario 5

In conclusion, considering the results obtained from the all scenarios, the integration scheme yields better prognostic capabilities. Even though both models, contributing to the hybrid model, are incomplete and weak, the integration scheme greatly deals with the problem and subsequently leads to and enhanced performance of the RUL estimations. The next section

presents the results obtained from the experimental clogging dataset case study.

5.3 Filter Clogging Modelling

A detailed discussion on the filter clogging modelling is provided in the previous chapter. In this section, we present the prognostic modelling results of the filter clogging case study. All prognostic models mentioned in the methodology chapter are implemented on the experimental pressure drop dataset. In this context, physics-based, data-driven and the hybrid modelling results are investigated. This section also entails the analysis of model performance evaluation.

The second case study, discussed in section 3.2, involves an experimental test rig setup to produce a prognostic benchmark dataset. The dataset consist of fifty-six run-to-failure samples obtained from well-controlled accelerated filter clogging experiments. The improvements in the system design and data collection mechanism resulted in the collection of reproducible and well organised dataset. A brief summary of the data collection mechanism is provided as follows.

Before the actual data collection, several errands are required to be conducted. The particles are sieved for narrowing the particle size distribution. Therefore, after the sieving, four different groups of particles having different size distribution are obtained. In addition, auxiliary tests with clean water are conducted prior to each run-to-failure experiment. The reason for these preliminary tests is to dispose air and bubbles within the system. Furthermore, these preliminary runs are also useful for calibrating the system parameters before the actual tests.

In addition to different particle size distributions, we have tested different rates of solid fractions in the suspension. Four different solid ratios are determined, ranging from 0.400% to 0.475% levels. As a result, data

collection has been conducted for sixteen different operational profiles each of which have four samples. Exceptionally, the last four profiles have fewer samples compared to the rest of the profiles. Operational profiles are the outcomes of predefined combinations of particle size distribution and solid ratio levels of the suspension.

The tests have been conducted by setting the pump with 211 RPM to produce 600 ml/min flow rate initially. The pressure and flow rate readings have been collected continuously as they are the main indicators of clogging. Each clogging experiment has been conducted and monitored until the filter has clogged up where the pressure drop value has reached its peak and entered into a stable pressure region. The sample rate for the data collection is kept 100Hz. However, for the modelling studies, the signals are down-sampled to 1Hz as shown in Figure 5.12. In the figure, the original signals are represented in blue whereas the sampled signal is the dotted red curve.

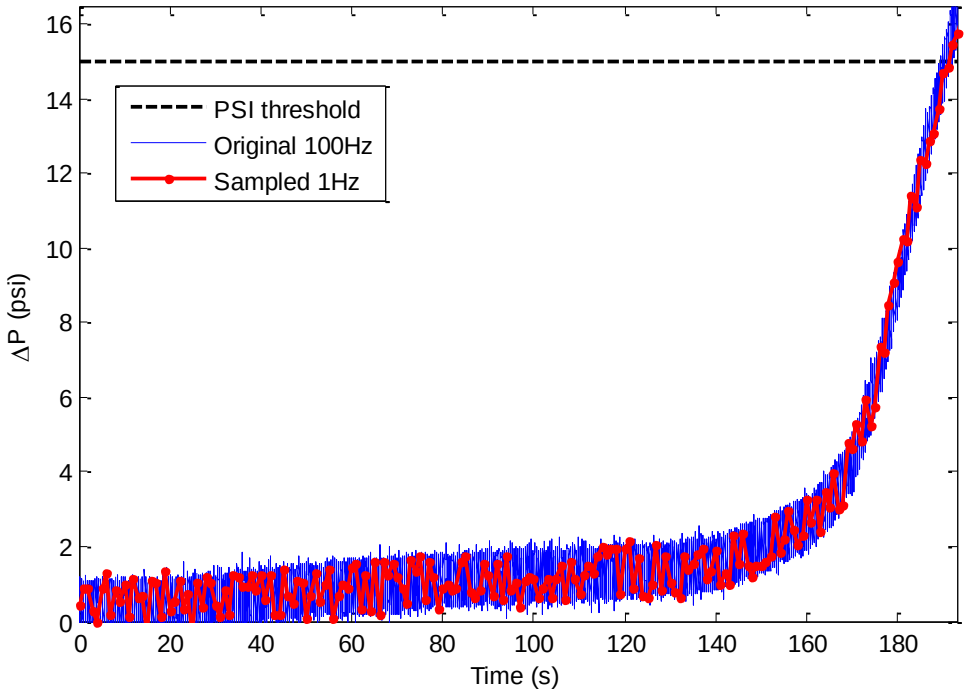

Figure 5.12. Original 100Hz vs 1Hz sampled data for filter clogging dataset

All prognostic models, discussed in the methodology chapter, employ the 1Hz sampled data in order to ease the computational time concerns. The

final look of the entire sampled dataset signals are visualised in Figure 5.13. It is evident in the figure that the signals have an intrinsic noise. If we are to explain the variation within the dataset from top-down level, the threshold hitting spread (i.e. as mentioned before: 36%) is due to the operational profile input variation (i.e. sixteen different operational profiles). For each set in the same operational profile, the variation is measured approximately 3%. The final uncertainty to be considered in the particular signal level is the noise due to the pump pulsations. Even though the system design and well-controlled operational procedures have minimised this effect, pressure drop signals still have the pulsation, hence the noise in the system.

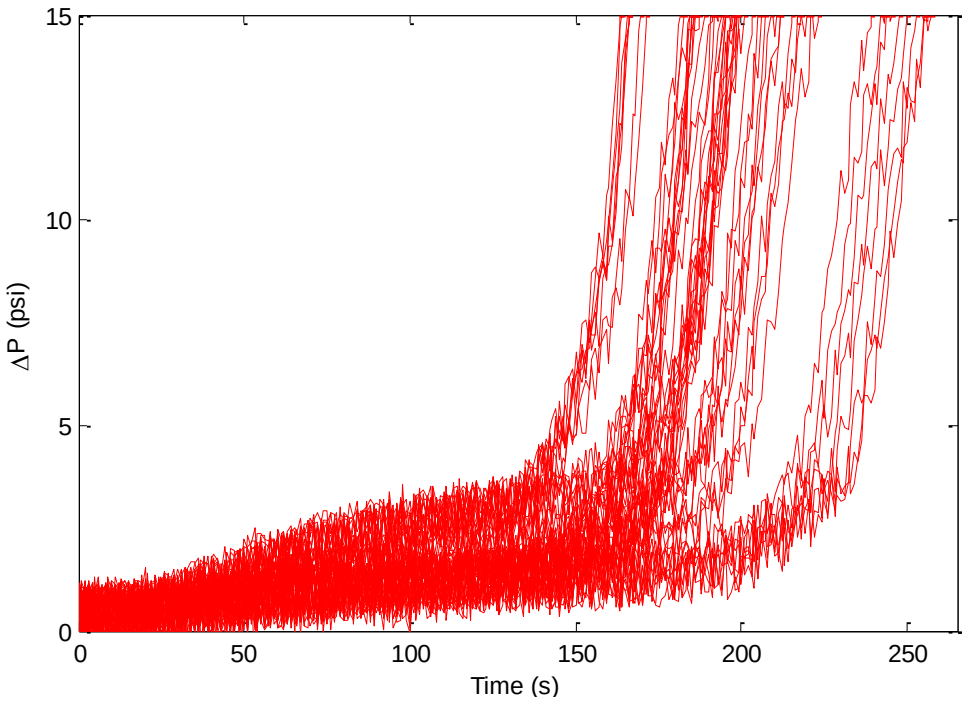

Figure 5.13. Final pressure drop trajectories for filter clogging dataset

However, true pressure drop levels can be estimated by using particle filters. The filter clogging physics-based model comprising of an analytic pressure drop equation and a particle filter mechanism is discussed in section 4.2.3. Briefly, the well-known Ergun equation is discretised and

integrated with particle filters to give a dynamic degradation modelling solution for the filter clogging case study (i.e. Equations. (32, 33)).

The hybrid integration scheme is analysed in five different scenarios, as previously illustrated in Figure 4.8. The same procedures are applied and discussed for the crack propagation degradation scenario in the previous section. Therefore, we will briefly introduce the results and move on to the discussion section, where the efficiency of the integration scheme is examined.

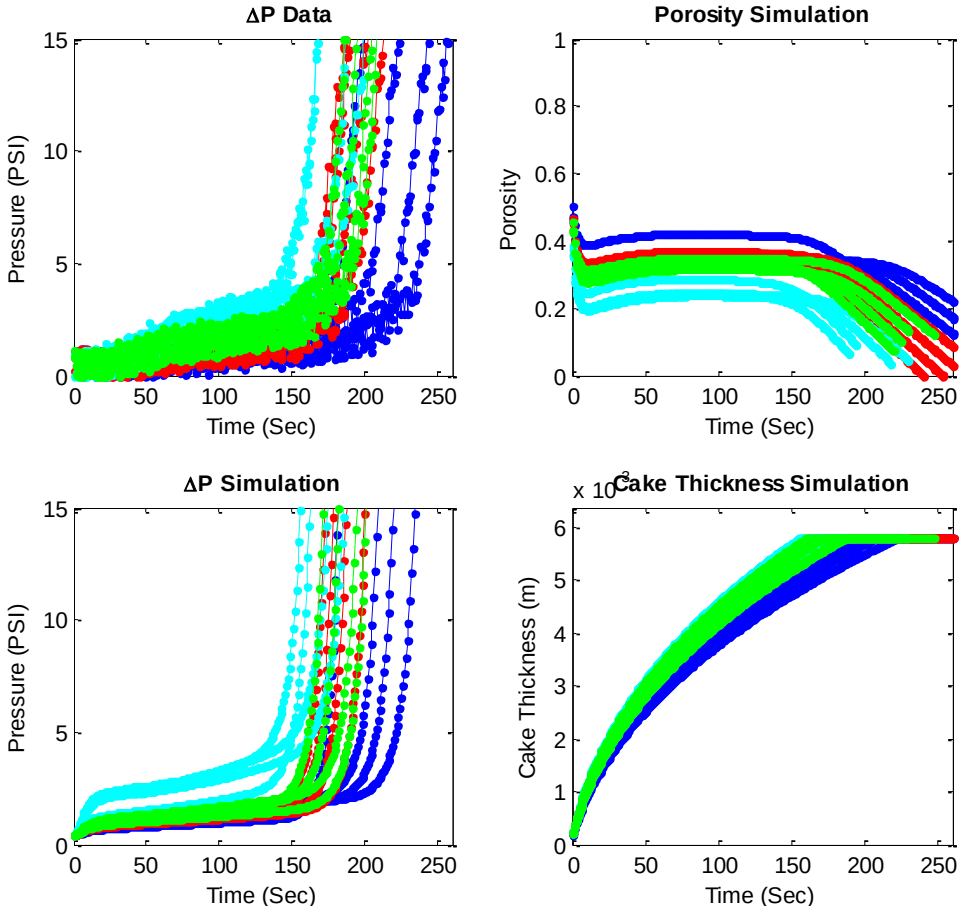

Figure 5.14. Simulation results before Particle Filter integration

The first scenario requires obtaining results from the complete physics-based model. The model we used is the modified Ergun equation integrated with particle filters. The dynamic parameters in the equation such as cake thickness and porosity are simulated via the sphere packing theory. The

simulation results prior to particle filter integration are displayed in Figure 5.14. In the figure, top left plots exemplify the actual pressure drop data for different particle size and solid ratio combinations. Each colour represents a different particle size distribution category. To be more precise, the blue, red, cyan and green colours represent the 45-53, 53-63, 63-75 and the original particle size distributions respectively.

Two separate particle filter mechanisms are integrated into the simulations. The first one tracks the sphere packing cake thickness model whereas the latter tracks the Ergun pressure drop model and its parameters. Figure 5.15 illustrates the demonstration of particle filter mechanisms integrated in the cake thickness and pressure drop modelling. The parameters are learned and updated until 150th second throughout the sample lifetime. Starting from the RUL estimation point, where the measurement input feed is terminated, the model parameters are extrapolated towards the future up to the maximum pressure drop threshold level using the discretised Ergun equation with Monte Carlo simulation. Thus, the RUL distribution at this specific point is obtained by calculating the differences between the RUL estimation starting point time and the times where trajectories (i.e. the number of trajectories is equal to the number of particles) hit the threshold for the first time. In the figure, blue lines represent the median values of the distribution whereas the green curves encapsulate the 95% of the spread within the distribution (i.e. confidence bounds).

For each test specimen, the RUL estimations are set to perform at every five seconds. RUL results of the individual physics-based modelling is analysed along with the fourth scenario. Similarly, the complete data-driven modelling results will be analysed in investigation of the third integration scenario.

The values chosen for the 'n_0' and 'n_1' are the same as the previous case study. Therefore, Table 5-1 is applicable in this case study as well. 'n_0'

stands for the number of latest data points within the signal to be used in similarity calculations for SBP and hybrid modelling. On the other hand, 'n_1' symbolise the number of estimations up to the future via the physics-based model. Therefore the numbers 'n_0' and 'n_1' can be used as the bias between the models. For instance, increasing 'n_0' means involving more data points from the past monitoring data into the similarity calculations which imply the hybrid integration system is biased towards the data-driven model. Contrarily, where the system is biased of physics-based modelling, can be achieved by increasing the 'n_1/n_0' ratio. The integration scheme is biased towards PbM and DDM for the scenarios three and four respectively. For the fifth scenario, the system is not biased as the models (i.e. PbM and DDM) contribute to the hybrid model equally.

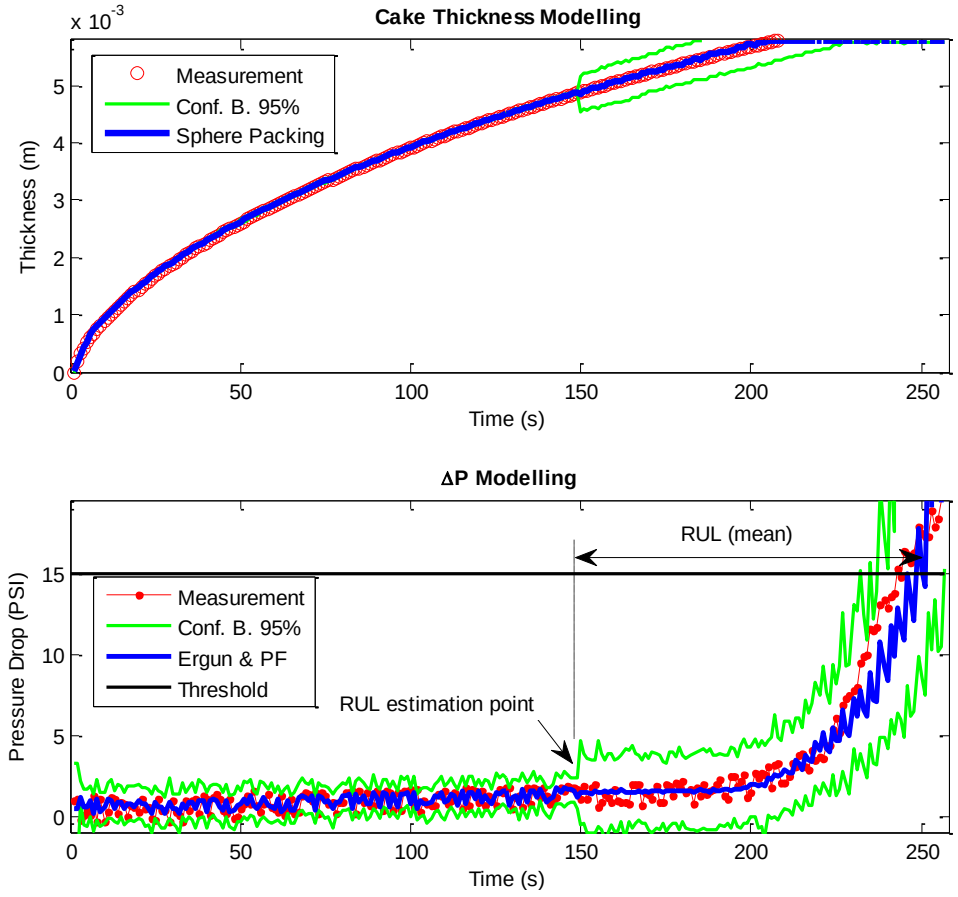

Figure 5.15. Cake thickness and pressure drop modelling

The standard deviation values selected for the measurement 'σ_v' and process noise 'σ_w' are 0.01 and 0.001 respectively. Five hundred numbers of particles are employed for particle filters for all scenarios.

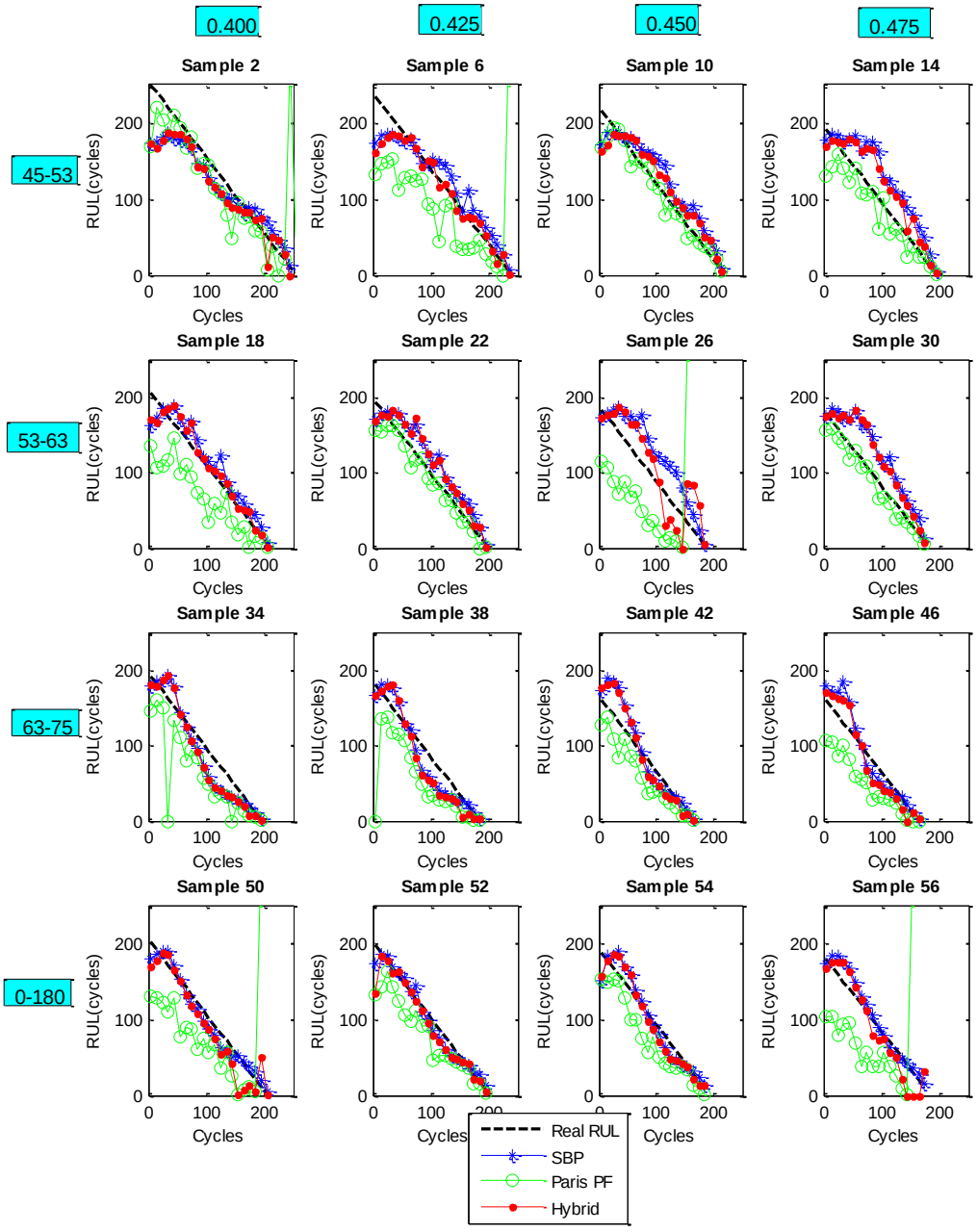

Figure 5.16. RUL results for filter clogging dataset scenario 3

Concisely, Figures (5.16-5.21) can be explained accordingly to the previous explanations of the figures (5.6-5.11) as the same conditions apply for each case study. In Figures (5.16, 5.18, and 5.20) RUL results for sixteen test

samples are shown. Each test sample is a representative of an operational profile. For these figures, the 4x4 matrix plotting mechanism is organised so that the rows represent the particle size distributions while the columns indicate the solid ratio levels. This figure organisation fits the order of operational profiles introduced previously in Table 3-5. For instance, the Sample 42 belongs to the 11th operational profile where the particle size distribution is 63-75 micron range and the solid ratio is 0.45%.

Figure 5.16 displays the RUL results obtained from the incomplete PbM (i.e. Ergun & PF), complete DDM (i.e. modified SBP), and the hybrid models. Figure 5.17 depicts the RUL performance results for each test specimen. Results achieved by the integration scheme outperform the incomplete model as the integration mechanism is biased towards the complete model ('$n_0 \gg n_1$').

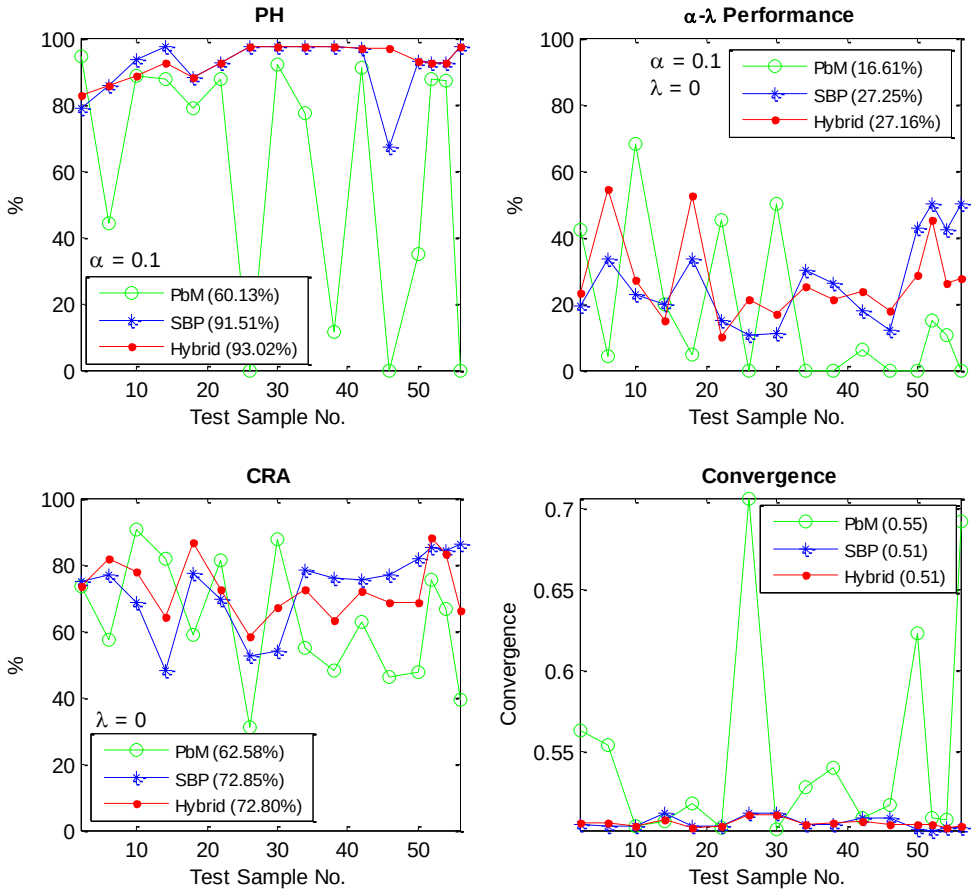

Figure 5.17. Performance results for filter clogging dataset scenario 3

Similarly, Figure 5.18 shows the RUL results obtained from the incomplete DDM, complete PbM and the hybrid models.

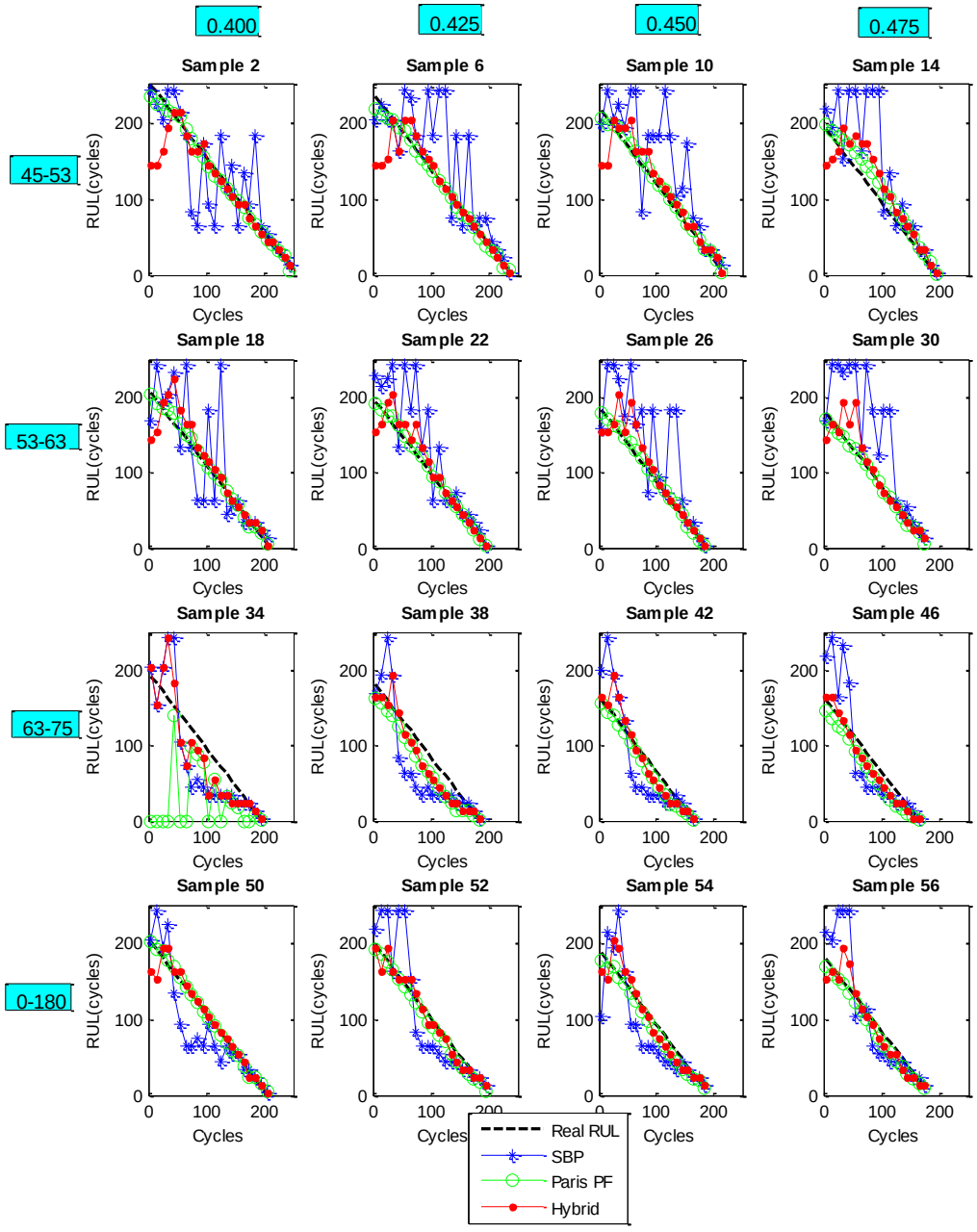

Figure 5.18. RUL results for filter clogging dataset scenario 4

As can be seen in Figure 5.19, the hybrid model increases the prognostic capability of the incomplete model. Finally, non-biased integration scheme results are displayed in Figure 5.20. Equivalently to the previous case

study, the hybrid model performed relatively better than the particular incomplete models, as seen in Figure 5.21.

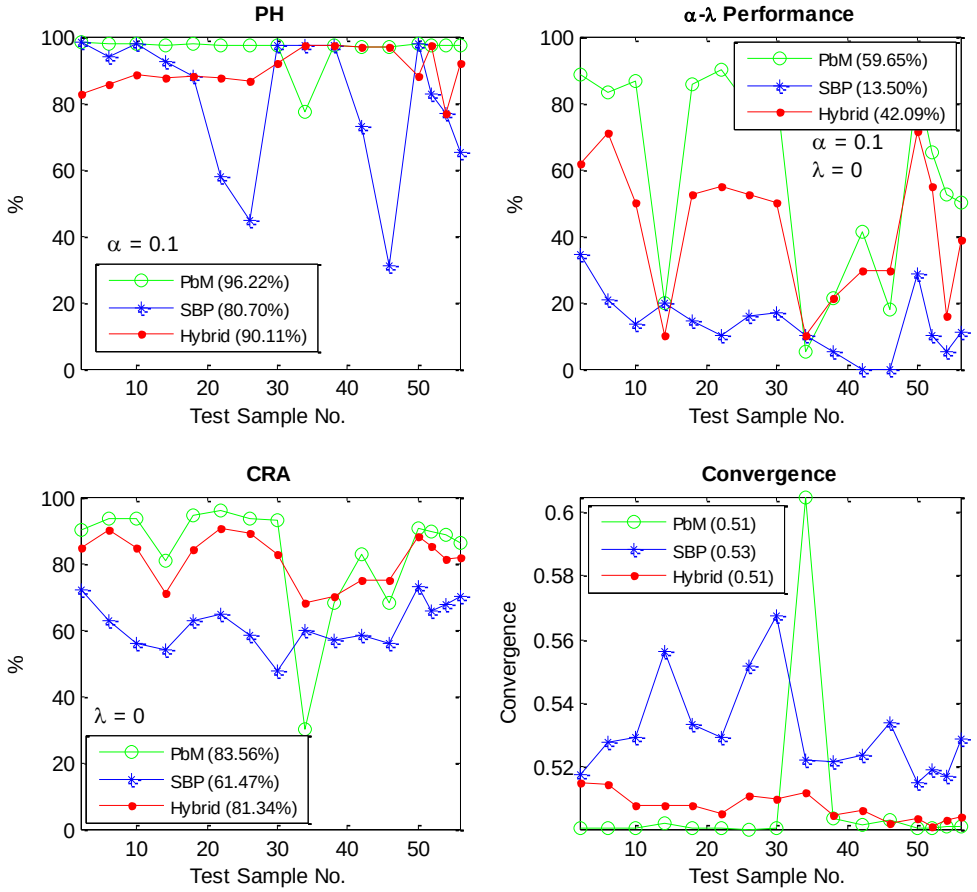

Figure 5.19. Performance results for filter clogging dataset scenario 4

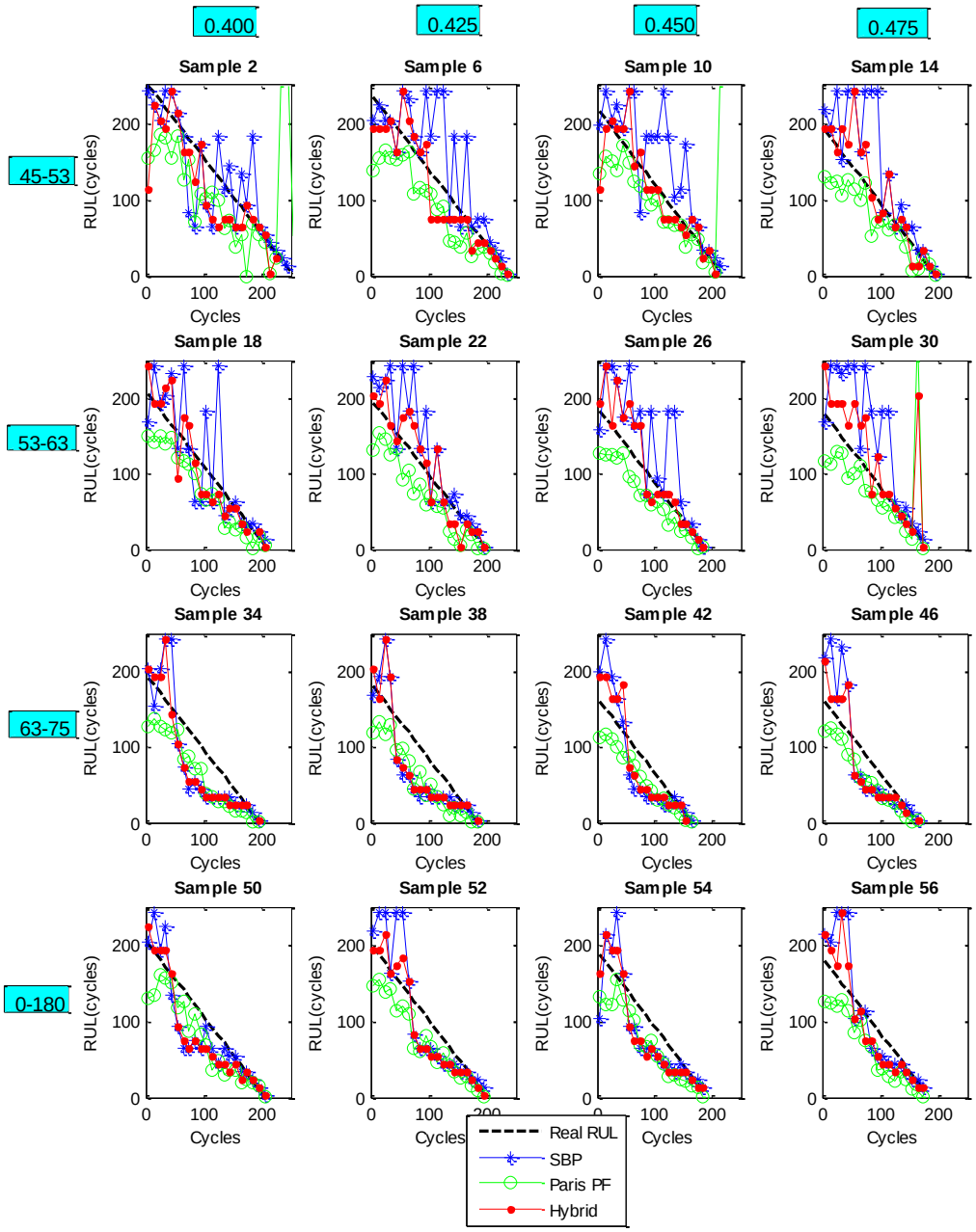

Figure 5.20. RUL results for filter clogging dataset scenario 5

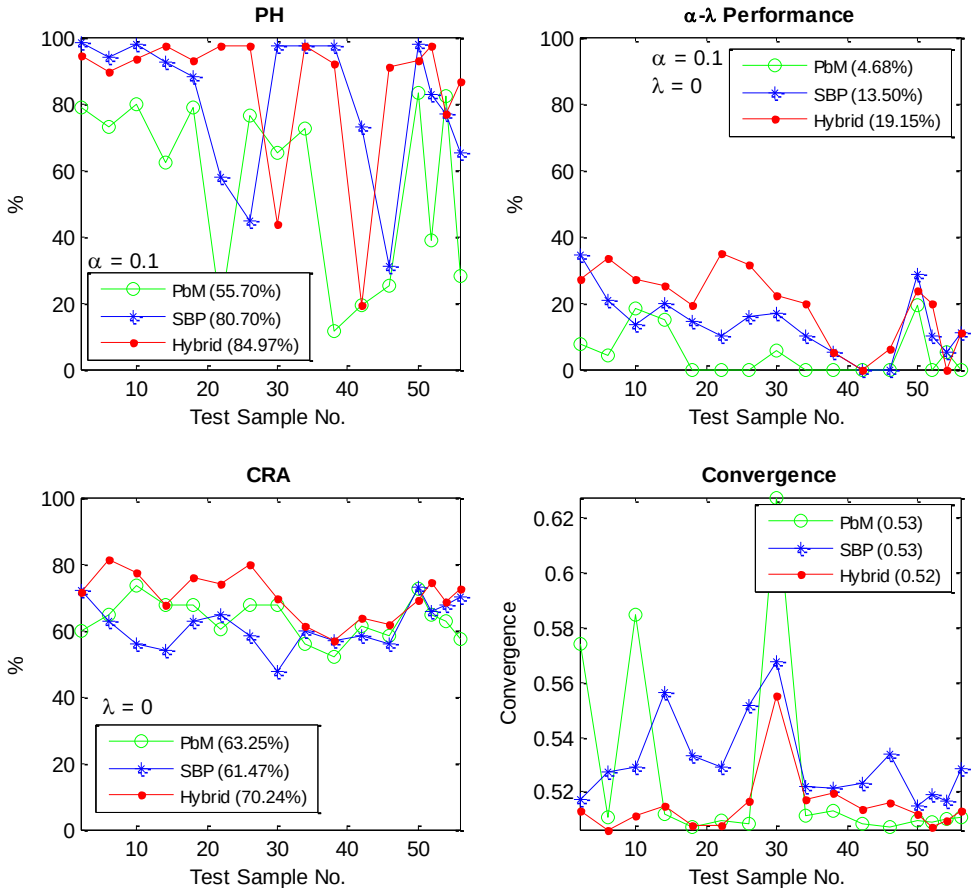

Figure 5.21. Performance results for filter clogging dataset scenario 5

To conclude, considering the results obtained from all scenarios, the integration scheme yields better prognostic capabilities for the filter clogging case study as well as the crack propagation study. Even though both models, contributing to the hybrid model, are incomplete and weak, the integration scheme greatly deals with the problem leading to better performance in RUL estimations. The next section presents the discussion on the RUL results for both case studies.

5.4 Discussion

In this section, we summarise and portray the prognostic performance results obtained from two different engineering case studies. In the first case study, a publicly available fatigue crack propagation dataset (Virkler dataset) is analysed and the prognostic results are obtained. The second

case study is an experimental degradation scenario where several fuel filters are gradually clogged using micron size polymer particles. Performance evaluation metric results are presented in previous sections. In this section, we examine the metric results thoroughly.

Table 5-2 and Table 5-3 organise all prognostic evaluation results for all integration scenarios. In these tables, scenario two and three; one and four are analysed together. PbM(c) and DDM(c) column names indicate that the model is complete, where they belong to the scenarios one and two respectively. Table 5-2 presents the metric measures for the Virkler dataset study, whereas Table 5-3 summarises the filter clogging study performance metric results.

Table 5-2. Performance metrics comparison for crack propagation case study

	Scenario								
	1	2	3		4		5		
	PbM(c)	DDM(c)	PbM	Hybrid	DDM	Hybrid	PbM	DDM	Hybrid
PH (%)	95.33	93.26	75.47	**93.60**	29.22	**52.04**	76.63	21.19	**89.95**
$\alpha - \lambda$ (%)	58.16	68.86	12.71	**67.13**	5.90	**15.19**	11.28	6.25	**18.63**
CRA (%)	85.99	88.42	61.64	**88.85**	60.36	**72.14**	61.26	56.03	**65.18**
Convergence	0.55	0.53	0.57	**0.52**	0.73	**0.65**	**0.59**	1.16	1.02
nRMSE (%)	5.97	4.63	22.46	**4.47**	15.43	**13.07**	23.09	16.56	**13.30**

Table 5-3. Performance metrics comparison for filter clogging case study

	Scenario								
	1	2	3		4		5		
	PbM(c)	DDM(c)	PbM	Hybrid	DDM	Hybrid	PbM	DDM	Hybrid
PH (%)	96.22	91.51	60.13	**93.02**	80.70	**90.11**	55.70	80.70	**84.97**
$\alpha - \lambda$ (%)	59.65	27.25	16.61	**27.16**	13.50	**42.09**	4.68	13.50	**19.15**
CRA (%)	83.56	72.85	62.58	**72.80**	61.47	**81.34**	63.25	61.47	**70.24**
Convergence	0.51	0.51	0.55	**0.51**	0.53	**0.51**	0.53	0.53	**0.52**
nRMSE (%)	7.17	11.09	26.24	**11.20**	25.04	**10.58**	20.30	25.04	**17.60**

In addition to the new prognostic evaluation metrics (i.e. PH, $\alpha - \lambda$ performance, CRA, and convergence), normalised root mean squared error (nRMSE) results are also included in the comparison table. nRMSE metric

results are obtained by normalising the RMSE results with mean lives in the relevant conditions. Thus and so, the nRMSE results can be read as percentage level errors.

The results highlighted with red colour in the tables indicate the highest performance under the group defined scenario. For instance in Table 5-2, for the scenarios one and four, the complete PbM performance levels are higher than the other two in terms of all evaluation metrics. The first three rows are occupied by the prognostic horizon (PH), '$\alpha - \lambda$' performance and cumulative relative accuracy metrics where the higher percentage levels indicate better prognostic performance. On the contrary, for the convergence and nRMSE, higher values indicate poorer performance.

For the combined scenarios one and four, the complete physics-based model is expected to perform the highest. Not surprisingly, the mature PbM outperforms the other two by scoring ten out of ten for both case studies. On the other hand, for the combined scenarios two and three, the complete model DDM was expected to perform the highest. However, the hybrid model produced significantly close results to the mature DDM model, and sometimes producing even better results for both filter clogging and crack propagation studies. This can be explained as the integration scheme is based on the similarity-based data-driven model. Hence, the PbM future estimations add value rather than corrupting the model. However, integrating these future estimations do not enhance the immatured SBP model as such.

The previous scenarios are the auxiliary cases to measure the efficiency of integration and bias adjusting. The fifth scenario can be taken as a basis for the hybrid performance as it is considered as the real life prognostic scenario, where both PbM and DDM are immature. If we inspect the tables for both cases, the hybrid model performance is the best for nine out of ten metrics. This indicates that integration mechanism enhances the prognostic

capability in general. Also the results show that using an individual model will not produce robust outputs. For example, the DDM prognostic horizon encapsulates 80% of filter clogging lifetime. However, the same data-driven model produces roughly 20% prognostic horizon levels for the crack propagation case. However, the integration scheme brings the robustness where the PH percentage level remains approximately 85% for both cases.

To conclude, one of the main goals for this research was to develop a generic integration scheme to be used in hybrid modelling, in which incomplete data-driven and physics-based models are integrated. The results obtained from two engineering case studies verify that the integration scheme produces better prognostic results compared to the particular models which contribute to the hybrid mechanism. Therefore, this integration scheme is anticipated to be applied to other engineering cases to enhance the accuracy of the estimations. The following chapter concludes the thesis work and outlines the future works.

Chapter 6

Conclusions & Future Work

Prognostics is the key component of IVHM technologies, which generally involves system monitoring, fault detection and diagnostics, failure prognostics and operating management. System monitoring, fault detection and diagnostics are relatively mature comparatively to prognostics. Despite the immaturity of prognostics field, in recent years the importance of the prognostics has been comprehended by the industry as well as research communities.

The heart of the prognostics is to calculate remaining useful life of the engineering asset precisely, which could lead to avoidance of the incidents / accidents peculiarly in the safety critical industry such as aviation, nuclear and military. The benefits of prognostics are to provide cost effectiveness, increased safety and availability via better maintenance planning.

There are several different approaches to achieve prognostic results. Physics-based and data-driven approaches are two of the most commonly used prognostic models in the industry / academia. Both approaches have their own pros and cons; therefore, the aim was to develop a hybrid prognostic model to leverage the strengths of both approaches whilst avoiding the cons where possible. The idea of combining prognostic models

to achieve hybrid prognostics is of great importance, hence the research community started to develop hybrid models.

In this research we provide a generic integration scheme for prognostic models to enhance the prediction accuracy and robustness. This research not only intends to make contribution on the concept of hybrid approach, but also manifests a generic prognostic integration scheme, an experimental prognostic benchmark dataset, a physics-based prognostic model of the clogging filter phenomena, and a number of modifications to improve a data-driven prognostic approach. Furthermore, a comprehensive literature survey on hybrid prognostic models is provided.

For this study, in order to be able to analyse the integration scheme, it is found to be necessary to work on an engineering case where the degradation mechanism is not extremely complex, enabling to model the component/system physics accurately as well as providing a means for data-driven modelling. For this reason, a comprehensive dataset eligibility analysis is conducted on the prognostic datasets available online. The Virkler fatigue crack growth dataset has found to be the suitable for this research purposes. However, an experimental rig has also setup to produce a prognostic benchmark dataset. Therefore, a simple filter clogging test rig has been designed and clogging indicators have been monitored throughout the accelerated aging experiments. In addition, several improvements have been made aiming to collect reproducible signals from different operational profiles.

A novel hybrid prognostic integration scheme has been developed where a data-driven and a physics-based model are integrated, aiming to improve the prognostic output. In this research, a similarity-based prognostics approach is explored for data-driven modelling purposes. A number of modifications have been made to increase the model's applicability and robustness. The modified model has been implemented on both case studies

and remaining useful life (RUL) estimation results are obtained. On the other hand, two physics-based models, accommodating two different degradation mechanisms, are implemented for each case study. The prognostic performance results show that the both physics-based and data-driven models predict the system behaviour accurately which led to successful RUL predictions. Note that, the physics-based model for the filter clogging scenario which involves the integration of particle filters with modified version of the Ergun equation is a novel contribution devoted to the literature.

However, in real-world conditions it is found to be very difficult to obtain highly accurate prognostic results due to the difficulties and limitations of data sources and the knowledge base. In order to mimic this fact, the models are deliberately weakened to produce less accurate and less price estimations. The integration methodology is tested on the mixture of these weakened and complete models. The results are scrutinised based on the new performance evaluation metrics designed for prognostic results. The results from the both case studies reveal that the integration scheme enhances the RUL prediction accuracy considerably. Furthermore, it can be observed the proposed generic hybrid integration scheme has potential to be applicable in a real world environment.

The key areas for the future work will include the investigation of the hybrid integration scheme capabilities. Several improvements can be made on the hybrid mechanism such as adapting more advanced similarity measures within the integration scheme. In addition, an investigation on the reduction of computational complexity for the integration methodology will greatly help in a potential instrumentation phase.

Furthermore, some future work can be expected to further explore the data collection mechanism, test rig design and publication of the collected clogging dataset for prediction and prognostic competitions. Also the dataset

can further serve a purpose as a benchmark dataset for prognostic algorithms to be tested on.

References

Abbas, M., Ferri, A. A., Orchard, M. E. and Vachtsevanos, G. J. (2007), "An Intelligent Diagnostic/Prognostic Framework for Automotive Electrical Systems", *Intelligent Vehicles Symposium, 2007 IEEE,* pp. 352.

Abboud, N. M. and Corapcioglu, M. Y. (1993), "Modeling of Compressible Cake Filtration", *Journal of colloid and interface science,* vol. 160, no. 2, pp. 304-316.

Advantech Mfg. (2013), *Test Sieving: Principles and Procedures*, available at: http://store.solutionsdirectonline.com/articles/test-sieves-technical-specifications.htm (accessed 05/15).

Agogino, A. and Goebel, K., (2007), *Mill Dataset*, BEST lab, UC Berkeley. NASA Ames Prognostics Data Repository, [http://ti.arc.nasa.gov/project/prognostic-data-repository], NASA Ames, Moffett Field, CA.

Ak, R., Li, Y. F., Vitelli, V. and Zio, E. (2013), "A Genetic Algorithm and Neural Network Technique for Predicting Wind Power under Uncertainty ", *Chemical Engineering Transactions,* vol. 33, pp. 925-930.

An, D., Choi, J. and Kim, N. H. (2013), "Prognostics 101: A tutorial for particle filter-based prognostics algorithm using Matlab", *Reliability Engineering & System Safety,* vol. 115, no. 0, pp. 161-169.

Banjevic, D. and Jardine, A. K. S. (2006), "Calculation of reliability function and remaining useful life for a Markov failure time process", *IMA Journal Management Mathematics,* vol. 17, no. 2, pp. 115-130.

Baraldi, P., Compare, M., Sauco, S. and Zio, E. (2012), "Fatigue Crack Growth Prognostics by Particle Filtering and Ensemble Neural Networks", *1st european conference of the prognostics and health management society 2012,* Vol. 3, 2012, Dresden, Germany, PHM Society, Dresden, Germany, .

Baraldi, P., Di Maio, F., Mangili, F. and Zio, E. (2013), "A belief function theory method for prognostics in clogging filters", *Chemical Engineering Transactions,* vol. 33, pp. 847-852.

Baraldi, P., Mangili, F. and Zio, E. (2015), "A prognostics approach to nuclear component degradation modeling based on Gaussian Process Regression", *Progress in Nuclear Energy,* vol. 78, no. 0, pp. 141-154.

Bartram, G. and Mahadevan, S. (2012), "Prognostics and health monitoring in the presence of heterogeneous information", *Annual Conference of the Prognostics and Health Management Society 2012,* Vol. 3, 2012, Minneapolis, Minnesota, USA, PHM Society, Minneapolis, Minnesota, USA, .

Baruah, P. and Chinnam, R. B. (2005), "HMMs for diagnostics and prognostics in machining processes", *International Journal of Production Research,* vol. 43, no. 6, pp. 1275-1293.

Bechhoefer, E. (2008), "A method for generalized prognostics of a component using Paris law", *ANNUAL FORUM PROCEEDINGS-AMERICAN HELICOPTER SOCIETY,* vol. 64, no. 2, pp. 1460.

Benedettini, O., Baines, T. S., Lightfoot, H. W. and Greenough, R. M. (2009), "State-of-the-art in integrated vehicle health management", *Proceedings of the Institution of Mechanical Engineers, Part G: Journal of Aerospace Engineering,* vol. 223, no. 2, pp. 157-170.

Biagetti, T. and Sciubba, E. (2004), "Automatic diagnostics and prognostics of energy conversion processes via knowledge-based systems", *Energy,* vol. 29, no. 12-15 SPEC. ISS., pp. 2553-2572.

Bigerelle, M., Najjar, D., Fournier, B., Rupin, N. and Iost, A. (2006), "Application of Lambda Distributions and Bootstrap analysis to the prediction of fatigue lifetime and confidence intervals", *International Journal of Fatigue,* vol. 28, no. 3, pp. 223-236.

Brotherton, T., Jahns, G., Jacobs, J. and Wroblewski, D. (2000), "Prognosis of faults in gas turbine engines", *IEEE Aerospace Conference Proceedings,* Vol. 6, pp. 163.

Brown, P. and Sondalini, M. (2014), *The Evolution of Maintenance Practices*, available at: http://www.lifetime-reliability.com/free-articles/maintenance-management/Evolution_of_Maintenance_Practices.pdf (accessed 17/11).

Bunks, C., McCarthy, D. and Al-Ani, T. (2000), "Condition-based maintenance of machines using hidden Markov models", *Mechanical Systems and Signal Processing,* vol. 14, no. 4, pp. 597-612.

Butler, K. L. (1996), "Expert system based framework for an incipient failure detection and predictive maintenance system", *Proceedings of the International Conference on Intelligent Systems Applications to Power Systems, ISAP,* pp. 321.

Butler, S. and Ringwood, J. (2010), "Particle filters for remaining useful life estimation of abatement equipment used in semiconductor manufacturing", *Control and Fault-Tolerant Systems (SysTol), 2010 Conference on,* pp. 436.

Byington, C. S., Watson, M. and Edwards, D. (2004a), "Data-driven neural network methodology to remaining life predictions for aircraft actuator components", *Aerospace Conference, 2004. Proceedings. 2004 IEEE,* Vol. 6, pp. 3581.

Byington, C. S., Watson, M., Edwards, D. and Stoelting, P. (2004b), "A model-based approach to prognostics and health management for flight control actuators", *IEEE Aerospace Conference Proceedings,* Vol. 6, pp. 3551.

Cadini, F., Zio, E. and Avram, D. (2009), "Monte Carlo-based filtering for fatigue crack growth estimation", *Probabilistic Engineering Mechanics,* vol. 24, no. 3, pp. 367-373.

Camci, F. (2005), *Process monitoring, diagnostics and prognostics using support vector machines and hidden Markov models* (PhD thesis), Graduate School of Wanye State University, Detroit, Lambert Academic Publishing.

Camci, F. and Chinnam, R. B. (2010), "Health-state estimation and prognostics in machining processes", *IEEE Transactions on Automation Science and Engineering,* vol. 7, no. 3, pp. 581-597.

Camci, F., Medjaher, K., Zerhouni, N. and Nectoux, P. (2012), "Feature Evaluation for Effective Bearing Prognostics", *Quality and Reliability Engineering International,* .

Carman, P. G. (1997), "Fluid flow through granular beds", *Chemical Engineering Research and Design,* vol. 75, no. 1 SUPPL., pp. S32-S46.

Celaya, J., Saxena, A., Saha, S. and Goebel, K. (2011), "Prognostics of power mosfets under thermal stress accelerated aging using data-driven and model-based methodologies", *Annual Conference of the Prognostics and Health Management Society,* 2011, Montreal, Canada, PHM Society, Montreal, Canada, .

Celaya, J., Wysocki, P. and Goebel, K., (2009), *IGBT accelerated aging data set*, NASA Ames Prognostics Data Repository, [/tech/dash/pcoe/prognostic-data-repository/], NASA Ames, Moffett Field, CA.

Cempel, C., Natke, H. G. and Tabaszewski, M. (1997), "A passive diagnostic experiment with ergodic properties", *Mechanical Systems and Signal Processing,* vol. 11, no. 1, pp. 107-117.

Chelidze, D. and Cusumano, J. P. (2004), "A dynamical systems approach to failure prognosis", *Journal of Vibration and Acoustics, Transactions of the ASME,* vol. 126, no. 1, pp. 2-8.

Chen, C., Zhang, B., Vachtsevanos, G. and Orchard, M. (2011), "Machine Condition Prediction Based on Adaptive Neuro–Fuzzy and High-Order Particle Filtering", *Industrial Electronics, IEEE Transactions on,* vol. 58, no. 9, pp. 4353-4364.

Chen, C., Vachtsevanos, G. and Orchard, M. E. (2012), "Machine remaining useful life prediction: An integrated adaptive neuro-fuzzy and high-order particle filtering approach", *Mechanical Systems and Signal Processing,* vol. 28, no. 0, pp. 597-607.

Chen, Z. (2003), "Bayesian filtering: From Kalman filters to particle filters, and beyond", *Statistics,* vol. 182, no. 1, pp. 1-69.

Cheng, S. and Pecht, M. (2007), "Multivariate state estimation technique for remaining useful life prediction of electronic products", *AAAI Fall Symposium on Artificial Intelligence for Prognostics,* November, Arlington, VA, USA, pp. 26-32.

Cheng, S. and Pecht, M. (2009), "A fusion prognostics method for remaining useful life prediction of electronic products", *2009 IEEE International Conference on Automation Science and Engineering, CASE 2009,* pp. 102.

Cheremisinoff, N. P. (1998), *Liquid Filtration,* Second Edition ed, Elsevier Inc.

Chinnam, R. B. and Baruah, P. (2004), "A neuro-fuzzy approach for estimating mean residual life in condition-based maintenance systems", *International Journal of Materials and Product Technology,* vol. 20, no. 1-3, pp. 166-179.

Choi, S. S., Kang, K. S., Kim, H. G. and Chang, S. H. (1995), "Development of an on-line fuzzy expert system for integrated alarm processing in nuclear power plants", *IEEE Transactions on Nuclear Science,* vol. 42, no. 4 pt 2, pp. 1406-1418.

Cox, D. R. (1972), "Regression models and life-tables", *Journal of the Royal Statistical Society. Series B (Methodological),* vol. 34, no. 2, pp. 187-220.

Cross, R.J., Makeev, A. and Armanios, E., (2006), *A comparison of predictions from probabilistic crack growth models inferred from Virkler's data*.

Cui, H. (2005), "Accelerated temperature cycle test and Coffin-Manson model for electronic packaging", *Reliability and Maintainability Symposium, 2005. Proceedings. Annual,* pp. 556.

Daigle, M., (2014), *Model based prognostics (Tutorial)*, PHM Society.

Daigle, M. and Goebel, K. (2010), "Model-based prognostics under limited sensing", *IEEE Aerospace Conference Proceedings,* .

Daigle, M. J. and Goebel, K. (2013), "Model-Based Prognostics With Concurrent Damage Progression Processes", *Systems, Man, and Cybernetics: Systems, IEEE Transactions on,* vol. 43, no. 3, pp. 535-546.

Dempsey, P. J., Kreider, G. and Fichter, T. (2006), "Investigation of tapered roller bearing damage detection using oil debris analysis", *Aerospace Conference, 2006 IEEE,* pp. 11 pp.

Diamanti, K. and Soutis, C. (2010), "Structural health monitoring techniques for aircraft composite structures", *Progress in Aerospace Sciences,* vol. 46, no. 8, pp. 342-352.

Dmitry, K. and Dmitry, V. (2004), "An algorithm for rule generation in fuzzy expert systems", *Pattern Recognition, 2004. ICPR 2004. Proceedings of the 17th International Conference on,* Vol. 1, pp. 212.

Dong, M. and He, D. (2007a), "Hidden semi-Markov model-based methodology for multi-sensor equipment health diagnosis and prognosis", *European Journal of Operational Research,* vol. 178, no. 3, pp. 858-878.

Dong, M. and He, D. (2007b), "A segmental hidden semi-Markov model (HSMM)-based diagnostics and prognostics framework and methodology", *Mechanical Systems and Signal Processing,* vol. 21, no. 5, pp. 2248-2266.

Dong, M., He, D., Banerjee, P. and Keller, J. (2006), "Equipment health diagnosis and prognosis using hidden semi-Markov models", *International Journal of Advanced Manufacturing Technology,* vol. 30, no. 7-8, pp. 738-749.

Dong, Y. -., Gu, Y. -., Yang, K. and Zhang, W. -. (2004), "A combining condition prediction model and its application in power plant",

Proceedings of 2004 International Conference on Machine Learning and Cybernetics, Vol. 6, pp. 3474.

Du, S., Lv, J. and Xi, L. (2012), "Degradation process prediction for rotational machinery based on hybrid intelligent model", *Robotics and Computer-Integrated Manufacturing,* vol. 28, no. 2, pp. 190-207.

Eker, O. F., Camci, F. and Jennions, I. K. (2013), "Filter Clogging Data Collection for Prognostics", *Proceedings of the Annual Conference of the Prognostics and Health Management Society,* 14-17 Oct 2013, New Orleans LA, USA, pp. 624-632.

Eker, O. F., Camci, F. and Jennions, I. K. (2014), "Physics-based Degradation Modelling for Filter Clogging", *2nd European Conference of the Prognostics and Health Management Society,* 2014, Nantes, France, PHM Society, Nantes, France, .

Eker, O. F. and Camci, F. (2012), "State-Based Prognostics with State Duration Information", *Quality and Reliability Engineering International,* .

Eker, O. F., Camci, F., Guclu, A., Yilboga, H., Sevkli, M. and Baskan, S. (2011), "A simple state-based prognostic model for railway turnout systems", *IEEE Transactions on Industrial Electronics,* vol. 58, no. 5, pp. 1718-1726.

Endo, Y., Chen, D. -. and Pui, D. Y. H. (1998), "Effects of particle polydispersity and shape factor during dust cake loading on air filters", *Powder Technology,* vol. 98, no. 3, pp. 241-249.

Ergun, S. (1952), "Fluid Flow through Packed Columns", *Chemical Engineering and Processing,* vol. 48, pp. 89-94.

Fan, J., Yung, K. and Pecht, M. (2015), "Predicting long-term lumen maintenance life of LED light sources using a particle filter-based prognostic approach", *Expert Systems with Applications,* vol. 42, no. 5, pp. 2411-2420.

Farrar, C.R. and Worden, K., (2007), *An introduction to structural health monitoring*.

Farrar, C. R. and Lieven, N. A. J. (2007), "Damage prognosis: the future of structural health monitoring", *Philosophical Transactions of the Royal Society of London A: Mathematical, Physical and Engineering Sciences,* vol. 365, no. 1851, pp. 623-632.

Feng, E., Yang, H. and Rao, M. (1998), "Fuzzy expert system for real-time process condition monitoring and incident prevention", *Expert Systems with Applications,* vol. 15, no. 3–4, pp. 383-390.

Garga, A. K., McClintic, K. T., Campbell, R. L., Chih-Chung Yang, Lebold, M. S., Hay, T. A. and Byington, C. S. (2001), "Hybrid reasoning for prognostic learning in CBM systems", *Aerospace Conference, 2001, IEEE Proceedings.* Vol. 6, pp. 2957.

Gebraeel, N. Z., Lawley, M. A., Li, R. and Ryan, J. K. (2005), "Residual-life distributions from component degradation signals: A Bayesian approach", *IIE Transactions,* vol. 37, no. 6, pp. 543-557.

Gebraeel, N., Elwany, A. and Jing Pan (2009), "Residual Life Predictions in the Absence of Prior Degradation Knowledge", *Reliability, IEEE Transactions on,* vol. 58, no. 1, pp. 106-117.

Gebraeel, N., Lawley, M., Liu, R. and Parmeshwaran, V. (2004), "Residual life predictions from vibration-based degradation signals: a neural network approach", *Industrial Electronics, IEEE Transactions on,* vol. 51, no. 3, pp. 694-700.

Gebraeel, N. Z. and Lawley, M. A. (2008), "A neural network degradation model for computing and updating residual life distributions", *IEEE Transactions on Automation Science and Engineering,* vol. 5, no. 1, pp. 154-163.

Goebel, K., Eklund, N. and Bonanni, P. (2006), "Fusing competing prediction algorithms for prognostics", *Aerospace Conference, 2006 IEEE,* pp. 10 pp.

Goebel, K. and Eklund, N. (2007), "Prognostic Fusion for Uncertainty Reduction", in American Institute of Aeronautics and Astronautics, .

Gola, G. and Nystad, B. H. (2011), "From measurements collection to remaining useful life estimation: defining a diagnostic-prognostic frame for optimal maintenance scheduling of choke valves undergoing erosion", *Annual Conference of the Prognostics and Health Management Society 2011,* Vol. 2, 2011, Montreal, Quebec, Canada, PHM Society, Montreal, Quebec, Canada, .

Goode, K. B., Moore, J. and Roylance, B. J. (2000), "Plant machinery working life prediction method utilizing reliability and condition-monitoring data", *Proceedings of the Institution of Mechanical Engineers, Part E: Journal of Process Mechanical,* vol. 214, no. 2, pp. 109-122.

A. Goodnough. (2005) "All 20 Killed as Seaplane Crashes Off Miami Beach", *The New York Times,* .

Gray, J. (1845), "On the causes of the great Versailles railway accident", *Journal of the Franklin Institute,* vol. 39, no. 6, pp. 371.

Guclu, A., Yilboga, H., Eker, O. F. and Camci, F. (2010a), "Classification of Uncertain Data Streams Using Modified K-Nearest Neighbor Method: A Case Study on Railway Turnouts", *International Symposium on INnovations in Intelligent SysTems and Applications, Kayseri & Cappadocia, Turkey,* 21-24 June 2010, .

Guclu, A., Yılboga, H., Eker, O. F., Camci, F. and Jennions, I. (2010b), "Prognostics with Autoregressive Moving Average for Railway Turnouts", *Annual Conference of Prognostics and Health Management Society, Portland, Oregon, USA,* 10-14 October 2010, .

Hamachi, M. and Mietton-Peuchot, M. (2001), "Cake thickness measurement with an optical laser sensor", *Chemical Engineering Research and Design,* vol. 79, no. 2, pp. 151-155.

Hansen, R. J., Hall, D. L. and Kurtz, S. K. (1995), "A New Approach to the Challenge of Machinery Prognostics", *Journal of Engineering for Gas Turbines and Power,* vol. 117, no. 2, pp. 320-325.

Hecht, H. (2006), "Why prognostics for avionics?", *IEEE Aerospace Conference Proceedings,* Vol. 2006, .

Heimes, F. O. (2008), "Recurrent neural networks for remaining useful life estimation", *Prognostics and Health Management, 2008. PHM 2008. International Conference on,* pp. 1.

Heng, A., Zhang, S., Tan, A. C. C. and Mathew, J. (2009), "Rotating machinery prognostics: State of the art, challenges and opportunities", *Mechanical Systems and Signal Processing,* vol. 23, no. 3, pp. 724-739.

Herzog, M. A., Marwala, T. and Heyns, P. S. (2009), "Machine and component residual life estimation through the application of neural networks", *Reliability Engineering & System Safety,* vol. 94, no. 2, pp. 479-489.

Hu, C., Youn, B. D. and Chung, J. (2012), "A multiscale framework with extended Kalman filter for lithium-ion battery SOC and capacity estimation", *Applied Energy,* vol. 92, no. 0, pp. 694-704.

Huang, R., Xi, L., Li, X., Richard Liu, C., Qiu, H. and Lee, J. (2007), "Residual life predictions for ball bearings based on self-organizing map and back propagation neural network methods", *Mechanical Systems and Signal Processing,* vol. 21, no. 1, pp. 193-207.

Hudak, S. J., Saxena, A., Bucci, R. J. and Malcolm, R. C. (1978), *Development of standard methods of testing and analyzing fatigue crack growth rate data,* ADA058320, Westinghouse Electric Corporation, Pittsburgh, Westinghouse R & D Center.

Irving, P. E., Eker, O. and Camci, F. (2012), "Prognostics control of cracking in structures and components operating in hydrogen environments", *Proc.Int.Hydrogen Conf,* .

Jardine, A. K. S., Lin, D. and Banjevic, D. (2006), "A review on machinery diagnostics and prognostics implementing condition-based maintenance", *Mechanical Systems and Signal Processing,* vol. 20, no. 7, pp. 1483-1510.

Jennions, I. K. (2011), *Integrated Vehicle Health Management: Perspectives on an Emerging Field,* SAE International.

Job, M. (1994), *Air disaster,* Aerospace publ. ; distributed in North America by Motorbooks International, Weston Creek (Act.); Osceola (Wis.).

Jones, M., (2008), *Engine Fuel Filter Contamination*, QTR_03 ed., Boeing AeroMagazine.

Jouin, M., Gouriveau, R., Hissel, D., Péra, M. and Zerhouni, N. (2014), "Prognostics of PEM fuel cell in a particle filtering framework", *International Journal of Hydrogen Energy,* vol. 39, no. 1, pp. 481-494.

Kacprzynski, G. J., Roemer, M. J., Modgil, G., Palladino, A. and Maynard, K. (2002), "Enhancement of physics-of-failure prognostic models with system level features", *Aerospace Conference Proceedings, 2002. IEEE,* Vol. 6, pp. 6-2919.

Kacprzynski, G. J., Sarlashkar, A., Roemer, M. J., Hess, A. and Hardman, W. (2004), "Predicting remaining life by fusing the physics of failure modeling with diagnostics", *JOM,* vol. 56, no. 3, pp. 29-35.

Khawaja, T. S. (2011), *A Bayesian Least Squares Support Vector Machines Based Framework for Fault Diagnosis and Failure Prognosis,* Proquest, Umi Dissertation Publishing.

Kothamasu, R. and Huang, S. H. (2007), "Adaptive Mamdani fuzzy model for condition-based maintenance", *Fuzzy Sets and Systems,* vol. 158, no. 24, pp. 2715-2733.

Kothamasu, R., Huang, S. H. and Verduin, W. H. (2006), "System health monitoring and prognostics - A review of current paradigms and practices", *International Journal of Advanced Manufacturing Technology,* vol. 28, no. 9, pp. 1012-1024.

Kotulski, Z. (1998), "On efficiency of identification of a stochastic crack propagation model based on Virkler experimental data", *Archives of Mechanics,* vol. Vol. 50, nr 5, pp. 829-847.

Kotzalas, M. N. and Harris, T. A. (2000), "Fatigue Failure Progression in Ball Bearings", *Journal of Tribology,* vol. 123, no. 2, pp. 238-242.

Kumar, S., Torres, M., Chan, Y. C. and Pecht, M. (2008), "A hybrid prognostics methodology for electronic products", *Neural Networks, 2008. IJCNN 2008. (IEEE World Congress on Computational Intelligence). IEEE International Joint Conference on,* pp. 3479.

Kwan, C., Zhang, X., Xu, R. and Haynes, L. (2003), "A novel approach to fault diagnostics and prognostics", *Proceedings - IEEE International Conference on Robotics and Automation,* Vol. 1, pp. 604.

Lawless, J. and Crowder, M. (2004), "Covariates and random effects in a gamma process model with application to degradation and failure", *Lifetime Data Analysis,* vol. 10, no. 3, pp. 213-227.

Lee, J., Qiu, H., Yu, G., Lin, J. and Rexnord Technical Services, (2007), *Bearing Data Set*, IMS, University of Cincinnati. NASA Ames Prognostics Data Repository [http://ti.arc.nasa.gov/project/prognostic-data-repository], NASA Ames, Moffett Field, CA.

Lee, C. C. (1990), "Fuzzy logic in control systems: fuzzy logic controller. I", *Systems, Man and Cybernetics, IEEE Transactions on,* vol. 20, no. 2, pp. 404-418.

Lee, J., Ni, J., Djurdjanovic, D., Qiu, H. and Liao, H. (2006), "Intelligent prognostics tools and e-maintenance", *Computers in Industry,* vol. 57, no. 6, pp. 476-489.

Lembessis, E., Antonopoulos, G. and King, R. E. (1989), "CASSANDRA: an on-line expert system for fault prognosis.", .

Lesieutre, G. A., Fang, L. and Lee, U. (1997), "Hierarchical failure simulation for machinery prognostics", *Critical Link: Diagnosis to Prognosis, Haymarket,* , pp. 103-110.

Li, C. J. and Choi, A. (2002), "Spur gear root fatigue crack prognosis via crack diagnosis and fracture mechanics", *Proceedings of Proceedings of the 56th Meeting of the Society of Mechanical Failures Prevention Technology,* Virginia Beach, VA, pp. 311-320.

Li, C. J. and Lee, H. (2005), "Gear fatigue crack prognosis using embedded model, gear dynamic model and fracture mechanics", *Mechanical Systems and Signal Processing,* vol. 19, no. 4, pp. 836-846.

Li, Y., Billington, S., Zhang, C., Kurfess, T., Danyluk, S. and Liang, S. (1999), "Adaptive prognostics for rolling element bearing condition", *Mechanical Systems and Signal Processing,* vol. 13, no. 1, pp. 103-113.

Li, Y., Kurfess, T. R. and Liang, S. Y. (2000), "Stochastic prognostics for rolling element bearings", *Mechanical Systems and Signal Processing,* vol. 14, no. 5, pp. 747-762.

Li, Z., Zhou, S., Choubey, S. and Sievenpiper, C. (2007), "Failure event prediction using the Cox proportional hazard model driven by frequent failure signatures", *IIE Transactions (Institute of Industrial Engineers),* vol. 39, no. 3, pp. 303-315.

Liao, L. and Kottig, F. (2014), "Review of Hybrid Prognostics Approaches for Remaining Useful Life Prediction of Engineered Systems, and an Application to Battery Life Prediction", *Reliability, IEEE Transactions on,* vol. 63, no. 1, pp. 191-207.

Liao, H., Qiu, H., Lee, J., Lin, D., Banjevic, D. and Jardine, A. (2005), "A predictive tool for remaining useful life estimation of rotating machinery components", *Proceedings of the ASME International Design Engineering Technical Conferences and Computers and Information in Engineering Conference - DETC2005,* Vol. 1 A, pp. 509.

Liu, Z., Li, Q. and Mu, V. (2012), "A Hybrid LSSVR-HMM Based Prognostics Approach", *Intelligent Human-Machine Systems and Cybernetics (IHMSC), 2012 4th International Conference on,* Vol. 2, pp. 275.

Liu, H., Shang, D., Liu, J. and Guo, Z. (2015), "Fatigue life prediction based on crack closure for 6156 Al-alloy laser welded joints under variable amplitude loading", *International Journal of Fatigue,* vol. 72, no. 0, pp. 11-18.

Liu, J., Swanson, J. J., Kittelson, D. B., Pui, D. Y. H. and Wang, J. (2013), "Microstructural and loading characteristics of diesel aggregate cakes", *Powder Technology,* vol. 241, pp. 244-251.

Liu, J., Wang, W., Ma, F., Yang, Y. B. and Yang, C. S. (2012), "A data-model-fusion prognostic framework for dynamic system state forecasting", *Engineering Applications of Artificial Intelligence,* vol. 25, no. 4, pp. 814-823.

Liu, J., Djurdjanovic, D., Ni, J., Casoetto, N. and Lee, J. (2007), "Similarity based method for manufacturing process performance prediction and diagnosis", *Computers in Industry,* vol. 58, no. 6, pp. 558-566.

Luo, J., Namburu, M., Pattipati, K., Qiao, L., Kawamoto, M. and Chigusa, S. (2003a), "Model-based prognostic techniques [maintenance applications]", *AUTOTESTCON 2003. IEEE Systems Readiness Technology Conference. Proceedings,* pp. 330.

Luo, J., Bixby, A., Pattipati, K., Qiao, L., Kawamoto, M. and Chigusa, S. (2003b), "An interacting multiple model approach to model-based prognostics", *Proceedings of the IEEE International Conference on Systems, Man and Cybernetics,* Vol. 1, pp. 189.

Luo, J. and Bowen, P. (2003), "A probabilistic methodology for fatigue life prediction", *Acta Materialia,* vol. 51, no. 12, pp. 3537-3550.

Mahamad, A. K., Saon, S. and Hiyama, T. (2010), "Predicting remaining useful life of rotating machinery based artificial neural network", *Computers & Mathematics with Applications,* vol. 60, no. 4, pp. 1078-1087.

Majidian, A. and Saidi, M. H. (2007), "Comparison of Fuzzy logic and Neural Network in life prediction of boiler tubes", *International Journal of Fatigue,* vol. 29, no. 3, pp. 489-498.

Marjanovic, A., Kvascev, G., Tadic, P. and Djurovic, Z. (2011), "Applications of predictive maintenance techniques in industrial systems", *Serbian Journal of Electrical Engineering,* vol. 8, no. 3, pp. 263-279.

Mathew, S., Das, D., Rossenberger, R. and Pecht, M. (2008), "Failure mechanisms based prognostics", *2008 International Conference on Prognostics and Health Management, PHM 2008,* .

Mattera, D. and Haykin, S. (1999), "Support Vector Machines for Dynamic Reconstruction of a Chaotic System", in *Advances in Kernel Methods,* MIT Press, Cambridge, MA, USA, pp. 211-241.

Medjaher, K., Tobon-Mejia, D. A. and Zerhouni, N. (2012), "Remaining Useful Life Estimation of Critical Components With Application to Bearings", *Reliability, IEEE Transactions on,* vol. 61, no. 2, pp. 292-302.

Mohanty, S., Chattopadhyay, A., Peralta, P., Das, S. and Willhauck, C. (2008), "Fatigue life prediction using multivariate gaussian process", *Collection of Technical Papers - AIAA/ASME/ASCE/AHS/ASC Structures, Structural Dynamics and Materials Conference,* .

Mohanty, S., Teale, R., Chattopadhyay, A., Peralta, P. and Willhauck, C. (2007), "Mixed Gaussian process and state-space approach for fatigue crack growth prediction", *International Workshop on Structural Heath Monitoring,* Vol. 2, pp. 1108.

Murthy, D. N. P., Atrens, A. and Eccleston, J. A. (2002), "Strategic maintenance management", *J of Qual in Maintenance Eng,* vol. 8, no. 4, pp. 287-305.

NASA (Oct. 1992), *Research and technology goals and objectives for Integrated Vehicle Health Management (IVHM),* report NASA-CR-192656.

NASA Ames (2012), *NASA Prognostics Center of Excellence Data repository*, available at: http://ti.arc.nasa.gov/tech/dash/pcoe/prognostic-data-repository/ (accessed 05/10).

Ni, L. A., Yu, A. B., Lu, G. Q. and Howes, T. (2006), "Simulation of the cake formation and growth in cake filtration", *Minerals Engineering,* vol. 19, no. 10, pp. 1084-1097.

Niculita, O., Irving, P. and Jennions, I. K. (2012), "Use of COTS Functional Analysis Software as an IVHM Design Tool for Detection and Isolation of UAV Fuel System Faults", *Annual Conference of the Prognostics and Health Management Society 2012,* Vol. 3, Sep 22- 27, Minneapolis, USA, pp. Paper #105.

Niculita, O., Jennions, I. K. and Irving, P. (2013), "Design for diagnostics and prognostics: A physical-functional approach", *Aerospace Conference, 2013 IEEE,* pp. 1.

Norwegian Public Reports (1981), *The 'Alexander L. Kielland' Accident,* 11, Global Book Resources Ltd.

Oppenheimer, C. H. and Loparo, K. A. (2002), "Physically based diagnosis and prognosis of cracked rotor shafts", *Proceedings of SPIE - The International Society for Optical Engineering,* Vol. 4733, pp. 122.

Orchard, M. E. (2007), *A Particle Filtering-based Framework for On-line Fault Diagnosis and Failure Prognosis* (PhD thesis), Georgia Institute of Technology, Georgia Institute of Technology.

Orchard, M. E. and Vachtsevanos, G. (2007), "A particle filtering approach for on-line failure prognosis in a planetary carrier plate", *International Journal of Fuzzy Logic and Intelligent Systems,* vol. 7, no. 4, pp. 221-227.

Orchard, M., Kacprzynski, G., Goebel, K., Saha, B. and Vachtsevanos, G. (2008), "Advances in uncertainty representation and management for particle filtering applied to prognostics", *Prognostics and Health Management, 2008. PHM 2008. International Conference on,* pp. 1.

Orsagh, R., Roemer, M., Sheldon, J. and Klenke, C. J. (2004), "A comprehensive prognostics approach for predicting gas turbine engine bearing life", *Proceedings of the ASME Turbo Expo 2004,* Vol. 2, pp. 777.

Orsagh, R. F., Sheldon, J. and Klenke, C. J. (2003), "Prognostics/diagnostics for gas turbine engine bearings", *Aerospace Conference, 2003. Proceedings. 2003 IEEE,* Vol. 7, pp. 3095.

Papazian, J. M., Anagnostou, E. L., Engel, S. J., Hoitsma, D., Madsen, J., Silberstein, R. P., Welsh, G. and Whiteside, J. B. (2009), "A structural integrity prognosis system", *Engineering Fracture Mechanics,* vol. 76, no. 5, pp. 620-632.

Paris, P. C. and Erdogan, F. (1963), "A critical analysis of crack propagation laws", *Journal of Basic Engineering, Trans. ASME,* vol. Ser. D, no. 85, pp. 528-534.

Park, M. (2002), "Engine failure caused by erosion-corrosion of fuel manifold", *Engineering Failure Analysis,* vol. 9, no. 6, pp. 673-681.

Patil, N., Das, D., Chunyan Yin, Hua Lu, Bailey, C. and Pecht, M. (2009), "A fusion approach to IGBT power module prognostics", *Thermal, Mechanical and Multi-Physics simulation and Experiments in Microelectronics and Microsystems, 2009. EuroSimE 2009. 10th International Conference on,* pp. 1.

Pecht, M. and Jaai, R. (2010), "A prognostics and health management roadmap for information and electronics-rich systems", *Microelectronics Reliability,* vol. 50, no. 3, pp. 317-323.

Peel, L. (2008), "Data driven prognostics using a Kalman filter ensemble of neural network models", *Prognostics and Health Management, 2008. PHM 2008. International Conference on,* pp. 1.

Peng, T., He, J., Liu, Y., Saxena, A., Celaya, J. and Goebel, K. (2012), *Integrated fatigue damage diagnosis and prognosis under uncertainties,* , NATIONAL AERONAUTICS AND SPACE ADMINISTRATION MOFFETT FIELD CA AMES RESEARCH CENTER.

Peng, Y., Dong, M. and Zuo, M. J. (2010), "Current status of machine prognostics in condition-based maintenance: A review", *International Journal of Advanced Manufacturing Technology,* vol. 50, no. 1-4, pp. 297-313.

Phelps, E., Willett, P. and Kirubarajan, T. (2001), "A statistical approach to prognostics", *Proceedings of SPIE - The International Society for Optical Engineering,* Vol. 4389, pp. 23.

Pintelon, L. and Parodi-Herz, A. (2008), "Part B, Maintenance: An Evolutionary Perspective", in *Complex System Maintenance Handbook,* Springer London, , pp. 21-48.

Pontikakis, G. N., Koltsakis, G. C. and Stamatelos, A. M. (2001), "Dynamic filtration modeling in foam filters for diesel exhaust", *Chemical Engineering Communications,* vol. 188, pp. 21-46.

Przytula, K. W. and Choi, A. (2007), "Reasoning framework for diagnosis and prognosis", *IEEE Aerospace Conference Proceedings,* .

Qiu, H., Lee, J., Lin, J. and Yu, G. (2006), "Wavelet filter-based weak signature detection method and its application on rolling element bearing prognostics", *Journal of Sound and Vibration,* vol. 289, no. 4–5, pp. 1066-1090.

Qiu, J., Seth, B. B., Liang, S. Y. and Zhang, C. (2002), "Damage mechanics approach for bearing lifetime prognostics", *Mechanical Systems and Signal Processing,* vol. 16, no. 5, pp. 817-829.

Righiniotis, T. D. and Chryssanthopoulos, M. K. (2003), "Probabilistic fatigue analysis under constant amplitude loading", *Journal of Constructional Steel Research,* vol. 59, no. 7, pp. 867-886.

Ritchie, R. O. (1999), "Mechanisms of fatigue-crack propagation in ductile and brittle solids", *International Journal of Fracture,* vol. 100, no. 1, pp. 55-83.

Rong, P. and Pedram, M. (2006), "An analytical model for predicting the remaining battery capacity of lithium-ion batteries", *Very Large Scale Integration (VLSI) Systems, IEEE Transactions on,* vol. 14, no. 5, pp. 441-451.

Rosunally, Y. Z., Stoyanov, S., Bailey, C., Mason, P., Campbell, S. and Monger, G. (2009), "Prognostics framework for remaining life rediction of cutty sark iron structures", *Annual Conference of the Prognostics and Health Management Society 2009,* 2009, San Diego, CA, USA, PHM Society, San Diego, CA, USA, .

Roussel, N., Nguyen, T. L. H. and Coussot, P. (2007), "General probabilistic approach to the filtration process", *Physical Review Letters,* vol. 98, no. 11.

Roychoudhury, I., Hafiychuk, V. and Goebel, K. (2013), "Model-based diagnosis and prognosis of a water recycling system", *Aerospace Conference, 2013 IEEE,* pp. 1.

Saarela, O., Hulsund, J. E., Taipale, A. and Hegle, M. (2014), "Remaining Useful Life Estimation for Air Filters at a Nuclear Power Plant", *2nd internatial conference of the Prognostics and Health Management Society,* .

Saha, B., Celaya, J. R., Wysocki, P. F. and Goebel, K. F. (2009), "Towards prognostics for electronics components", *Aerospace conference, 2009 IEEE,* pp. 1.

Saha, B. and Goebel, K., (2007), *Battery Data Set*, NASA Ames Prognostics Data Repository, [http://ti.arc.nasa.gov/project/prognostic-data-repository], NASA Ames, Moffett Field, CA.

Saha, B., Goebel, K. and Christophersen, J. (2009), "Comparison of prognostic algorithms for estimating remaining useful life of batteries", *Transactions of the Institute of Measurement and Control,* vol. 31, no. 3-4, pp. 293-308.

Saha, B., Goebel, K., Poll, S. and Christophersen, J. (2007), "An integrated approach to battery health monitoring using bayesian regression and state estimation", *Autotestcon, 2007 IEEE,* pp. 646.

Saha, B., Goebel, K., Poll, S. and Christophersen, J. (2009), "Prognostics Methods for Battery Health Monitoring Using a Bayesian Framework", *Instrumentation and Measurement, IEEE Transactions on,* vol. 58, no. 2, pp. 291-296.

Samie, M., Perinpanayagam, S., Alghassi, A., Motlagh, A. and Kapetanios, E., (2014), *Developing Prognostic Models Using Duality Principles for DC-to-DC Converters*.

Sappok, A., Rodriguez, R. and Wong, V. (2010), "Characteristics and effects of lubricant additive chemistry on ash properties impacting diesel particulate filter service life", *SAE International Journal of Fuels and Lubricants,* vol. 3, no. 1, pp. 705-722.

Satish, B. and Sarma, N. D. R. (2005), "A Fuzzy BP approach for diagnosis and prognosis of bearing faults in induction motors", *2005 IEEE Power Engineering Society General Meeting,* Vol. 3, pp. 2291.

Saxena, A., Celaya, J., Saha, B., Saha, S. and Goebel, K. (2010), "Metrics for Offline Evaluation of Prognostic Performance", *International Journal of Prognostics and Health Management,* vol. 1, no. 001, pp. 20.

Saxena, A. and Goebel, K., (2008), *C-MAPSS Data Set*, NASA Ames Prognostics Data Repository, [http://ti.arc.nasa.gov/project/prognostic-data-repository], NASA Ames, Moffett Field, CA.

Saxena, A., Celaya, J., Saha, B., Saha, S. and Goebel, K. (2009), "On applying the prognostic performance metrics", *International Conference on Prognostics and Health Management (PHM),* San Diego, CA, USA, .

Saxena, A., Celaya, J., Balaban, E., Goebel, K., Saha, B., Saha, S. and Schwabacher, M. (2008), "Metrics for evaluating performance of prognostic techniques", *2008 International Conference on Prognostics and Health Management, PHM 2008,* .

Saxena, A., Celaya, J., Saha, B., Saha, S. and Goebel, K. (2009), "Evaluating algorithm performance metrics tailored for prognostics", *IEEE Aerospace Conference Proceedings,* .

Saxena, A., Celaya, J., Saha, B., Saha, S. and Goebel, K. (2010), "Evaluating prognostics performance for algorithms incorporating uncertainty estimates", *IEEE Aerospace Conference Proceedings,* .

Sheppard, J. W. and Kaufman, M. A. (2005), "Bayesian diagnosis and prognosis using instrument uncertainty", *AUTOTESTCON (Proceedings),* Vol. 2005, pp. 417.

Shetty, P., Mylaraswamy, D. and Ekambaram, T. (2008), "A hybrid prognostic model formulation and health estimation of auxiliary power units", *Journal of Engineering for Gas Turbines and Power,* vol. 130, no. 2.

Si, X. -., Wang, W., Hu, C. -. and Zhou, D. -. (2011), "Remaining useful life estimation - A review on the statistical data driven approaches", *European Journal of Operational Research,* vol. 213, no. 1, pp. 1-14.

Sikorska, J. Z., Hodkiewicz, M. and Ma, L. (2011), "Prognostic modelling options for remaining useful life estimation by industry", *Mechanical Systems and Signal Processing,* vol. 25, no. 5, pp. 1803-1836.

Sonnenfeld, G., Goebel, K. and Celaya, J. R. (2008), "An agile accelerated aging, characterization and scenario simulation system for gate controlled power transistors", *AUTOTESTCON, 2008 IEEE,* pp. 208.

Sparks, T. (2011), *Solid-Liquid Filtration: A User's Guide to Minimizing Cost & Environmental Impact, Maximizing Quality & Productivity,* First Edition ed, Elsevier Science & Technology Books.

Sutherland, K. (2010), "Mechanical engineering: The role of filtration in the machinery manufacturing industry", *Filtration and Separation,* vol. 47, no. 3, pp. 24-27.

Swanson, D. C. (2001), "A general prognostic tracking algorithm for predictive maintenance", *IEEE Aerospace Conference Proceedings,* Vol. 6, pp. 62971.

Thissen, U., van Brakel, R., de Weijer, A. P., Melssen, W. J. and Buydens, L. M. C. (2003), "Using support vector machines for time series prediction", *Chemometrics and Intelligent Laboratory Systems,* vol. 69, no. 1–2, pp. 35-49.

Tien, C. and Ramarao, B. V. (2013), "Can filter cake porosity be estimated based on the Kozeny-Carman equation?", *Powder Technology,* vol. 237, pp. 233-240.

Tien, C. and Bai, R. (2003), "An assessment of the conventional cake filtration theory", *Chemical Engineering Science,* vol. 58, no. 7, pp. 1323-1336.

Vachtsevanos, G., Lewis, L., Roemer, M., Hess, A. and and Wu, B. (2006), *Intelligent Fault Diagnosis and Prognosis for Engineering Syst,* Wiley.

Vachtsevanos, G. and Wang, P. (2001), "Fault prognosis using dynamic wavelet neural networks", *AUTOTESTCON Proceedings, 2001. IEEE Systems Readiness Technology Conference,* pp. 857.

Vachtsevanos, G. J. and Valavanis, K. P. (2009), *Applications of Intelligent Control to Engineering Systems: In Honour of Dr. G. J. Vachtsevanos,* Springer.

Vichare, N. M. and Pecht, M. G. (2006), "Prognostics and health management of electronics", *IEEE Transactions on Components and Packaging Technologies,* vol. 29, no. 1, pp. 222-229.

Virkler, D. A., Hillberry, B. M. and Goel, P. K. (1979), "The Statistical Nature of Fatigue Crack Propagation", vol. 101, no. 2, pp. 148-153.

Wakeman, R. (2007), "Filter media: Testing for liquid filtration", *Filtration and Separation,* vol. 44, no. 3, pp. 32-34.

Wang, T. (2010), *Trajectory Similarity Based Prediction for Remaining Useful Life Estimation* (PhD thesis), UNIVERSITY OF CINCINNATI, UNIVERSITY OF CINCINNATI.

Wang, T., Yu, J., Siegel, D. and Lee, J. (2008), "A similarity-based prognostics approach for remaining useful life estimation of engineered systems", *2008 International Conference on Prognostics and Health Management, PHM 2008,* .

Wang, W. and Carr, M. (2010), "An adapted brownion motion model for plant residual life prediction", *2010 Prognostics and System Health Management Conference, PHM '10,* .

Wang, W. Q., Golnaraghi, M. F. and Ismail, F. (2004), "Prognosis of machine health condition using neuro-fuzzy systems", *Mechanical Systems and Signal Processing,* vol. 18, no. 4, pp. 813-831.

Wegerich, S. W. (2004), "Similarity based modeling of time synchronous averaged vibration signals for machinery health monitoring", *Aerospace Conference, 2004. Proceedings. 2004 IEEE,* Vol. 6, pp. 3654.

Wei Wu, Jingtao Hu and Jilong Zhang (2007), "Prognostics of Machine Health Condition using an Improved ARIMA-based Prediction method", *Industrial Electronics and Applications, 2007. ICIEA 2007. 2nd IEEE Conference on,* pp. 1062.

Weiming Xian, Bing Long, Min Li and HouJun Wang (2014), "Prognostics of Lithium-Ion Batteries Based on the Verhulst Model, Particle Swarm Optimization and Particle Filter", *Instrumentation and Measurement, IEEE Transactions on,* vol. 63, no. 1, pp. 2-17.

Wilfong, D., Dallas, A., Yang, C., Johnson, P., Viswanathan, K., Madsen, M., Tucker, B. and Hacker, J. (2010), "Emerging challenges of fuel filtration", *Filtration,* vol. 10, no. 2, pp. 107-117.

Wu, W. F. and Ni, C. C. (2003), "A study of stochastic fatigue crack growth modeling through experimental data", *Probabilistic Engineering Mechanics,* vol. 18, no. 2, pp. 107-118.

Xing, Y., Williard, N., Tsui, K. -. and Pecht, M. (2011), "A comparative review of prognostics-based reliability methods for Lithium batteries", *Prognostics and System Health Management Conference (PHM-Shenzhen), 2011,* pp. 1.

Xiong, Y., Cheng, X., Shen, Z. J., Mi, C., Wu, H. and Garg, V. K. (2008), "Prognostic and warning system for power-electronic modules in electric, hybrid electric, and fuel-cell vehicles", *IEEE Transactions on Industrial Electronics,* vol. 55, no. 6, pp. 2268-2276.

Xu, J. and Xu, L. (2011), "Health management based on fusion prognostics for avionics systems", *Systems Engineering and Electronics, Journal of,* vol. 22, no. 3, pp. 428-436.

Xue, G., Xiao, L., Bie, M. and Lu, S. (2005), "Fault prediction of boilers with fuzzy mathematics and RBF neural network", *2005 International Conference on Communications, Circuits and Systems - Proceedings,* Vol. 2, pp. 1012.

Yam, R. C. M., Tse, P. W., Li, L. and Tu, P. (2001), "Intelligent Predictive Decision Support System for Condition-Based Maintenance", *The International Journal of Advanced Manufacturing Technology,* vol. 17, no. 5, pp. 383-391.

Yan, J. and Lee, J. (2007), "A Hybrid Method for On-line Performance Assessment and Life Prediction in Drilling Operations", *Automation and Logistics, 2007 IEEE International Conference on,* pp. 2500.

Yen, Y., Söhner, J., Lilly, B. and Altan, T. (2004), "Estimation of tool wear in orthogonal cutting using the finite element analysis", *Journal of Materials Processing Technology,* vol. 146, no. 1, pp. 82-91.

Yilboga, H., Eker, O. F., Güçlü, A. and Camci, F. (2010), "Failure prediction on railway turnouts using time delay neural networks", *CIMSA 2010 - IEEE International Conference on Computational Intelligence for Measurement Systems and Applications, Proceedings,* pp. 134.

Yu, W. K. and Harris, T. A. (2001), "A New Stress-Based Fatigue Life Model for Ball Bearings", *Tribology Transactions,* vol. 44, no. 1, pp. 11-18.

Zemouri, R., Racoceanu, D. and Zerhouni, N. (2003), "Recurrent radial basis function network for time-series prediction", *Engineering Applications of Artificial Intelligence,* vol. 16, no. 5-6, pp. 453-463.

Zhang, G., Lee, S., Propes, N., Zhao, Y., Vachtsevanos, G., Thakker, A. and Galie, T. (2002), "A novel architecture for an integrated fault diagnostic-prognostic system", *Proc. AAAI Symp.* 2002, Stanford, California, AAAI, Stanford, California, .

Zhang, H., Kang, R. and Pecht, M. (2009), "A hybrid prognostics and health management approach for condition-based maintenance", *IEEM 2009 - IEEE International Conference on Industrial Engineering and Engineering Management,* pp. 1165.

Zhang, J., Sato, T. and Iai, S. (2006a), "Support vector regression for on-line health monitoring of large-scale structures", *Structural Safety,* vol. 28, no. 4, pp. 392-406.

Zhang, L., Li, X. and Yu, J. (2006b), "A review of fault prognostics in condition based maintenance", *Proceedings of SPIE - The International Society for Optical Engineering,* Vol. 6357 II, .

Zhang, X., Xu, R., Kwan, C., Liang, S. Y., Xie, Q. and Haynes, L. (2005), "An integrated approach to bearing fault diagnostics and prognostics", *Proceedings of the American Control Conference,* Vol. 4, pp. 2750.

Zhigang Tian (2009), "An artificial neural network approach for remaining useful life prediction of equipments subject to condition monitoring", *Reliability, Maintainability and Safety, 2009. ICRMS 2009. 8th International Conference on,* pp. 143.

Zio, E. and Di Maio, F. (2010), "A data-driven fuzzy approach for predicting the remaining useful life in dynamic failure scenarios of a nuclear system", *Reliability Engineering & System Safety,* vol. 95, no. 1, pp. 49-57.

Zio, E. and Peloni, G. (2011), "Particle filtering prognostic estimation of the remaining useful life of nonlinear components", *Reliability Engineering & System Safety,* vol. 96, no. 3, pp. 403-409.